MODEL TEST DATA ANALYSIS OF SHIP MANEUVERABILITY IN ICE

YU SHI

Faculty of Engineering and Applied Science
Memorial University of Newfoundland

Model Test Data Analysis of Ship Maneuverability in Ice

by

Yu Shi, B. Eng.

A thesis submitted to the School of Graduate Studies
in partial fulfillment of the requirement for
the degree of M. Eng.

May 2002

St. John's Newfoundland Canada

Acknowledgements

I would like to specially thank Dr. F. M. Williams and Dr. M. R. Haddara, my thesis supervisors, for their guidance and support through my study at Memorial University of Newfoundland. Their friendship, encouragement, experience and insightful suggestions have greatly facilitated the successful completion of my research.

Financial supports from Canada-Newfoundland Cooperation Agreement on Economic Renewal, supports from Faculty of Engineering and Applied Science and School of Graduate Studies of Memorial University of Newfoundland are highly appreciated.

Finally, I would like to thank all IMD staff who designed, planned and performed the model test and provides the raw test data for my research.

Abstract

This thesis presents a detailed analysis of planar motion mechanism model test data in various ice conditions. A comprehensive literature investigation on ship maneuverability in ice was performed. The main focus of this work is better understanding of the effects of different ice conditions on ship maneuverability and information for an effective and accurate mathematical model for estimating ship maneuverability in ice. Because of high forces and high accelerations in icebreaking operation, the data are complex. A complete procedure for the analysis of the raw test data, including wavelet transform and neural network calculation, was developed. A ship turning radius predictor based on the data gives internally consistent results. The proposals for further research, to achieve a more accurate model, are provided.

CONTENTS

List of Figures

List of Tables

List of Abbreviations

PMM	Planar Motion Mechanism
IMD	Institute for Marine Dynamics
CWT	Continuous Wavelet Transform
DWT	Discrete Wavelet Transform

List of Symbols

V	Instant Velocity at the center of gravity of the ship
ψ_0	Voyage Angle
ζ	Axis fixed to the earth
χ	Axis fixed to the ship
ψ	Yaw Angle
β	Drift Angle
r	Yaw Rate
R	Turning Radius of the ship
X, Y, N	Surge force, Sway force and Yaw moment, respectively
u, v, r	Instant Surge velocity, Sway velocity and Yaw rate, respectively
u_1	Velocity at the time of initial equilibrium condition
Δ	Displacement of ship
I_z	Mass moment inertia of ship
δ_R	Rudder Angle
N_δ	Rudder Moment Coefficient
Y_δ	Rudder Force Coefficient
Y_{pmm}	PMM Force
N_{pmm}	PMM Moment
Y_r	Sway Force / Yaw Rate Coefficient
N_r	Yaw Moment / Yaw Rate Coefficient
Y_v	Sway Force / Sway Velocity Coefficient
N_v	Yaw Moment / Sway Velocity Coefficient

Chapter 1 Introduction

1.1 Background

Naval Architects have long faced the problem of estimating the performance of ships navigating in ice-covered oceans. Exploitation of oil and gas reserves from hydrocarbon reservoirs below the seabed has increased rapidly since the early 1960s. A number of offshore structures have been designed, fabricated and deployed in the arctic and sub-arctic waters, areas with tremendous potential for deposits. The most effective means of transportation between the mineral deposit and the plant is shipping. More and more crude oil tankers, bulk carriers and other service ships will navigate this area. The presence of large fields of ice, which are common in this geographic area, provides a primary impediment to transportation. There is little operational experience with merchant vessels in severe ice conditions. So it is necessary to understand how to design, evaluate and estimate ship's controllability in various ice conditions.

Ice-ship interaction has various aspects. These include ice-propeller interaction, ice-rudder interaction, ice floe impact, and ship resistance in ice. The study of ship resistance in ice has made substantial advances over the years. A considerable effort was spent in documenting ice properties and characteristics, and measuring ice resistance acting on different ship hulls. Many model experiments were carried out and numerous empirical formulae were developed by researchers to predict ship resistance in ice. [13] Much less attention has been paid to the study of ship maneuverability in ice. [1]

Maneuverability is one of the aspects of controllability. Controllability of ships includes all aspects of regulating ship's trajectory, speed and orientation in various environmental conditions. The maneuverability is the ability to change ship's course as necessary in a timely and predictable fashion. The investigation of the maneuverability of a ship in ice is of great practical importance because icebreakers and arctic cargo ships move in ice for most of their navigation seasons. In comparison with open water condition, ships experience great difficulty in moving through ice-covered water even if the ice cover has been thoroughly broken into small pieces. Thus good maneuvering performance is an important part of safe navigation. The most widely used method to study ship maneuverability in ice is still model tests. Data obtained from maneuvering tests require complex methods of analysis: measured ice forces have large random variations and show irregular sawtooth patterns.

Model tests to study the effect of different ice conditions on ship's maneuverability were performed in July 1998 at the Institute for Marine Dynamics. The planar motion mechanism was used to maneuver an R-Class model in the ice tank of the institute. The analysis presented in this work is based on the data obtained during these tests.

1.2 Objectives

The main focus of this work is to better the understanding of the effects of different ice conditions on ship maneuverability and to develop an effective and accurate mathematical model for estimating ship maneuverability in ice. The present study of the maneuvering qualities of a ship in ice has the following specific objectives:

1. To develop a procedure for the manipulation and analysis of the raw test data.
2. To evaluate different data analysis techniques.
3. To correlate the ship motions in ice with the corresponding ice forces acting on the ship.
4. To develop an effective approach to predict the ship maneuvering performance in different ice conditions.
5. To provide proposals for further work

1.3 Methodology

Two types of PMM maneuvering experiments were carried out: constant radius arcs and sinusoidal maneuvers. They were performed in four ice conditions and in open water in order to compare ship maneuverability in different ice conditions. Details of the PMM experiments are given in Chapter 4.

The data were converted to MATLAB format and manipulated in a methodical way for further analysis. The details are given in Appendix 1. Measured forces acting on the model and the corresponding responses of the model were obtained from the test data. The derivation of basic equations is given in Chapter 3.

The work focuses on the different method of data analysis. Wavelet filters which preserve the characteristic information of the data were developed and applied. Neural networks and Regression techniques were employed to identify the relationship between sway force, yaw moment and sway velocity, yaw rate. Statistical Analysis of the results was used to correlate the ice forces acting on ship during a maneuver with various ice conditions. A model to predict the ship maneuverability in ice condition was developed.

Chapter 2 Literature Survey

2.1 Review of ship maneuverability in ice

The development of icebreaking technology in the past several decades has proven that the maneuverability of a ship can be improved by modifying specific features of the hull and the propulsion system and by using of maneuvering aids, such as a thruster, or a bubbler.

But it is still a tremendous task to obtain comprehensive insight into the physical actions involved when a ship performs all types of maneuvers in ice. To develop an analytical procedure which will account for the behavior observed and will indicate the significant variables and their effects on the processes of maneuvering in ice is still an incomplete mission of many researchers.

Before we touch the "ship in ice" issues, ship maneuverability in open water should be mentioned to make a comparison with the different phenomenon for a ship in ice.

2.1.1 Ship Maneuverability in open water

It is reasonable to review ship maneuverability in open water before we turn to the same topic in ice. Although the influenced parameters differ in the two cases, in both cases no completely satisfactory mathematical model has yet been developed, and the

most accurate predictions of ship maneuverability are dependent on model testing. Empirical estimates may be used at early stages in the design process.

After the beginning of the turning motion, the lateral movement of the ship is opposed by the inertial reactions. If the rudder remains at a fixed angle of deflection, a steady turning condition will develop when hydrodynamic and inertial forces and moments reach a balance.

Generally, there are four types of forces acting on a ship during a maneuver:

- Hydrodynamic forces acting on the hull and appendages due to ship velocity and acceleration, rudder deflection, and propeller rotation.
- Inertial reaction forces caused by ship acceleration.
- Environmental forces due to wind, waves and currents
- External forces such as tugs, thrusters and other maneuvering aids.

The first two types of forces generally act in the horizontal plane and involve only surge, sway and yaw responses. Usually, the simplest case of maneuverability, assuming a calm open sea without wind, waves, current, and external forces, is considered by most researchers. Thus, the surge, sway and yaw motions have been extensively studied by researchers.

From a previous study [1], some basic empirical rules have been developed relating maneuverability to certain ship parameters. (Table 2-1)

Table 2-1 effect of the ship parameters on maneuverability in open water

Characteristic		Influence
Length/Beam Ratio	L/B	Increase reduces Maneuverability
Length/Draught Ratio	L/D	Increase increases Maneuverability
Block Coefficient	C_B	Increase increases Maneuverability
Stern Trim (stern draft increased)		Increase reduces Maneuverability
Bow Shape		Sharp forms reduce Maneuverability

2.1.2 Ship Maneuverability in Ice

So far only very limited work has been carried out to obtain a physical understanding of the processes which control the maneuvering performance of a ship in ice. The development of reliable modeling techniques for ship maneuvering in ice would constitute a major advance in the design of new ice-worthy vessels and in the simulation of their navigating characteristics.

Ship resistance in ice has received much more attention than ship maneuverability in ice. So some numerical models of ship maneuverability in ice were developed from the models of ship resistance in ice. The ship maneuvering performance in continuous level ice also attracted much more attention than in any other ice condition. A majority of available literature concerning the ship maneuverability in ice is the study of ship performance in level ice with a solitary dominant icebreaking mode. But in actual operations in arctic and sub-arctic regions, the ship will encounter a mixture of ice formations. According to the Captain's experience, [1] ships still have great difficulty

not only in level ice but also in moving through water covered with layers broken ice fragments. The ideal approach would be of course to take all actual ice conditions into account when aiming at real optimization of an ice-worthy vessel's design.

So a thorough literature review of ship maneuvering performance in ice should include the following aspects:

1. Brief introduction to the morphology and physical properties of sea ice
2. The process of a ship executing maneuvers in ice
3. Important ship parameters governing maneuverability in ice

2.1.2.1 Morphology and physical properties of sea ice

Sufficient knowledge of the formation of ice and its various forms, conditions, and properties can facilitate a better understanding of issues of ice mechanics and ice loads on ships. [2]

Ice is a granular material. The typical size and shape of an ice grain, which actually is an individual ice crystal, varies greatly. The ice grain ranges from 1 mm to several centimeters and its shape can be tabular, granular, or columnar. The structure of ice may be complicated further by the presence of salt and air. It is generally believed that these impurities play a more important role than microstructure in determining large-scale deformation and strength.

Generally, sea ice is classified as first-year or multi-year. The characteristics and properties of each type of ice are highly variable. The basic ice condition is a uniform, level ice sheet. On calm water, supercooled condition, the smooth ice sheet grows continuously throughout the winter season in cold regions. First-year sea ice can be overridden by the ice sheets of the same or varying thickness which tend to consolidate quickly into a single thicker sheet. Much of the sea ice is present in the form of ridges and rubble fields. When ridges extend because of pressure acting from several directions they are often referred to as an ice rubble field. The pack ice is formed by ice movement breaking the ice sheet or by the passage of vessels. The diameter of pack ice ranges from 2m (Brash Ice) to 10 km (vast floe). An important characteristic in the study of pack ice is the concentration, which is the ratio in tenths of the sea surface actually covered by ice to the total area of sea surface over a defined area. The parameter of concentration obviously means the total volume of ice, which is very important in predicting ship resistance in confined navigation channels.

The mechanical properties of sea ice, which are necessary to predict ice load on ships, usually include compressive, tensile, flexural, shear, adhesion strengths, friction coefficient and also its deformation characteristics such as elastic modulus and Poisson's ratio. All of above properties heavily depend on brine volume, which can be calculated from the empirical formula developed by Cox, and Weeks, [36]. Other useful references are given in the list of reference. [3] [4] [27]

2.1.2.2 Physical description of a ship maneuvering in ice

A full review of the noticeably sparse literature on this issue was carried out, but necessary information is far from complete. There are almost an infinite variety of ice conditions found in cold regions and this greatly complicates the problem of determining ship dynamics in ice. For example, at least three ice conditions are typical in Northern Labrador: level, pack ice and rubble ice. It also should be remembered that the forces acting on a ship in ice are unsteady, quasi-periodic phenomena since ship-ice interaction may involve varying degrees of ice ingestion, blockage, or ice milling. The vessel may undergo motions in six degrees of freedom unless restricted.

In order to simplify the problem, it is assumed throughout this thesis that the ice-worthy ship in question moves continuously (as opposed to ramming) through a homogeneous, uniform ice field of constant thickness and mechanical / physical properties, without any internal pressure. Real ice fields, of course, are not this simple. Instead, they are frequently interwoven with pressure ridges of varying size or rafted ice. The actual ice field may also be in various states of stress due to wind and water drag. In this paper, we only consider three dynamic modes, which constitute the steady turning motion in ice, surge, sway and yaw. The other three modes, heave, pitch and roll become important when unsteady motions in non-uniform ice are considered such as ramming a ridge. Roll may have some effects on maneuverability. A heel of ship hull can improve its ability to break the ice sheet.

The ice conditions a ship experiences in cold regions can be grossly divided into three categories. The first is uniform, unbroken, level ice; the second is pack ice, the third is multi-layer broken ice, including rubble ice, brash ice, and mush ice.

Level Ice

First, we give an introduction of the dynamics of a ship maneuvering in level ice.

While the flexural failure mode is the dominant pattern in a straight-line forward icebreaking, the turning motions of a ship in level ice cause ice failure in a combination of compressive, buckling, and flexural modes. This further makes it difficult to set up an accurate mathematical model for ship maneuverability in level ice.

Kendrick et al. [1] presented a description of the process of ship maneuvers in a continuous, homogeneous ice sheet. In the initial phase of a turn, at a small angle, the ship will be entirely within the channel broken by the inclined portion of the bow. The forces and moments opposing the turn will, therefore, be as a result of displacing broken ice fragments. When the ship reaches a certain turning rate, the sides of the ship will also be required to start breaking additional ice sheet. Its ability to do this will be dependent on the turning moment applied by the rudders and on the efficiency of the hull side in icebreaking, in particular the mid-body flare angle. For all vessels, in ice over a certain thickness, it will be impossible to turn beyond a critical turning rate.

Menon et al. [5] gave an explanation of the maximum thickness concept. The process of steady turns ahead in level ice is governed by a number of phenomena. In a very thin ice sheet, with thickness typically in the range 0 to 10cm, the ship will normally turn with a turning radius very nearly the same as that in open water. In this range, the breaking process is primarily the result of bow wave actions. With the increase in the ice thickness, icebreaking by bow waves stops and the ice cover begins to interact with the hull. Most of the breaking processes occur around the bow and the channel is wider than the beam so that the stern moves out to point the bow into the turn. With the continuous augmentation of the ice thickness, the sides of the hull also break the ice. In this phase, the rudder force together with hydrodynamic force is sufficient to clear the broken ice between the hull and the channel edge. Beyond a certain thickness, more and more broken ice in the gap will restrict the outward movement of the stern, thereby preventing the hull from adopting sufficient drift angle to obtain the required moment for a turn. So there is a maximum ice thickness under which the ship can continuously break ice and execute a turn maneuver.

The total resistance due to ice when a ship is performing a maneuver in level ice is assumed to be composed of a component due to breaking the ice, a component due to submerging and clearing the broken ice pieces around the ship, and a frictional drag component between ship hull and ice. Turning in level ice is dependent on the failure of the ice sheet, which occurs as a succession of discrete events. The basic frequency of these will most probably be dependent on ice strength and thickness and on ship velocity.

When a ship is performing turning maneuvers in an ice field, since breaking and submerging the ice normally occurs at the bow of the ship, the ship must maintain a certain forward speed in order to execute a yaw motion. Thus the observed motion in tests or trials is generally restricted to yaw with a small drift angle. Sway velocity and sway acceleration are relatively very small. Short term surge and yaw accelerations may be significant at the moment of ice failure or yield, but on the time scale of the ship making maneuvers, ship velocities vary slowly. Experience from ship resistance in ice indicates that ice resistance is quasi-static in nature, that is it depends on instantaneous ship velocity, and not on the history of the velocity or the acceleration. As the ship yaws, ice fragments may be accelerated along the length of the hull.

Pack Ice

A large field of pack ice is a typical ice form in cold regions. The visual feature of pack ice can be described as various sizes of ice fragments floating on the water surface.

When a ship is maneuvering in pack ice, the forces on the ship due to ice are likely to be much greater than the usual hydrodynamic forces. The resistance against turning is derived from the consideration of mass, momentum and energy conservation. Instead of breaking ice as in the motion of a ship in continuous ice, the motion of a ship in pack ice results in pushing the ice aside and in compression of ice. Several different processes are happening when a ship moves through pack ice. [38] [39]

The most typical interaction process is: impact between an ice floe and the ship hull, followed by submerging and overturning of the floe. When there are many ice floes, they are packed at the side of the hull as they are being pushed away by the hull. In addition, neighboring ice floes (not in contact with the hull) participate in the process.

In accordance with the described nature of movement of a ship in pack ice it is possible to analyze and clarify the force components due to ice involved in ship maneuvering. So far the different terms of ice force are difficult to separate exactly. Some of the components do indeed affect one another.

- Inertia component due to the loss of kinetic energy of the ship in collision with ice floes. During the motion of ship, the side of the ship comes into contact with ice floes which are originally motionless. Therefore, momentum is transferred to the ice floes which cause their translational motion. The process follows the law of conservation of momentum.

- Dissipation component due to dissipation of the energy of the ship, predominantly frictional. It can be subdivided into two terms: water resistance to separation of ice floes (overcome water resistance), and friction between ice floes. The water resistance to the motion of an ice floe on the surface of water is proportional to the area of water surface covered by the ice floes, and to the resistance coefficient. The second term is proportional to the contact area of separated ice floes and the resistance coefficient between ice floes.

- Component due to deformation of ice when ice is being separated. This process is independent of velocity, and hence we call it static resistance. It comes from the volume force (buoyancy), and depends on the length of ice floe and its thickness.

- Component due to submersion and overturning of ice, due to creation of waves and change of the position of the ship. One thing should be mentioned is the pattern of motion of a ship in broken ice depends significantly on the density of ice floes. The submerging of ice floes by the sides of the hull is seldom observed in broken ice of low density. The number of ice floes participating in the motion is relatively small.

Rubble Ice

The vessel is likely to travel through a highly dynamic ice environment, which consists of many miles of multiple layers of small ice floes. This is formed when ice is pushed by wind and ocean current into multiple layers. This ice was also subject to pressure and consolidation, which can make ship movement even more difficult. Ship performance in these ice conditions has not yet been studied in depth.

Ice rubble broadly indicates fragmented ice. As such, ice rubble occurs in many sizes and forms. Although more strictly speaking it is categorized as fragments whose major linear dimension exceeds about 2 m, smaller ice fragments in the size range of 2 to

0.02 m are categorized as brash ice. Ice fragments that are yet finer usually form mush ice.

Heavy pack ice, or rubble ice, resembles a viscous plastic material. Thick brash ice can perhaps be regarded as a floating granular solid that is homogeneous and isotropic. Inter-particle cohesion is not likely to be significant unless the mixture remains stationary for long time periods and fuses. The effects of any intrinsic cohesion between ice blocks have been ignored in this discussion.

During a ship maneuver, the total resistance encountered in multi-layer rubble ice can be divided into the following components:

- Resistance associated with the shearing or compression of the layer;
- Resistance attributable to the submergence of ice floes;
- Resistance caused by momentum exchange between the hull and ice rubble;
- Resistance due to friction between ice rubble and hull;
- Resistance associated with the breaking of ice rubble, which is significant if the layer is comprised of relatively large, plate-like ice pieces whose plane diameter approaches hull beam, and open water hydrodynamic resistance.

2.1.2.3 Parameters Influencing Ship Maneuverability in Ice

Ship maneuverability in ice has received much less attention than have other ship-in-ice issues. But some reports or papers have now commented on at least some aspects of the subject.

It has been shown that the position of the pivot point is a major factor affecting the turning circle capability of a ship. In the case of a vessel turning under the action of a stern rudder, the pivot point (zero moment) is located within 0.2 of the ship's length from the bow. [6] Its position will depend upon the efficiency of the bow geometry in terms of lateral resistance. In general, it appears that the higher the lateral bow resistance, the further forward will be the location of the pivot which increases the turning radius.

The forward location is particularly obvious in icebreakers where, although the system of motions, forces, and moments governing the vessel's turning dynamics is similar to that in open-water, the magnitude of the turning resistance is greatly increased by the presence of the ice. The net effect is to move the pivot point further forward and so increase the turning circle. Two approaches are available to move the pivot point nearer to midship, either a reduction of lateral resistance of the hull or the development of an increased lateral force of the hull in the direction of the turn. Thus, the central focus of the researcher's consideration was directed towards the achievement of a more effective turning performance by means of reduced lateral resistance and increased lateral forces.

Edwards et. al. [6] represented the results of two model tests. The two models were identical except for the block coefficient. The increase in the block coefficient from 0.555 to 0.625 has resulted in an increase in the dimensionless turning radius of 95 percent. The turning radius of the longer ship is significantly greater than that of the

shorter model. An increase in ship length of 20 percent caused an increase in turning radius per ship length of 300 percent. A simplified explanation for this greater turning radius is that for a ship to turn in ice, the hull side must break ice. The longer model must break ice over a greater length than the shorter model in a turn of equal radius. Hence, the tests predict much higher forces and moments for the longer ship to achieve the same radius turn, and, conversely, the ship will execute a much greater radius turn with the same available turning forces. The turning radius is greatly influenced by ice thickness. Edwards reported that by increasing the ice thickness from 3 to 6 ft, the turning radius per ship length increased from 3.3 to 37.5 at a rudder angle of 35 deg.

Peirce et. al. [7] conducted a survey over a database of twenty current icebreakers covering a representative range of size, proportions and capability coupled with an extensive literature search to identify and quantify those factors which contribute to good maneuverability in ice. The following are their conclusions.

Maneuverability was greatly improved by the reduction of the vessel's length to breadth ratio. The L/B ratio has a powerful influence on the turning circle. The turning circle increased five fold for a doubling in the L/B ratio.

It must be emphasized that bow geometry plays a vastly more important role in a ship's total performance than any other underwater portion of the hull. One method of producing the additional lateral force is by creating a differential geometry between the two sides of the bow by heeling the ship. The effect of heeling is to change the flare

angles on either side and this will result in a differential resistance across the bow. The basic principle involves an increase in lateral resistance on the outer side of the turning path and a reduction on the inner side. The modification to the stern lines near the waterline could be made to improve turning in ice. Providing a little more slopes at the waterline would assist the stern sections to break ice in bending rather than crushing. A model with the greatest section forward of amidships might also show a better maneuvering performance, as this allows room for the stern to swing. Vessels having high-energy downward icebreaking hull forms characterized by large waterline flare angles, such as elliptical and spoon bows, reduce lateral resistance and increasing turning ability compared with conventional bows.

The adoption of nozzles and one-for-one propeller/rudder arrangements has improved icebreaker turning ability. It has been found that the use of reamers also contributes significantly to improving turning capability. Bubbler systems also can improve ship's maneuverability in ice to some degree by reducing the friction coefficient between the ship and the ice sheet. [7]

Some conclusions from the above discussions are shown in Table 2-2, which should be compared with Table 2-1 for the open water case.

Table 2-2 effect of the ship parameters on ship maneuverability in ice

Characteristic		Influence
Length/Beam Ratio	L/B	Increase reduces Maneuverability
Block Coefficient	C_B	Increase reduces Maneuverability
Bow asymmetry		Increased lateral force
Bow thruster		Increased lateral force
Bubbler		Reduced lateral resistance
Mid-Body flare angle		Reduced lateral resistance
Stern thruster		Increased lateral force
Bow, Stern, Hull Shape		See detailed description

Bow asymmetry means that the two sides of a ship's bow have different shapes

2.2 Survey of current methods to predict ship maneuverability in ice

Theories and techniques for predicting the important maneuvering abilities of ships in open water have been improved to a satisfactory level. Unfortunately very little effort has been exerted to understanding these abilities of ships in ice. Good maneuverability is also considered to be an important requirement for the design of ice – worthy ships.

Generally speaking, the methods for predicting ship maneuverability can be divided into three categories, full-scale ship trials, model tests, and analytical approaches.

A reliable analytical approach is the ultimate goal of all ice-ship researchers. This would be a method based on a physical representation of the mechanics of ship-ice interaction and the building of a matching mathematical model. So a thorough understanding of ship-ice interaction is a prerequisite for this method. The process of the motion of a ship in various ice conditions is quite complicated. So far the study of the complex nature of ship-ice interaction leaves too much to be improved. This tremendous task has been tackled by several investigators over the years. [5] [13]

Full-scale ship voyage trials obviously represent the most valid performance of ship in ice. The data of trials also give a most powerful database for the validation of results of the model tests and analytical methods. The major shortcoming of such trials is that the trials are related to a particular type of ship and to a specific ice condition under which the measurement was made. Thus, full-scale trials are not generally valid for all ice conditions. Due to the limitations of this approach and the prohibitive cost of full-scale tests, not too much work has been done using this approach.

The most widely used method in predicting ship maneuverability in ice is model tests. For the case of open-water model testing, more than 100 years of experience led to the highly reliable techniques for estimating ship's maneuverability. The determination of hydrodynamic derivatives for the motions and control of a hull is a well-advanced science. The accomplishments in open water encouraged researchers to apply this method in the study of ship maneuverability in ice. Considering the complexity of the loads imposed by ice, a physical model experiment is currently the best method available

for investigating the maneuverability of ships in ice. Hence this literature review emphasizes the theory and application of a variety of model tests.

2.2.1 Full scale voyage trials

The first documented full-scale turning test was conducted on the CCGS Labrador in sea ice during the winter of 1973, and thus provided the first full-scale data for model and full-scale correlation study.

There are few available reports of full-scale trials to review. Menon's report [5] documented the maneuvering performance data from trials conducted onboard 35 ships, which is the most complete record of full-scale trials. The data were used to identify the principal parameters controlling ship's maneuverability in ice.

The 1985 summer Antarctic Development of USCGC Polar Star provided an opportunity to obtain full scale maneuvering performance data in level ice. The dedicated maneuvering tests were planned with the main objective of quantifying the maneuvering capability of the Polar class vessel in ice considering ship speed and rudder angle as parameters.

Although the single voyage was useful in providing benchmark data for a ship operating in this specific condition, it did not give sufficient information for the evaluation of ship maneuverability in other ice conditions. It is the principle drawback of this approach that the results of full-scale tests are of limited value to a general solution.

Furthermore, it is very difficult to find a place where the ice condition is homogeneous over sufficient length for a ship to accomplish a maneuvering pattern. For instance, in level ice, the distance between successive arcs must be sufficient to avoid interaction through the ice. Another shortcoming of this approach is the prohibitive cost and sophisticated equipments used in the trials.

However, data obtained from full-scale trials, in controlled conditions, are of value for research purposes. The data can be used to identify the main parameters governing maneuverability in ice and to develop functional relationship between the turning radius and the main parameters. The full-scale data can assist in the development and validation of numerical models of vessels maneuvering in ice. The success of theoretical or model experiment methods depends on establishing reliable correlation with the full-scale ship.

2.2.2 Model Experiments

Up to now, model experiments are the most successful technique in assessing ship maneuverability. Although numerical simulation is the eventual goal, physical model tests are an essential step in determining ship maneuvering equations and parameters. There are two distinct types of model tests used in evaluating of ship maneuverability: forced captive model tests and free running model tests. Free-running model tests are more direct and make use of a self-propelled ship scale model fitted with all appendages and remote control, so that actual maneuvers can be performed and maneuverability can be evaluated. This test requires a large maneuvering basin, and the model tests have to be

conducted in different ice thickness with different rudder angles; thus, the test is very expensive. Captive model tests are useful in developing coefficients for use in ship trajectory prediction equations. This experimental method provides the information on hull force and moment derivatives and is more versatile to apply to the prediction of maneuvering performance. Among these, the planar motion mechanism, oscillator, and rotating arm methods were considered.

This section provides an overview of the current state of the art techniques used in the testing of ships in simulated ice cover. Validity of model test results only can be determined in comparison with available full-scale measurements. It is unreasonable to carry out model experiments at all possible combinations of ship and ice conditions. The variables currently thought to have the most effect on ship performance are ice thickness, ice flexural strength, ship speed. The complex nature of the ice imposes minimum run length requirements. The maximum test pattern dimensions are restricted by the tank size, and by the cost of producing each ice sheet. Finally, the experiments must provide information which can be correlated with full-scale ship performance.

The formation of model ice and full-scale/model-scale correlation are also considered as important aspects of the model experiments in ice.

Free-running Model Test

For accurate prediction of ship behavior, the model must represent as closely as possible the ship and its operating condition both geometrically and dynamically. The

self-propelled free-running model is one of the choices. Free-running maneuvering model tests in ice were performed recently, at IMD. [18]

These free-running tests are similar to full scale trials and are generally used to confirm predictions, to evaluate or demonstrate the vessel's maneuverability. For the free running model tests, all aspects of the flow and resulting forces are accurately simulated. One of the main disadvantages of using free running models is the large space required to perform specific maneuvers. This means a large maneuvering basin is required. Often this limits the size of the model to a scale not considered suitable for tests. But a specific test maneuver of a free-running model is difficult to achieve in the ice tank due to the random interaction between ice and the hull of the ship model.

The results from the free-running maneuvering programs conducted provide further empirical data to refine our maneuvering predictions. However, they only demonstrate the effect of various design alternatives but do not provide much insight into the physical cause for the behavior.

Captive Model Test

Captive model tests provide the basic data to determine the cause of problems and are essential for the researchers to improve their knowledge of ship maneuverability in ice.

Most captive model tests are now carried out using a planar motion mechanism (PMM) or a rotating arm. In either case the model is tested over a suitable range of important variables such as drift angle, yaw rate, sway acceleration, yaw acceleration and rudder angle, and the results are analyzed to obtain the hydrodynamic coefficients required in the equations of motion. The derivatives of forces and moments with respect to transverse velocity or yaw rate can also be measured in what is termed an oblique tow test in a conventional long ship tank. Another approach, impulse-response technique has recently been developed by researchers at the Berkeley which is used to evaluate ship maneuverability in open water. The following text gives introductions to the several captive model test methods.

Straight-line Oblique Tow model test

Straight-line oblique tow tests can be carried out in a traditional towing tank. In the straight-line oblique test, the models are towed at constant velocity along a straight line parallel to centerline of the the basin over a range drift angles varying in a range of degrees. This straight-line towing of a model with a drift angle generates a transverse velocity component and thus provides the data to plot the forces and moments against the transverse velocities. So the velocity dependent derivatives Y_v and N_v of a ship at any draft and trim can be determined from measurements on a model of the ship towed in a conventional towing tank at a constant velocity.

[6] and [15] both demonstrated that the standard oblique straight-line tests could be applied to a ship model in simulated ice. This is a convenient and inexpensive means by

which the designer can obtain much useful information about the vessel's turning performance characteristics in ice.

Rotating-Arm Test

To measure the rotatary derivatives Y_r and N_r on a model, a special type of towing tank and apparatus called a rotating-arm facility is employed. In the rotating tests, the models are towed along an arc segment by the rotating arm. This rotation generates a pure yaw angular velocity in the model while its transverse velocity component v is at all times zero (drift angle equal to zero). The rotating tests thus provided the data to plot the longitudinal forces and moments versus the yaw angular velocity. Edwards et. al. [6] presented a modified rotating arm experimental and analysis technique to assess the maneuverability of ship in level ice. The model is rotated at a constant linear speed at various radii and a dynamometer measures the force and the moment acting on the model. One way to vary angular velocity is to vary radii at constant linear speed. The rotating-arm facility can also be used to determine Y_v and N_v as well as Y_r and N_r. This accomplished by towing the model at a variety of values of drift angles for each yaw rate. In order to obtain the values of the derivatives Y_r and N_r, small values of r are necessary. This means that the ratio of the radius of turn R/L should be large. For large models, a large facility is required. Thus a major drawback associated with the rotating-arm test is that it requires a specialized facility in a large basin and cannot be conducted in the long narrow tank conventionally used for resistance and propulsion testing. There

are only a few rotating-arm facilities in the world. Smaller models may use a smaller tank, but models too small will lead to scale effects in the ship prediction.

Impulse test

An impulse-response technique [43] has been developed at Berkeley which is capable of providing the designer with a very complete description of a ship's maneuvering qualities in open water. This impulse-response technique is also simple and inexpensive because it is conducted in the traditional towing tank with a considerable savings in "setup" time and facilities costs. This method will yield the added-mass and damping coefficients as functions of frequency, while rotating-arm and straight-line tests yield no information about added masses and only zero-frequency value of the damping coefficients.

This method might be applicable to the prediction of ship maneuverability in ice, although some researchers have rejected the possibility of applying this technique to maneuverability in ice because of the discontinuous nature of the ice forces on the hull as individual ice cusps break off. Due to the abundant frequency information showed in the data of measured ice forces of the PMM test practiced in IMD ice tank, I would recommend that it be considered before further studies are undertaken. In chapter 5, we examine the power spectra of measured ice forces and ship motions to understand that the added-mass (acceleration) coefficients and frequency dependent damping (velocity) coefficients are necessary in ice-ship interaction problems.

Planar Motion Mechanism (PMM) Test

In order to avoid the large expense of a rotating-arm facility, a device known as a Planar Motion Mechanism (PMM) was developed for use in the conventional long and narrow towing tank to measure the velocity dependent derivatives, rotary derivatives, as well as acceleration derivatives. This research is the first one to attempt a detailed and comprehensive analysis of PMM in ice tests. Basically the PMM consists of two oscillators to control a ship model's trajectory. The PMM, however, is more than a mechanical means of oscillating a model in a prescribed manner. The transducers used to measure the forces on the model, and the special instrumentation required for the proper resolution of the forces, are vital parts of the PMM. The PMM also measure the displacements, rotations of the model in the test. The essence of these tests is that the model is forced to oscillate at the same time as being towed below the carriage of a conventional ice tank giving rise to sinusoidal yawing and swaying motions.

PMM techniques allow a better understanding of the maneuvering problem by allowing us to force a model to follow prescribed path. Test results obtained using PMM can provide the most complete information on the hull force and moment derivatives.

Although PMM test yields satisfactory result in the research, the construction of a PMM system suitable for ice tests and the reduction of the data obtained during the PMM tests in ice were expected to be very complex and costly. In addition, the statistical time-varying nature of icebreaking forces would complicate the analysis of such tests where turning rate is constantly varying. The rates of turn or curvature that can be

applied in PMM tests are limited and the tests do not provide useful information on non-linearities and cross-coupling terms. Thus the oblique tow, rotating arm and PMM tests are complementary to one another.

Full-scale/model-scale correlation

Ship designers rely heavily on the results of tests on scaled models in order to predict whether the ship, as designed, will have satisfactory performance when in service at sea. A valid model is one in which the force coefficient measured on the model will have the same value as the force coefficient that will occur on the ship. The results in the force coefficient on the model test are not necessarily equal to the force coefficient of the ship. The difference in the result of force coefficient obtained from model test and full-scale ship is called "scale error" and is attributed to "scale effects". Model test results suffer from "scale effects", and the development of accurate methods of extrapolation to full size have been hindered by the lack of reliable "measurements" from full-scale trials (often expensive) of resistance, thrust deduction factor, propeller thrust and hydrodynamic maneuvering coefficients. A scale effect is evident in model ice tests. In a resistance in ice test, the $1/48^{th}$-scale models predict higher resistance than the $1/36^{th}$-scale models with divergence increasing from zero to 10 percent as ice thickness Froude number increases from zero to 2.0. [5] At low speeds typical of the limiting conditions of icebreaker performance, scale effect is negligible.

Model Ice

Numerous materials have been used over the years in an effort to find the ideal material for testing, one which maintains the required scale ratios for all dimensional and mechanical properties simultaneously. Most recently, three materials have been used for the simulation of the ice sheet. [2] These are: Saline ice, Carbamide ice and MOD-ice. The first two of these materials are formed by freezing solutions of salt or urea, respectively. The third is a synthetic ice formulation requiring no refrigeration formerly used by ARCTEC (no longer in use). The target properties for the ice to be modeled can vary greatly with loading conditions, structural shapes, and geographical area of interest.

The concept of model testing with saline ice was initially developed in the Soviet Union in 1955 and has been shown to give good results for cases where ice failure occurs in the flexural mode. Saline ice was considered to be the more flexible and cost-effective medium for subsequent tests. But the turning motions of ship cause ice failure in a combination of failure modes in full scale. This dynamic process unfortunately cannot be duplicated with saline model ice, which only can break in a flexural mode.

This section gives an introduction of formulation of the model ice. All ice-testing facilities now use some kind of doped ice as the modeling material. This model ice is grown from a water bath in which a dopant, either salt, carbamide (urea), or ethylene glycol has been added. Growth of the ice sheet at the surface of the towing tank, the dopant is trapped within the pure ice matrix, forming the equivalent of brine pockets. Once the ice sheet has nearly reached the target ice thickness, the ice sheet is usually

tempered until the flexural strength of the model ice is within an acceptable range of its target value. Columnar ice is initiated by the wet seeding method: a fine water mist is sprayed in the cold air (-10 to 20C) where it freezes into small ice crystals that deposit at the water surface. The columnar ice sheet grows from the top down at a rate that depends primarily on the air temperature. Fine-grain ice is grown by continuously spraying, throughout the growth period, fine water droplets in the frigid air that settle as ice crystals on the water surface; the ice sheet therefore grows from the bottom up.

Uncertainty Analysis

Uncertainty analysis is a true and important aspect in the design of experiments. Especially in the study of ship-ice interaction, we observed that the ice forces are transient and irregular. It is possible that the jagged pattern ice forces initiate the instantaneous velocity of the ship. The magnitude of this instant velocity is perhaps in the range of measurement uncertainty of the sensors. *Hermanski et. al.* preformed the uncertainty analysis on the results of the ship experiments at IMD in 2001.[30] Although, in this paper, the model test database did not include the data in ice conditions, we can also have a general idea about what is the level of uncertainty in the measured data. Uncertainties associated with ship motions, wave impact forces and pressures were calculated in this paper. The results of uncertainty analysis reveal that the measured errors possibly cause the unreliable outcome. (Details in Chapter 5) In the summary of total uncertainty of this paper, we can notice the maximum error in ship speed measurement in calm water is 0.30 m/s, 1.42 degree in angle measurement, 4.1 N in force measurement.

2.2.3 Development of numerical models

We know the analytical approach or a perfect mathematical model is the final goal of every researcher. However the ice forces have a different dynamic mode than the hydrodynamic forces. The ice forces, which are governed by ice failure processes, are transient and irregular. The force amplitudes may be much larger than the mean thrust or turning moment which the ship can generate, and the ship is effectively restrained from lateral motion. Because of the lack of a satisfactory analytical expression for ship maneuvering resistance in ice, numerical models of vessel maneuvering performance are considered. Due to the complexity of ship-ice interaction, such numerical tools are obtained by simplifying the dynamic processes. Therefore, several assumptions are normally applied in the development of mathematical models. Development, application and validation of numerical tools for the prediction and simulation of ship maneuvers will provide an efficient and versatile aid to ship design valuation, navigation route selection, and operational training. Such tools exist for ship maneuvers in open water. But satisfactory simulations in ice are unlikely to be accomplished by a simple extension to existing methods, and there is a requirement for new tools to support the simulation of ship operations in ice.

Various attempts have been made in the past several decades to numerically model the maneuvering performance of ships in ice. The earliest one dated back to 1969, when Tronin [50] attempted to express analytically the components of ice forces and resulting

moment acting on an icebreaking hull form performing steady turns in consolidated pack ice.

Canmar Numerical Model

The first predictive mathematical model of the steady turning performance of icebreakers with conventional bow forms in level, unbroken, homogeneous ice fields is the model developed by Canadian Marine Drilling Limited (Canmar) [5]. This approach developed directly from Carter's straight-ahead icebreaking resistance model and used simplified hull geometry to develop a balance equation for the forces acting on an icebreaker whilst turning. The force balance is then used to predict the radius of the turn.

Generally, there are three dynamic modes which constitute the steady turning motion in level unbroken ice, surge, sway and yaw. (Ch. 2.1.1) A simplified vessel model is presented for only the three primary variables of motion (or degrees of freedom) in the horizontal plane. The primary simplifications of this approach are the elimination of higher order terms in the hydrodynamic force formulation. Further, the hull hydrodynamic forces are assumed to be independent of the ice interaction forces.

The co-ordinate system, x-axis referred to as surge axis, y-axis referred to as sway axis, z-axis referred to as yaw axis. The mathematical model of a maneuvering ship can be described by the equations in the surge, sway and yaw modes of motion, with reference to the body axes given below:

$$\begin{aligned} m(\dot{u} - rv - x_G r^2) &= \sum X = X_I + X_H + X_P + X_R \\ m(\dot{v} + ru + x_G \dot{r}) &= \sum Y = Y_I + Y_H + Y_P + Y_R \\ I_Z \dot{r} + mx_G(\dot{v} + ru) &= \sum N = N_I + N_H + N_P + N_R \end{aligned} \qquad (2.1)$$

Where

$\sum X, \sum Y, \sum N$. Summation of X and Y forces and the moments about the Z-axis:

m . Mass of the vessel:

I_z . Mass moment of inertia of the vessel about the z-axis:

u, v, r . Surge, sway and yaw velocities relative to water:

$\dot{u}, \dot{v}, \dot{r}$. Surge, sway and yaw accelerations relative to water:

x_G . Longitudinal position of the center of gravity of the vessel:

X_I, Y_I, N_I . Ice forces and Moments:

X_P, Y_P, N_P . Forces and Moments from propeller:

X_R, Y_R, N_R . Forces and Moments from rudder:

X_H, Y_H, N_H . Hull hydrodynamic forces and moments.

The ice forces and moments are computed using a modified version of Carter's model of level ice resistance. The algorithm that computes the forces and moments resulting from ice failure around the hull uses the hull angles along the waterline to define the hull/ice interface geometry, and the angular and lateral velocities to define the relative velocity on the hull surface interacting with the ice edge. The three modes of ice failure along the interface, bending, buckling and compressing, determine the local forces on the bow and the shoulder. Breaking forces are concentrated around the bow, while the parallel midbody and the stern contribute to frictional and ice clearing forces. The local forces are integrated along the length of the ship to determine the net (global) longitudinal and transverse forces and the yaw moment. In order to facilitate the computation of the ice forces, the distribution of the contact force was idealized.

Ellipsoidal, triangular or trapezoidal force distributions were adopted in the numerical algorithm based on full-scale observations and operational experience. The hydrodynamic forces and moments on the hull, the propeller thrusts and the rudder forces were calculated by using standard semi-empirical formulations in this approach. The governing nonlinear equations of motion of a maneuvering vessel are numerically integrated to give the trajectory of the vessel center of gravity in the time domain.

Correlation of predicted maneuvering performance with full-scale measurements did not yield acceptable results. Since the model was developed from a straight-ahead resistance model, ice forces in the X direction seem to be predicted with a reasonable degree of accuracy. But, ice forces in the Y direction and the resulting moment on the vessel appear to be overestimated in comparison with measured data. The results of the numerical calculation show that the model properly predicts the expected trend of the turning radii in ice. The ship turning radii increases with increasing ice thickness; the ship turns with a smaller turning circle with greater power and at higher rudder angle. The Canmar model, for a particular ship, also predicts greater turning radius for turns to port and tends to underestimate the turning radius for turns to starboard when compared to the corresponding full-scale measurements.

The prediction capability of the model can be greatly improved by taking into account the following aspects: a better estimate of the location of the mid-body side force and center of rotation by calibration with other full-scale data; a better estimate of

rudder lift force taking into account the effects of the propeller race; the direct influence of the propeller on turning; the effect of wind and current;

Menon Time Domain Model

A numerical model of a time domain maneuvering simulation is presented by *Menon et. al.* [5]. This numerical model is based on conventional maneuvering equations with coefficients obtained from model test. It has limitations which prevent it from taking sufficient account to prevailing circumstances, and was unable to provide a general and powerful prediction.

One method that is amenable to the calculation of three horizontal modes of motion which constitute the steady turning motion in level unbroken ice is to utilize the principles of rigid body dynamics and functional representations of external forces. Such a method is used in the development of the mathematical model that allows computation of the turning trajectory as a time-stepping process. The mathematical details of the nonlinear equations of motion are given by *Abkowitz*. [8]

When the full-scale data were applied to take a comparison with the results of time-domain simulation, the result of T-D model of vessel maneuvering in level ice [5] consistently over-predicted the steady turning radius. The model also failed to give steady turning radii, at 40000 and 18000HP, in 1.5 and 1.8 m of ice respectively. It is seen that the result of T-D model consistently under-predicted at lower ice thickness and over predicted at higher ice thickness.

A number of factors contributed to this discrepancy: the hull derivative coefficients which were extracted from model test data of icebreaking hull forms do not account for changes in flexural strength. The T-D model in its present form takes into account equal thrust on the three propellers (Polar Star Class vessels involved in full-scale trials) in the calculation of forward motion and its effect on the rudder.

Lindstrom's model

Traditionally, theoretical ice force calculation, such as ice resistance predictions, has been based on the static solution of a semi-infinite plate on an elastic foundation. Yet, full scale observations, model tests and calculations by the finite element method all show that ice-breaking is a dynamic phenomenon. Lindstrom [33] observed that the static equation cannot take into account the influence of speed on the ice load and on the size of the broken ice floe etc. Consequently, the following dynamic equation for an elastic plate on elastic foundation is used in this approach:

$$\nabla^4 w + \frac{c\partial^2 w}{D\partial t^2} + \frac{\gamma}{D} w = 0 \qquad (2.2)$$

where w is the vertical deflection of the ice sheet and c is the vertical mass per unit area. D is the flexural rigidity of the ice plate and γ describes the relation between the pressure from the underneath water and the deflection of the ice.

Sorensen [41] has solved the equation for a semi-infinite plate with a linearly growing vertical force distribution on the free edge. He gave expressions for the

deflection of the ice sheet as well as for the bending moments in the ice. The results are, however, in integral form but can be solved by means of numerical methods. So when the response of the ice sheet is known, the time history of the force in a contact point between the ship and the ice could be calculated together with bending stresses in the ice sheet. The total stresses in the ice sheet are the sum of the bending stresses and membrane stresses caused by the horizontal component of the contact force. The horizontal stresses are calculated by the static equation. An application of Tsai-Wu failure criterion will give us the impact duration, the maximum ice force. In the simulation calculations, the interesting ice force is the average force acting on the entire ship. The average force in the assumed contact point can be estimated by integrating the force from first contact until the broken ice floe has been turned parallel to the hull. The hydrodynamic forces and rudder forces are calculated using semi-empirical methods developed for ships in open water.

The presented model is tested by numerical simulation of turning maneuvers in level ice with the Finnish patrol vessel Tursas, the USCG Mobile Bay and the Finnish icebreaker Kontio Thus. The results of simulations show relatively good correlation with results from full-scale measurements. The model is believed to be a helpful tool in the design of ice transiting vessels. The main disadvantage of the model is that the bending failure of the ice is the only mode of ice breaking. Because of this, the model cannot be used for ships with vertical sides.

A brief introduction of several numerical models is presented above. The development of every model is similar. First, quite a few approximations are considered to simplify the complex interaction between ship and ice. Second, a selected failure criterion is applied in the calculation. Next, a specified ship hull, especially the shape of bow and side, is chosen as the rigid body under the ice load. Finally, the average ice force and yaw moment is calculated by integrating (numerical method) the force in contact point along the ship hull. From the summary of the general procedures of the numerical method, we can understand why each one of them is only limited to a special hull and ice. The disagreement between the results of numerical methods and full-scale measurements is developed from the approximation of the ship-ice interaction and the ice failure criterion. A universal numerical method is not available. So it is still necessary to develop an efficient approach of physical model testing in ice.

2.2.4 Evaluation of the applications and limitations of current approaches

A comprehensive comparison of present approaches in the research of ship maneuverability in ice is clearly demonstrated in the following table, including the advantages, disadvantages, cost, accuracy, prospect, etc.

Table 2-3 comparison of current approaches used in ship maneuverability in ice

	Full Scale Trial	Model Test	Numerical methods
Advantage	Provide the most accurate information about ship responses in ice and the most appropriate data used in the validation of other math models	Study the influences of different ship parameters and ice conditions on ship maneuverability; data can be used in the validation of various math models; evaluation of ship maneuverability in the phase of design is available.	Give an accurate prediction of ship maneuverability; programmable, it is convenient to improve a ship's maneuverability in the phase of design and to train mariners by using simulation program.
Shortcoming	Limited to a specific ship type	Scale effect exists	Limited to a specific ship hull and a single failure mode
Cost	Prohibitive	Expensive for set up; affordable in testing	Cost effective
Accuracy	Perfect (actual ship responses)	Approximation	Approximation
Difficulty	It is difficult to find a place with a homogeneous ice condition which is large enough to make maneuvers; adjustment and compatibility of the sophisticated onboard equipment ; results influenced by other parameters, e.g. condition of propellers.	Uncertainty of test system; insufficient test database for the development of the model	A series of simplifications are applied because of the complexity of the ship-ice interaction; limited to one type of failure mode and specific ship hull; inadequate data for the validation of the model.
Prospect	Indispensable (Validation)	Promising (most popular)	Promising

Chapter 3 Derivation of the Basic Equations of Motion

3.1 Linear Newtonian Equations

The basic dynamics of maneuvering can be studied using Newton's equations of motion in the horizontal plane. It is customary to consider the dynamic equations with reference to two different right-hand coordinate systems: one set of axes fixed relative to the earth, and the other set fixed relative to the ship.

Figure 3-1 shows the orientation of the coordinate systems. $O_0X_0Y_0$ is fixed in space and OXY is fixed in the ship. O is located at the center of gravity of the ship, with the x-axis pointing forward. The y-axis is pointing to the starboard side of the ship. The two origins coincide when the ship is in her initial position.

Figure 3-1 Two Coordinate Axes

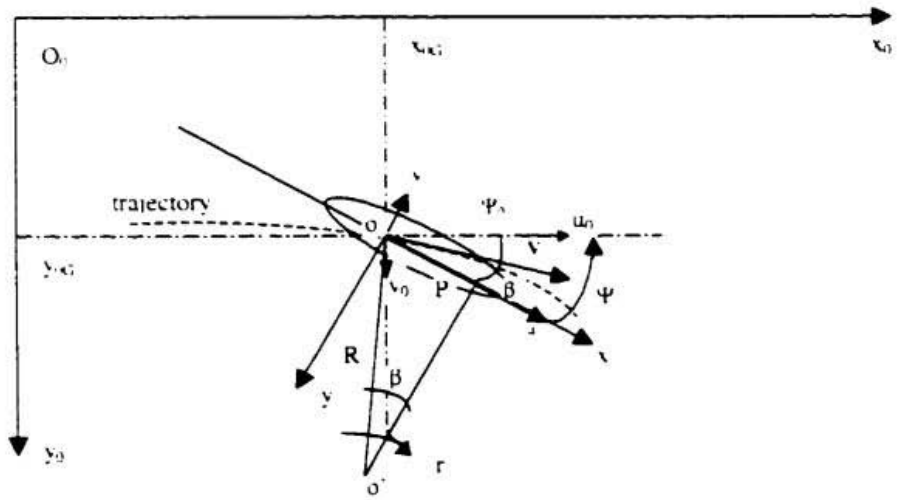

The yaw angle, Ψ, is the angle between the ship's longitudinal axis x and the fixed axis (x_0), drift angle, β, is the difference between the x axis and the tangent to the actual course of the ship (direction of the velocity vector at the center of gravity). The motion of the ship is completely defined by the coordinates x_{0G}, y_{0G} and the yaw angle ψ.

With reference to the fixed coordinate system, according to Newton's second law of motion, the equations of motion of the ship can be written as:

$$X_0 = \Delta\ddot{x}_{0G} \quad \text{(Surge)}$$

$$Y_0 = \Delta\ddot{y}_{0G} \quad \text{(Sway)} \qquad (3.1)$$

$$N = I_z\ddot{\psi} \quad \text{(Yaw)}$$

Where,

X_0, Y_0 and N, are the total forces and moments acting at the center of gravity of ship, in the x_0, y_0 direction and about an axis parallel to the z_0-axis; earth coordinate system.

Δ, is the displacement of ship;

I_z is the mass moment inertia of ship about the z-axis;

ψ, is the yaw angle.

Coordinate transformation

The motion of a ship is more conveniently expressed with respect to the axes x and y fixed in the ship. The moving axes x, y form a right-hand orthogonal system whose origin is fixed at the center of gravity. The x-axis is along the longitudinal center line of the ship. The instantaneous linear velocity of the center of gravity, always tangent to the

real course of the ship. is indicated by the vector **V** in Fig 3-1. As noted earlier. the orientation of the x-axis is the heading angle of the ship. named yaw angle ψ: and the so-called drift angle β is measured from direction of motion **V** to the moving axis x.

Now we can rewrite the Equations (3.1) in the moving coordinate (ship axis) using the following coordinate transformation:

$$\begin{aligned} X &= X_0 \cos\psi + Y_0 \sin\psi \\ Y &= Y_0 \cos\psi - X_0 \sin\psi \end{aligned} \qquad (3.2)$$

Similarly. velocity transformations are given as:

$$\begin{aligned} \dot{x}_{0G} &= u\cos\psi - v\sin\psi \\ \dot{y}_{0G} &= u\sin\psi + v\cos\psi \end{aligned} \qquad (3.3)$$

Where u and v are the components of **V** along ship axes x and y and a dot above the variable indicates the first derivative with respect to time.

Next. differentiate equations (3.3) with respect to time to obtain the acceleration transformation:

$$\begin{aligned} \ddot{x}_{0G} &= \dot{u}\cos\psi - \dot{v}\sin\psi - u\dot{\psi}\sin\psi - v\dot{\psi}\cos\psi \\ \ddot{y}_{0G} &= \dot{u}\sin\psi + \dot{v}\cos\psi + u\dot{\psi}\cos\psi - v\dot{\psi}\sin\psi \end{aligned} \qquad (3.4)$$

Substituting equations (3.2) and (3.4). Equations (3.1) arrives at (ship axis):

$$\begin{aligned} X &= \Delta(\dot{u} - v\dot{\psi}) \quad \text{(Surge)} \\ Y &= \Delta(\dot{v} + u\dot{\psi}) \quad \text{(Sway)} \\ N &= I_z\ddot{\psi} \qquad \text{(Yaw)} \end{aligned} \qquad (3.5)$$

Linear Equations of Motion

In the most general case, the force components X, Y and the moment component N are functions of the velocities and the accelerations of the ship, i.e. the motion of the ship. For the present study, X, Y, and N are assumed to be expressed functionally as:

$$\begin{aligned} X &= F_x(u, v, \dot{u}, \dot{v}, \dot{\psi}, \ddot{\psi}) \\ Y &= F_y(u, v, \dot{u}, \dot{v}, \dot{\psi}, \ddot{\psi}) \\ N &= F_\psi(u, v, \dot{u}, \dot{v}, \dot{\psi}, \ddot{\psi}) \end{aligned} \qquad (3.6)$$

The functional expressions shown above must be simplified. Taylor expansion of a function of several variables is one of the choices. Consider a small disturbance which deflects the ship through a small angle ψ relative to its initial path. The velocity of the ship is still substantially along the direction of the initial path. The ship hull, at an angle of attack ψ, develops a lift force which is in the direction of the perpendicular to the ship's heading. This force can be replaced by a parallel force acting at the center of gravity of the ship and a turning moment about the vertical axis passing through the c.g. of the ship. The direction of the moment is such that it leads to decrease the angle ψ. Considering only small deviations from a straight path so that second order terms can be neglected, linear equations can be used to describe ship maneuverability. The linearized form of Taylor expansion for the force Y, can be written as:

$$Y = F_y(u_1, v_1, \dot{u}_1, \dot{v}_1, \dot{\psi}_1, \ddot{\psi}_1) + (u - u_1)Y_u + (v - v_1)Y_v + \cdots\cdots + (\ddot{\psi} - \ddot{\psi}_1)Y_{\dot{\psi}} \qquad (3.7)$$

where the subscript 1 means the values of the variable at the initial equilibrium condition and $Y_u = \frac{\partial Y}{\partial u}$ Using Taylor Expansions, initial equilibrium conditions and symmetry properties of ship, linearized Taylor expansion equations can be reduced to:

$$X = X_{\dot{u}}\dot{u} - X_u(u - u_1)$$

$$Y = Y_v v + Y_{\dot{v}}\dot{v} + Y_r r + Y_{\dot{r}}\dot{r} \qquad (3.8)$$

$$N = N_v v + N_{\dot{v}}\dot{v} + N_r r + N_{\dot{r}}\dot{r}$$

Dynamic Equations

Finally, substituting above linear expansion equations into Newton Equations of Motion, for small perturbation (control force is zero), one get

$$-X_u(u - u_1) + (\Delta - X_{\dot{u}})\dot{u} = 0 \qquad \text{(Surge)}$$

$$-Y_v v - (\Delta - Y_{\dot{v}})\dot{v} - (Y_r - \Delta u_1)r - Y_{\dot{r}}\dot{r} = 0 \qquad \text{(Sway)} \qquad (3.9)$$

$$-N_v v - N_{\dot{v}}\dot{v} - N_r r + (I_z - N_{\dot{r}})\dot{r} = 0 \qquad \text{(Yaw)}$$

where

$X_{\dot{u}}, X_u, Y_{\dot{v}}, Y_v, Y_{\dot{r}}, Y_r, N_{\dot{v}}, N_v, N_{\dot{r}}, N_r$, refers to derivative coefficients:

and subscripts u v r denote differentiation with respect to surge velocity (longitudinal component of velocity), sway velocity (lateral component of velocity) and yaw rate (rate of changing heading) respectively, i.e. $Y_v = \partial Y / \partial v$, etc.

X, Y, N Surge force, Sway force and Yaw moment, respectively;

u, v, r Instant Surge velocity, Sway velocity and Yaw rate, respectively; $r = \partial\psi / \partial t$

u_1 Velocity at the time of initial equilibrium condition;

Δ displacement of ship:

I_z Mass moment inertia of ship:

These equations are based on a Taylor series expansion of the Newtonian Dynamic Equations with the assumption that all non-linear terms in the series are either zero or small enough to be neglected. All derivative coefficients can be obtained from model tests or estimated from mathematical modeling of the ship hull.

It is important to notice that equations (3-9) are homogeneous equations. These equations express the equilibrium condition without control forces or moments acting on the hull. When a ship makes a maneuver in water, the control forces on the right sides of the equations are generated by rudder deflection and any other control devices. In a PMM model test, it is created by the carriage of the PMM.

3.2 Derivation of Equations for PMM Model Tests.

To consider the motion of a ship model during a PMM maneuver, we used to modify the right hand side of equation (3-9) to reflect the effect of the PMM on the model.

Firstly, we should return to figure (3-1) to review the relationship between the fixed coordinate system and moving coordinate system. Using figure (3-1), we can derive the following relationships:

$$\psi = \psi_0 - \beta \tag{3.10}$$

Velocity Relationship:

$$u = V'\cos\beta$$

$$v = V'\sin\beta$$

$$V' = \sqrt{u_0^2 + v_0^2}$$

$$\psi_0 = \tan^{-1}\frac{v_0}{u_0} \tag{3.11}$$

So sway velocity of ship v is

$$v = \sqrt{u_0^2 + v_0^2}\,\sin\left[\tan^{-1}\left(\frac{v_0}{u_0}\right) - \psi\right] \tag{3.12}$$

surge velocity of ship u is

$$u = \sqrt{u_0^2 + v_0^2}\,\cos\left[\tan^{-1}\left(\frac{v_0}{u_0}\right) - \psi\right] \tag{3.13}$$

$$r = \frac{d\psi}{dt} = \frac{d\psi_0}{dt} - \frac{d\beta}{dt}$$

Figure 3-2 Ship turning motion diagram

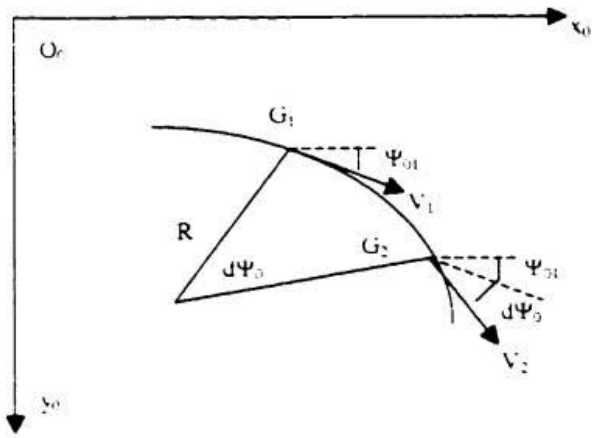

From above graph figure (3-2), we get

$$G_1G_2 = Vdt$$

$$G_1G_2 = Rd\psi_0$$

Thus, from $Vdt = Rd\psi_0$ obtain

$$\frac{d\psi_0}{dt} = \frac{V}{R}$$

$$r = \frac{d\psi}{dt} = \frac{V}{R} - \frac{d\beta}{dt} = \frac{V}{R} \qquad (3.14)$$

so turning radius / length ratios is

$$\frac{R}{L} = \frac{V}{rL} \qquad (3.15)$$

In the graph, where

x_{0G}, y_{0G}, Center of gravity of the ship:

V Instant Velocity at the center of gravity of the ship:

ψ_0 Voyage Angle. Angle measured from x_0 axis to the direction of V. from x_0 to V. Positive direction is Clockwise:

ψ Yaw Angle. Angle measured from x_0 axis (fixed) to x axis (moving). from x_0 axis to x axis. Positive direction is Clockwise:

β Drift Angle. Angle measured from x axis (moving) to the direction of V. from x to V. Positive direction is Clockwise:

r Yaw Rate: instant angular velocity of ship's rotation:

R Instant Turning Radius of the ship

In the PMM test, we carry out two kinds of tests.

(The unit of x-axis in the following figures is sample number, with sample rate 50Hz. Thus, 50 data points equal to 1 second.)

3.2.1 Sinusoidal Tests

A pure yaw test should satisfy:

$$v = 0, \dot{v} = 0, \beta = 0$$

Figure 3-3 Sinusoidal test data velocity plots (rclassmano_40, level ice, 50mm)

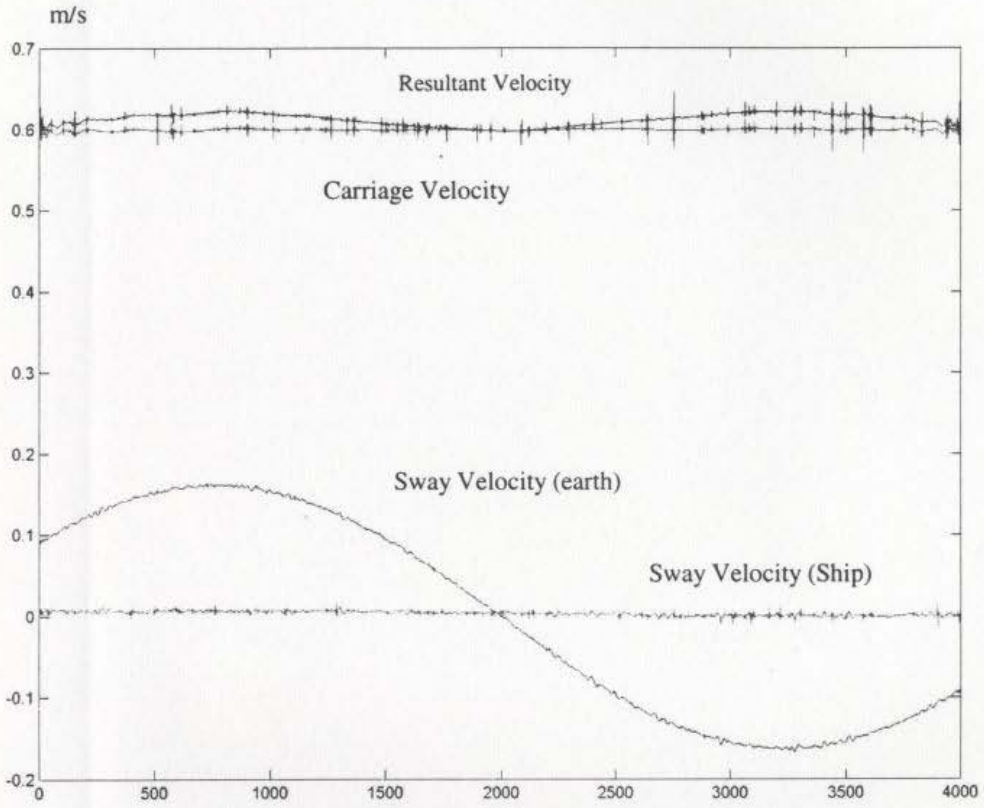

Figure 3-3 shows the results from the raw sinusoidal test data according to equation (3-12). From above graph, we can observe that the carriage velocity (u_0) and sway velocity (in ship coordinate system) of the ship (v) are almost constant in a

comparison with resultant velocity. Sway velocity (v) is nearly zero. The resultant velocity and the sway velocity with respect to the fixed axes are denoted V and v_0, respectively. These results also can be verified using the following plot of drift angle from the same test data.

Figure 3-4 Sinusoidal test data drift angle plot (rclassmano_40, level ice, 50mm)

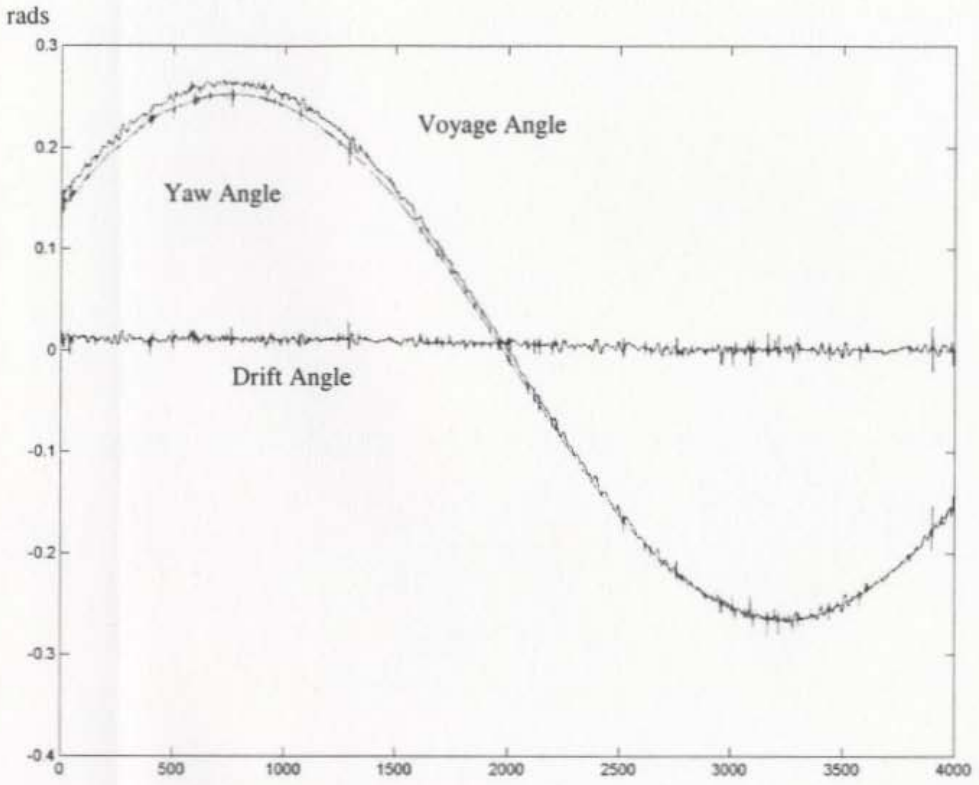

From figure 3-4, we can find that the drift angle (voyage angle minus yaw angle) is close to zero. So the sway velocity (resultant velocity times cosine of drift angle) is a very small value.

Figure 3-3 and figure 3-4 were obtained from the same test file (rclassmano_40, level ice, 50mm). The results can validate the test program. The prescribed maneuvers were achieved exactly under the control of PMM.

Since $v = 0, \dot{v} = 0$, the dynamic equations (3.9) in a sinusoidal test can be simplified to:

$$\begin{aligned} -(Y_r - \Delta u_1)r - Y_{\dot{r}}\dot{r} &= Y_{pmm} \\ -N_r r + (I_z - N_{\dot{r}})\dot{r} &= N_{pmm} + N_{prop} \end{aligned} \tag{3.16}$$

3.2.2 Constant Radius Tests

$\frac{d\beta}{dt} = 0$

$r = \frac{d\psi}{dt} = \frac{V}{R}$ and V, R are constants, so

$v = cons., \therefore \dot{v} = 0$

$r = cons., \therefore \dot{r} = 0$

Figure 3-5 Constant Radius test data velocity plots (rclassmao_28, level ice, 50mm)

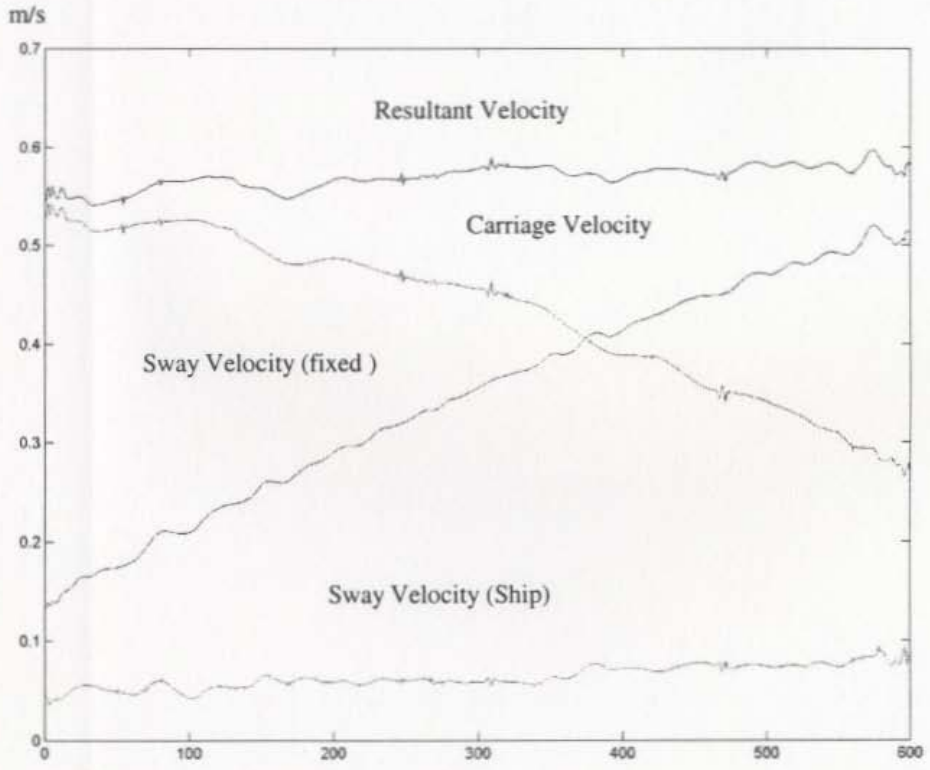

From above Figure 3-5, we can find that the resultant velocity (V) and sway velocity (v) are approximately constant.

The variances in the sway velocity measurement reflect the nature of ship passage in ice.

Figure 3-6 Constant Radius test data drift angle plot (rclassmano_28, level ice, 50mm)

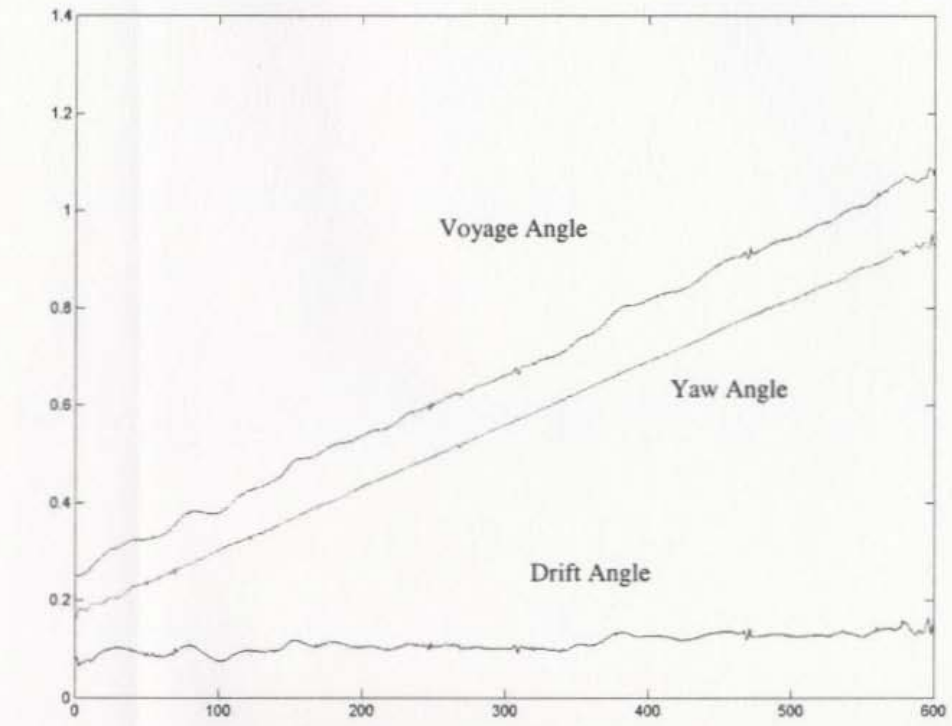

From above Figure 3-6, we notice that the drift angle (voyage angle minus yaw angle) is nearly constant.

So the sway velocity (resultant velocity times cosine of drift angle) is a constant.

Since $v = cons.., \dot{v} = 0, r = cons.., \dot{r} = 0$, the dynamic equations simplify to:

$$\begin{aligned} -Y_{\cdot}v - (Y_{\cdot} - \Delta u_1)r &= Y_{prop} \\ -N_{\cdot}v - N_{\cdot}r &= N_{prop} - N_{prop} \end{aligned} \tag{3.17}$$

Chapter 4 Experimental Program

The present work is based on the analysis of data that was obtained during an experimental program to study the maneuverability of ship models in ice. The program was carried out at the Institute for Marine Dynamics using their PMM and an R-class model. This program was preceded by two series of tests of the same model. The previous tests were recorded in [18] and [37].

4.1 The Planar Motion Mechanism (PMM)

The advantages of using the PMM were reviewed in Chapter 2. In what follows, we will provide a brief description for the IMD facility.

This apparatus is a new multi-purpose planar motion mechanism designed by Marineering Limited, which has been specially manufactured for use at the Institute for Marine Dynamics in St. John's. The PMM consists of two primary components: a sway sub-carriage which mounts beneath the IMD main towing carriages and a yawing assembly that bolts to the sway sub-carriage. The combinations of sway and yaw carriages enable the PMM to conduct a variety of maneuvers. The sway sub-carriage, the largest component of the PMM, was first developed to tow structures through ice with changing drift angles. The sway carriage is a 2m x 2m open steel frame suspended on linear bearings between the two 10m long rails allowing the sway carriage a net travel of

8m. It is driven by a stepper server motor coupled through a gear box to a chain drive. Therefore the sway carriage is able to travel ±4 m at a maximum velocity of 0.7m/s.

The PMM digital control system allows great flexibility in managing the sway and yaw motors. Actually, any complex planar motion can be programmed using this system. The window-based control program has two components: a motion generation component and another for motion implementation. The motion generator component generates ASCII files containing control instructions for the motors. The motion generator module has six predefined motion types: Static, Sway, Yaw, Drift, Surge, Circle. During the generation phase the software estimates loads and checks rates to make sure the maneuver can be safely performed. The execution module loads these files and transfers them to the computer controlling the motors. Once the file is transferred, the program could be executed and the computer begins to take the control of the machine.

Table 4-1 Particulars of IMD's PMM

Maximum Sway Amplitude (m)	±4.0
Maximum Yaw Amplitude (degree)	±175
Maximum Sway Velocity (m/s)	±0.70
Maximum Yaw Amplitude (degree/s)	±60.0
Maximum Sway Force (N)	±2200
Maximum Yaw Moment (N-m)	±3000

4.2 Maneuvering Test Program

4.2.1 Data Acquisition and Instrumentation

It is necessary to check and adjust the data acquisition instrumentation used in the tests as an initial preparation for the test. This task includes recording relevant information e.g. sample rates, units, ...etc. Table 4-2 shows a typical information sheet.

Table 4-2 Data Acquisition and Instrumentation Parameters

Name	Device	Units	Range	Tolerance	Sign convention	Sample rates	Critical level
Fwd Sinkage	LVDT	M	0-0.03	± 0.005	down	20	2
Aft Sinkage	LVDT	M	0-0.03	± 0.005	down	20	2
Torque Port	R33	N-m	0-6	± 0.05	outboard	20	2
Torque Stbd	R33	N-m	0-6	± 0.05	outboard	20	2
Thrust Port	R33	N	0-300	± 10	ahead	20	1
Thrust Stbd	R33	N	0-300	± 10	ahead	20	1
Model Speed	Carriage	m/s	0-2	± 0.1	ahead	20	1
Carriage Position	Carriage	M	0-70	± 0. 5	ahead	20	1
Port Shaft Speed	Controller	rps	15	± 1	outboard	20	1
Stbd Shaft Speed	Controller	rps	15	± 1	outboard	20	1
PMM Sway Position	LVDT	M	± 4	± 0.5	stbd	20	1
PMM Sway Velocity	LVDT	m/s	± 0.5	± 0.05	stbd	20	1
PMM Yaw	RVDT	Deg	-0.6-1.2	± 0.05	stbd	20	1
PMM Surge	load cell	N	1000	± 10	forward	20	1
PMM Fwd Sway	load cell	N	2000	± 10	stbd	20	1
PMM Aft Sway	load cell	N	2000	± 10	stbd	20	1

Critical level

1= stop test and repair immediately

2= stop at earliest convenience and repair

4.2.2 Ship Conditions

The ship model 491A used in this test is a 1:20 scale model of the Canadian Coast Guard R-Class Icebreaker. The model was fitted with twin propellers and a single centerline rudder. The model was ballasted to the correct condition. The model's initial condition is: Forward Perpendicular Draft. 0.338m: After Perpendicular Draft. 0.362m: Draft in Midship. 0.35m: Trim. 0.024m: Displacement. 965Kg. The ship parameters changed in the test were model speed. propeller speeds. and rudder angle. Model speed was chosen to be 0.6 m/s for tests both in open water and in ice. Propeller speeds were steady in the ice tests. The rudder angle was constant at 0° all the time in the ice tests.

4.2.3 Ice Conditions

Tests were carried out in a variety of ice conditions. Ice conditions were Level ice. Pack ice and Rubble ice. Two nominal ice thicknesses. 30mm and 50mm. were used in the tests. corresponding to 0.6 m and 1.0m of the full scale level ice.

The EG/AD/S C.D. model ice [42] was prepared for these tests in the ice tank at IMD. EG/AD/S C.D. refers to the model ice composed of 0.39% **E**thylene **G**lycol (Antifreeze). 0.0036% **A**liphatic **D**etergent (Dishliquid) and 0.04% **S**ugar. C.D. refers to

controlled density in which the density of the ice is controlled using an air bubbler system. This technique has been developed to provide the model ice with kinematic and mechanical properties required to model the ship-ice interaction correctly. The ice is grown at finely controlled temperatures in a mild EG/AD/S solution, resulting in uniform thickness, with standard deviation normally less than 3%. Fine bubbles are selectively incorporated into the ice to produce the required ice density and plate stiffness. The ice is tempered for a period of time before the test, until the required flexural strength is achieved. Shear strength and compressive failure stresses are established as functions of the flexural strength, similar to the full-scale relationships. Ice flexural strength was measured by sets of cantilever beam tests at different times and locations in the tank. For each ice sheet, flexural strength-ice curves were developed, and strength was interpolated to test time and location. Ice density, shear strength, and compressive failure stress were determined from flexural strength relations, calibrated by measurements in each ice sheet. The flexural strength of model ice in this test was 20kPa.

Level ice refers to the original and unbroken ice sheet.

Pack ice refers to level ice that has been broken into pieces. In the tests, pack ice was created by breaking the ice with the paddles on the ice tank service carriage. First, the ice was broken into a series of approximately parallel fractures across the tank. Then it was broken by hand so that floe shapes were approximately square. Pack ice concentration was determined from digitized overhead photographs of each ice condition, before the start of experiments. For pack ice, the thickness was measured directly.

Rubble ice refers to pack ice that has been compressed along the length of the tank. After completion of the pack ice experiments, the ice was made into a wide rubble field. The pack ice was compressed longitudinally using the paddles on the service carriage. This resulted in rafting of the ice, in a process not observed in nature, where ice floes naturally moved over one another under the action of wind and current. The nominal ice thickness was based on the volume of ice, but this did not take into account the porosity which resulted from uneven stacking of the ice floes. Ice concentration is given in tenths. For example 20/10 rubble is the pack ice that has been compressed half the length of the tank and is nominally twice as thick as the level ice sheet. Actual ice thickness can be measured manually or an underwater acoustic array of ultra-sonic probes, mounted on an underwater carriage that moved at the same speed as the model.

4.2.4 Experimental Maneuvers

There are two types of maneuvering tests conducted in the plan: constant radius and sinusoidal maneuver. They were carried out in four ice conditions and in open water. The constant radius arcs are performed for three radii, corresponding radius to ship length ratios: 2, 10, and 20. The middle value was chosen close to the turning radii from the free running tests in order to provide a good comparison with the free running tests. The pure yaw test was performed as a single sinusoidal along the length of the tank. The sway amplitude of the sinusoidal was chosen to be 2.5m.

A 4-day test plan was conducted. Table 4-3 shows a summary of the experimental program.

Table 4-3 table of tests

Filename	Test type	thickness	Ice condition	Friction Coe.	Radius m
rclassmano_001	sinusoidal	30 mm	level	0.06	
rclassmano_002	sinusoidal	30 mm	pack	0.06	
rclassmano_003	sinusoidal	30 mm	20/10 rubble	0.06	
rclassmano_004	sinusoidal	30 mm	30/10 rubble	0.06	
rclassmano_017	Const. Radius	30 mm	level	0.06	9.3
rclassmano_018	Const. Radius	30 mm	level	0.06	93
rclassmano_019	Const. Radius	30 mm	level	0.06	20
rclassmano_021	Const. Radius	30 mm	pack	0.06	9.3
rclassmano_022	Const. Radius	30 mm	pack	0.06	20
rclassmano_023	Const. Radius	30 mm	pack	0.06	93
rclassmano_024	Const. Radius	30 mm	20/10 rubble	0.06	9.3
rclassmano_025	Const. Radius	30 mm	20/10 rubble	0.06	20
rclassmano_026	Const. Radius	30 mm	30/10 rubble	0.06	20
rclassmano_028	Const. Radius	50 mm	level	0.06	9.3
rclassmano_029	Const. Radius	50 mm	level	0.06	20
rclassmano_030	Const. Radius	50 mm	level	0.06	93
rclassmano_032	Const. Radius	50 mm	pack	0.06	9.3
rclassmano_033	Const. Radius	50 mm	pack	0.06	20
rclassmano_034	Const. Radius	50 mm	pack	0.06	93
rclassmano_035	Const. Radius	50 mm	20/10 rubble	0.06	9.3
rclassmano_036	Const. Radius	50 mm	20/10 rubble	0.06	20
rclassmano_037	Const. Radius	50 mm	30/10 rubble	0.06	20
rclassmano_040	sinusoidal	50 mm	level	0.06	
rclassmano_041	sinusoidal	50 mm	pack	0.06	
rclassmano_042	sinusoidal	50 mm	20/10 rubble	0.06	
rclassmano_043	sinusoidal	50 mm	30/10 rubble	0.06	
rclassmano_045	Const. Radius	50 mm	level	0.01	9.3
rclassmano_046	Const. Radius	50 mm	level	0.01	20
rclassmano_047	Const. Radius	50 mm	level	0.01	93
rclassmano_049	Const. Radius	50 mm	pack	0.01	9.3
rclassmano_050	Const. Radius	50 mm	pack	0.01	20
rclassmano_051	Const. Radius	50 mm	pack	0.01	93
rclassmano_052	Const. Radius	50 mm	20/10 rubble	0.01	9.3
rclassmano_053	Const. Radius	50 mm	20/10 rubble	0.01	20
rclassmano_054	Const. Radius	50 mm	30/10 rubble	0.01	20
rclassmano_056	Const. Radius	30 mm	level	0.01	9.3
rclassmano_057	Const. Radius	30 mm	level	0.01	20
rclassmano_058	Const. Radius	30 mm	level	0.01	93
rclassmano_060	Const. Radius	30 mm	pack	0.01	9.3
rclassmano_061	Const. Radius	30 mm	pack	0.01	20
rclassmano_062	Const. Radius	30 mm	pack	0.01	93
rclassmano_063	Const. Radius	30 mm	20/10 rubble	0.01	9.3
rclassmano_064	Const. Radius	30 mm	20/10 rubble	0.01	20
rclassmano_066	Const. Radius	30 mm	30/10 rubble	0.01	20
rclassmano_067	Sinusoidalal	50 mm	level	0.01	
rclassmano_069	Sinusoidalal	50 mm	pack	0.01	

Two sets of tests were carried out in this research. One group of tests is from rclassmano_001 to rclassmano_043, and another group from rclassmano_045 to rclassmano_069. The only difference between the two groups of tests is that different hull-ice friction coefficients of the model were applied. In the first group of tests, the ship hull was tested with a hull-ice friction coefficient 0.06. This value corresponds to the average condition of a new ship based on IMD' data for icebreakers. The model also tested at a much lower friction coefficient (0.01) to investigate the influence of hull-ice coefficient on the ship maneuverability in ice conditions.

The purpose of the tests is to obtain further information on ship-ice interactions in a variety of ice conditions. The incentive to perform PMM maneuvering tests comes from two series of maneuvering tests previously done [18] [37]. The test data will expand the database for ship maneuvering in ice [37] and compare PMM test results with those free-running test results [18]. The goal is to produce reliable data from which accurate predictions can be made about ship maneuvering in various ice conditions.

Chapter 5 Data Analysis

In previous chapters, we discussed recent developments in the study of ship maneuverability in ice. An evaluation of current methodologies in this area was presented in chapter 2. Basic dynamic equations in the test were derived and validated by raw test data in chapter 3. The experimental program on which this thesis is based is given in chapter 4. In this chapter, we concentrate on analysis techniques which could extract valuable information from test results to achieve the objectives of this work.

5.1 Data Manipulation

The raw test data were prepared for further analysis. The data were initially analyzed using GEDAP ("General Experimental Data Acquisition, Control and Analysis Package", developed and used by NRC) command procedures. The first step, was to convert all .DAC files to .MAT files using a VMS program named "convert.com" and transfer the test data from VMS system to a Window System. The next step was to examine the data structure of the files, extract the useful columns of data from raw data, cut the valuable segment of data to eliminate the unusual effects of the towing carriage start and stop, execute a filter process by using a designed Wavelet filter, and calculate the required forces and ship motions. A MATLAB program implements the whole process including extract, cut, filter and arithmetic calculations. The details of the data preparation are given in Appendix 1.

5.2 Wavelet Analysis

In chapter 2, we discussed the irregular nature of the ice forces and the scale of the force variations. After an examination of the raw test data, we found significant noise contaminating the original signals. It is necessary to remove the noise from the original signal in order to obtain accurate results.

Conventional analysis techniques apply a low pass Fourier filter to the time series to remove the high frequency noise, or a Fourier transform to separate the phase at the test pattern frequency. Typical filter design methods include Butterworth, Chebyshev, may also be used. It is convenient to design these filters in MATLAB. But, there are problems with this approach. This filter will arbitrarily get rid of the components in the original signal whose frequency is higher than the value we initially set in the filter design. When the data is low pass filtered, the retained information is the sum of the low frequency Fourier coefficients, each of which is an integral over a large portion of the data. Localized information is lost. When taking a look at a Fourier transform of a signal, it is impossible to identify when a special event took place in time. Observing the plots of the raw test data, the signals contain numerous transitory characteristics, abrupt changes, localized trends, beginnings and ends of events. These characteristics are often the most important part of the signal in the research of ice forces. Fourier analysis is not a good way to detect these phenomena. So the usual Fourier methods used to determine hydrodynamic coefficients from open water PMM tests are not appropriate for the ice maneuvering analysis.

A powerful technique which can remove the high frequency noise and still retain the localized information involves the use of wavelet filters. Wavelet analysis allows the use of long time intervals where we need more precise lower frequency information, and shorter regions where we need higher frequency information. Wavelet coefficients represent both scale and frequency information. At small scale, there is high frequency information, and at large scale, the low frequency is retained.

A wavelet is a waveform of effectively limited duration that has an average value of zero [34]. Wavelets tend to be irregular and asymmetric in comparison with sinusoids in Fourier analysis. Fourier analysis consists of breaking up a signal into sine waves of various frequencies. Similarly, wavelet analysis is the breaking up of a signal into shifted and scaled versions of the original wavelet.

In this work, two wavelet techniques were applied. Continuous Wavelet Transform (CWT) and Discrete Wavelet Transform (DWT). CWT was used to qualitatively analyze the frequency information of measured data at different phases in a test run. The DWT algorithm is the basis of the wavelet filter. We used a wavelet filter to implement the de-noise task.

5.2.1 Continuous Wavelet Transform Application

The continuous wavelet transform (CWT) is defined as the sum over all time of the signal multiplied by scaled, shifted versions of the wavelet function ψ :

$$C(scale, position) = \int_{-\infty}^{\infty} f(t)\psi(scale, position, t)dt \qquad (5.1)$$

The results of the CWT are many wavelet coefficients C, which are functions of the scale and the position. Multiplying each coefficient by the appropriately scaled and shifted wavelet yields the constituent wavelets of the original signal. The factor C represents how closely correlated the wavelet is with a segment of the signal. The higher C is, the more the similarity. The process produces the coefficients of different scales at different sections of the signal. A plot of CWT coefficients is usually used to inspect the signal's frequency characteristics. The x-axis of the plot represents time, and the y-axis represents the scale and the color at each x-y point represents the magnitude of the wavelet coefficient C. The continuous wavelet transform coefficient plots precisely display the time-scale view of the signal. It is a different view of signal data than the time-frequency Fourier view, but it is not unrelated. The scales on the coefficients plots (shown as y-axis labels) run from minimum to maximum values. The higher scales correspond to the most "stretched" wavelets. The more the stretched the wavelet, the longer the portion of the signal with which it is being compared, and thus the coarser the signal features being measured by the wavelet coefficients. Thus, the low scale in the CWT plot represents rapid changing details. CWT operates at every scale, from that of the original signal up to some maximum scale determined by the need for detailed analysis. The CWT is also continuous in terms of shifting: during computation, the wavelet kernel is shifted smoothly over the full time domain of the analyzed signal. We present the CWT coefficient plots of two raw test data channels as examples to explain how to use this technique.

The first one is the raw data of a sinusoidal test, file name: rclassmano_001, ice condition: level, 30mm. We performed CWT on the measured sway force and yaw moment:

Figure 5-1 CWT Coefficients Plots of Sway Force (rclassmano_001, level, 30mm)

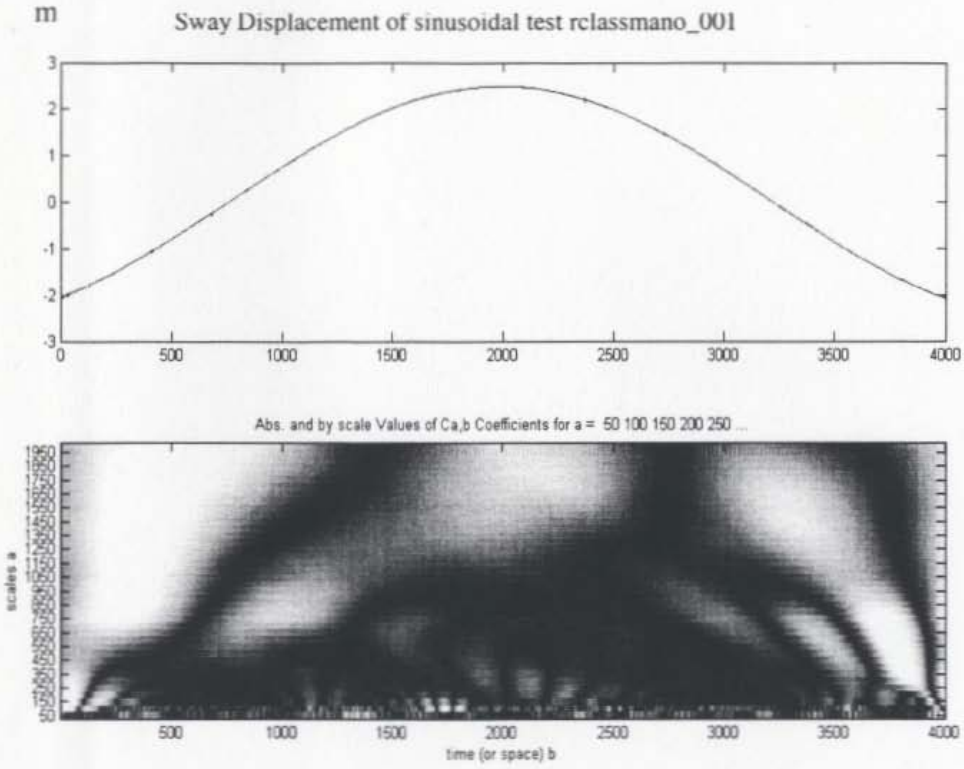

The upper plot in the figure recorded the sway displacement of the model. The lower plot presents the calculated CWT coefficients for the measured sway force data. Brighter areas represent larger coefficients. Larger scale represents lower frequency information. Thus we can provide an initial evaluation of the sway force the ship encountered when it executed a sinusoidal maneuver. It is noted that different forces (frequency) were generated in different locations in a sinusoid. In this run, we can observe that a low frequency force dominated around time 500, 2000 and 3000(highlight area in large scale). In other parts of the sinusoid, higher frequency force is the primary component due to the

ship-ice interaction. It is not easy to find a clear frequency component in the test data. The data of the sway force consist of different frequency components without a clear trend during the maneuvers.

The following figure is CWT plot of yaw moment in the same test.

Figure 5-2 CWT Coefficients Plots of Yaw Moment (rclassmano_001, level, 30mm)

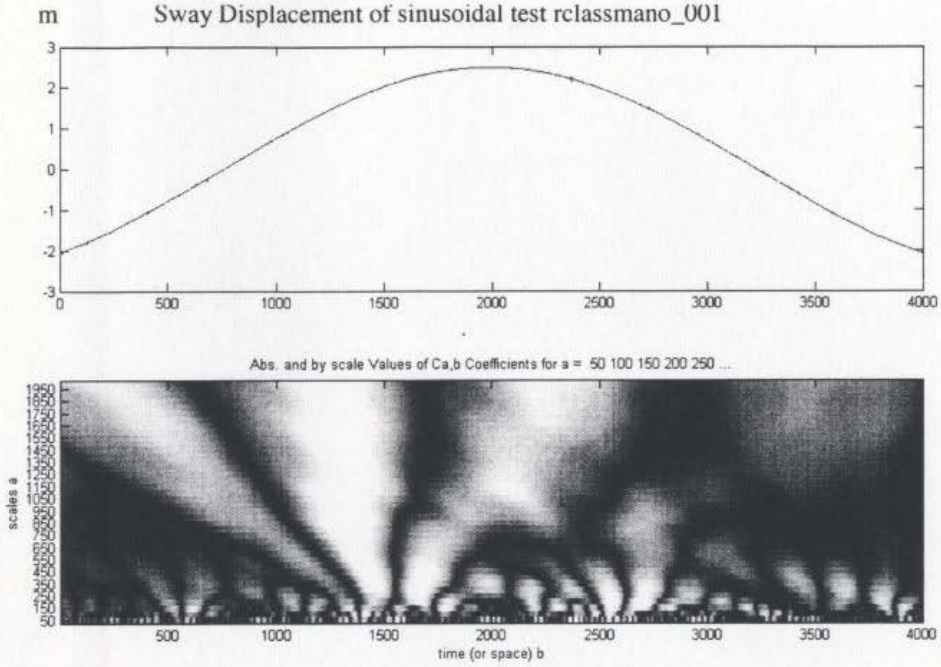

Another example is the application of CWT to a constant radius test, file name: rclassmano_028, ice condition: level, 50mm.

Figure 5-3 CWT Coefficients Plots of Sway Force (rclassmano_028, level, 50mm)

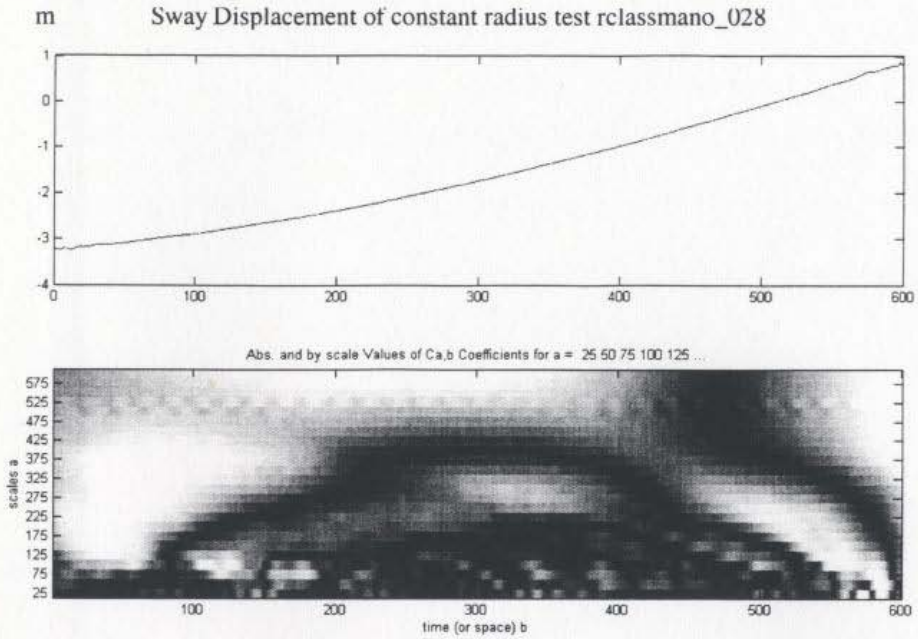

Figure 5-4 CWT Coefficients Plots of Yaw Moment (rclassmano_028, level, 50mm)

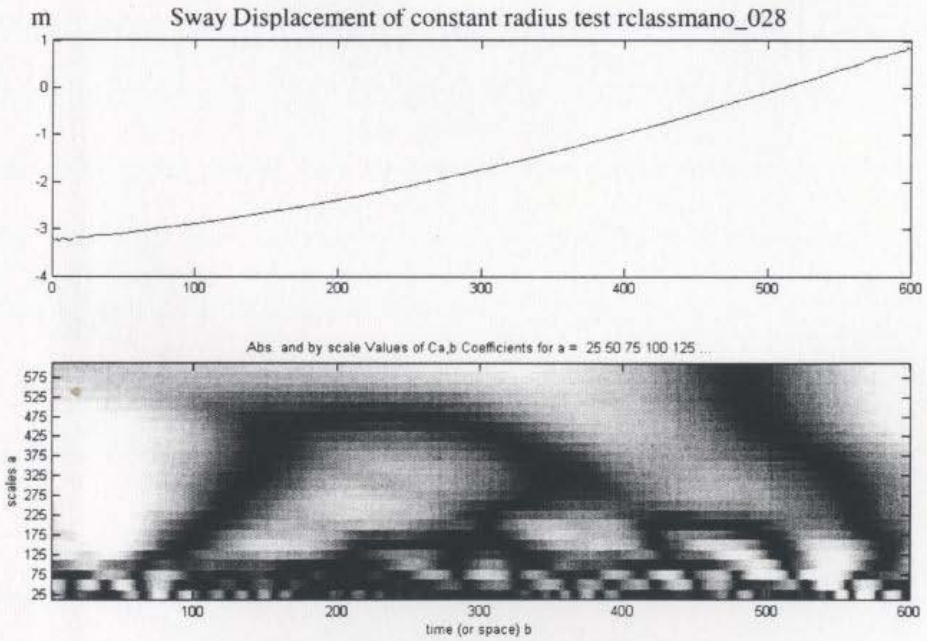

The frequency of force and moment in constant radius tests still cannot demonstrate a clear frequency component.

The CWT technique is helpful in the study of the physics of a ship maneuver in ice conditions, such as, an observation of different frequency components of ice force at different phases in a turning maneuver. But it can just offer a qualitative evaluation and leaves much to be developed. The main problem of this method is that calculating wavelet coefficients at every possible scale requires a large amount of work.

5.2.2 Discrete Wavelet Transform (DWT) application

For many signals, the low frequency content is the most important part. One of the most important applications of DWT is de-noising. After a one-stage discrete wavelet transform of a signal, the outcome is a vector of detail coefficients cD consisting mainly of the high-frequency noise; while the approximation coefficients cA contain much less noise than the original signal does. The decomposition process can be iterated, with successive approximations being decomposed sequentially, so that one signal is broken down into many lower-resolution components. Since the process is iterative, in theory it can be continued indefinitely. In practice, one selects a suitable number of iterations based on the nature of the signal.

Using DWT to remove the noise from a signal requires identifying which component or components contain the noise and then reconstructing the signal without these components. In a coarse de-noising method, a multi-layer decomposition process is

performed. The successive approximations become less and less noisy as more and more high-frequency information is filtered out of the signal.

But, in discarding all the high-frequency information, we also lose many of the original signal's sharpest features. Optimal de-noising requires a more subtle approach. A traditional linear smoother is to cut the series, starting from some prescribed term, for example, to keep only the first five terms of the expansion. Another way is to keep only those coefficients, whose absolute value is greater than some threshold values. The result is a nonlinear smoothing function. Such a technique is called threshholding. Wavelet threshholding provides a way to automatically adapt to the irregularity of the function to be estimated. Note that the "detail coefficients" obtained from the Discrete Wavelet Transform are MATLAB vectors. Then we manipulate each vector, setting each element to some fraction of the vectors' peak or average value and removing the coefficients within the threshhold. Finally, we can use the new "detail coefficients" to reconstruct the signal in order to get the filtered signals. Notice that it is a strength of the wavelet filter that we can remove the noise without compromising the sharp detail of the original signal. This advantage is particularly helpful in the study of ice related forces.

The details of the wavelet filter are documented in Appendix 2.2.

Now we can compare the original signal with de-noised signals. These plots correspond to a 10 second segment of measured forward sway force (data from rclassmano_001, sinusoidal test, 50mm level ice). The upper one is the raw test data plot.

The lower plot is the data filtered by using wavelet filter. The noise components in the original signal were removed and some sharp details which reflect the nature of ship-ice interaction are retained.

Figure 5-5 Raw test data and filtered test data of sway force in rclassmao_001

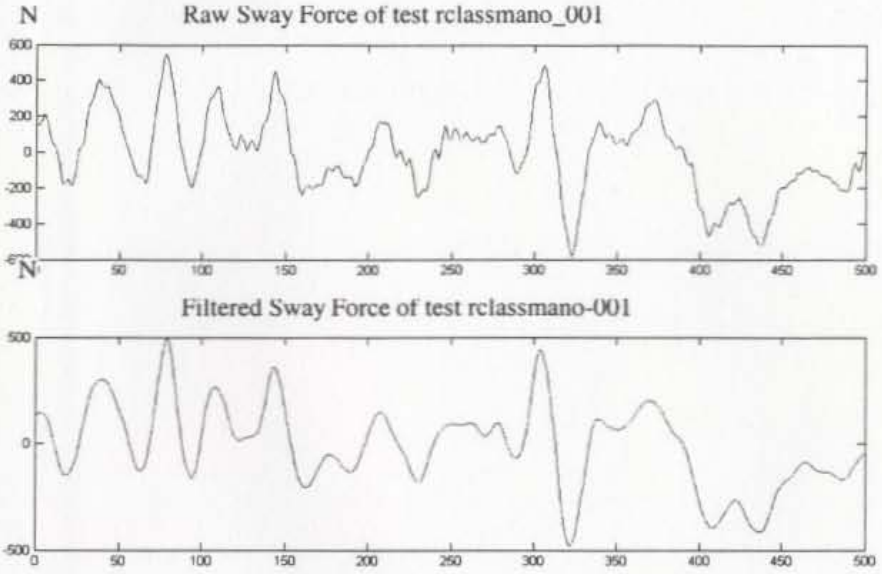

5.3 Neural Network Calculations

Interest in the Neural Network technique has grown rapidly over the past few years. The field initially grew from 1930s ideas about how biological systems work, particularly the human brain. Later research in human development and neurological systems proved those early theories about how people learned were not quite accurate but neural network research continued. Today neural network systems are being used in business, government, and academic research because of their ability to model data quickly and to produce better results than other more traditional data analysis techniques. Neural Computing also can be used to solve complex problems which defy practical

solution by other more traditional methods. Neural Network Identification does not use a physical model. Because of this, it is more robust than the classical parametric identification techniques. The input-output relationship of the system is represented by a network consisting of different layers of neurons. One of the problems of this approach is that its convergence is not always guaranteed. In addition, usually a tremendous amount of computer time is needed for the parameters to converge to their true values.

In this section we show how to calculate the yaw rate using neural networks. In the constant radius test, we have:

$$r = \frac{V}{R} \tag{5.2}$$

But, in the sinusoidal test, the radius of turn is not a constant value. So we have to carry out differentiation $r = \frac{d\psi}{dt}$ to obtain the nominal yaw rate.

The first idea which comes to our mind is the most common numerical method in differential calculation: "finite difference method". The yaw acceleration, and yaw rate time series can be calculated from yaw angles time series in the raw test data. The yaw velocity is the 1st derivative of the yaw angle and the yaw acceleration is the 2nd derivative of the yaw angle. The numerical methodologies are given below:

$$r = \frac{\theta_{i+1} - \theta_{i-1}}{2\Delta t}$$

$$\dot{r} = \frac{\theta_{i+1} - 2\theta_i + \theta_{i-1}}{(\Delta t)^2}$$

where, θ_i is the yaw angle.

Unfortunately, this methodology did not work due to the nature of the signal. Although we ammended the governing equation to $r = \frac{\theta_{i-10} - \theta_{i-10}}{20\Delta t}$ in order to remove the effect of the rapid, sharp local variations in the signal, still the results were not satisfactory.

The neural network method is a possible alternative which can be used to find the first derivative of the yaw angle. To achieve this purpose we need understand the structure and detailed algorithm of the neural network.

First, we can set the time as the only input and yaw angle as the only output. Then the neural network program can generate a network after calculation. When the time series passes through the network the yaw angle is obtained. It is actually a function which correlates time with yaw angle. If we differentiate this function (the network) with time, we can get the time series of yaw rate. The detailed algorithm:

Figure 5-6 Neural network Structure

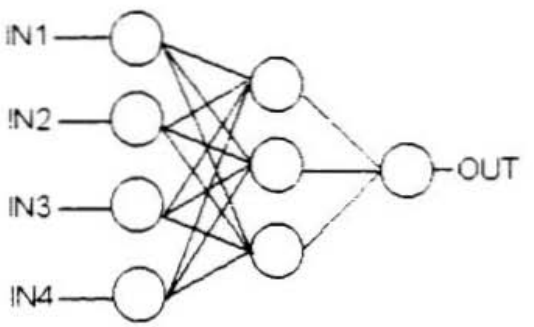

First. the variable must be scaled from its original values to a range [-1.1]. The scaled input is given by

$$x_i = \frac{2x_{ij} - \max(x_{ij}) - \min(x_{ij})}{\max(x_{ij}) - \min(x_{ij})} \qquad (5.3)$$

$$X = \{x_i\} = [1.1], \qquad i = 1$$

Where, x_{ij} is the original data. The input to the j node in the intermediate layer is given by

$$A_j = \sum_{i=1} w_{ij} x_i, \qquad j = 1, \ldots\ldots 15 \qquad (5.4)$$

Where j is the number of neurons in the middle layer. The input to the j-node in the middle layer is acted upon by an activation function. $H(A_j)$ is given by

$$H(A_j) = \frac{1 - e^{-A_j}}{1 + e^{-A_j}} \qquad j = 1, \ldots\ldots 15 \quad H_0 = 1 \qquad (5.5)$$

The output of the network is given by

$$y = \sum_{j=1}^{h} \beta_j H(A_j) \qquad (5.6)$$

Once y has been determined, then the result is rescaled to the range of the data.

$$y_{ij} = \frac{\max(y_{ij}) - \min(y_{ij})}{2} y_k + \frac{\max(y_{ij}) + \min(y_{ij})}{2}$$

y_{ij} is the real output test data

Differential coefficients

After transformation and simplification, the derivative is:

$$\frac{\partial y_k}{\partial x_i} = \frac{\max(y_o) - \min(y_o)}{\max(x_o) - \min(x_o)} \sum_{j=1}^{15} \beta_{kj} w_{ji} \frac{\left[1 + H_j(A_j)\right]\left[1 - H_j(A_j)\right]}{2}$$

Figure 5-7 r40 test yaw rate calculated by finite difference method and neural network

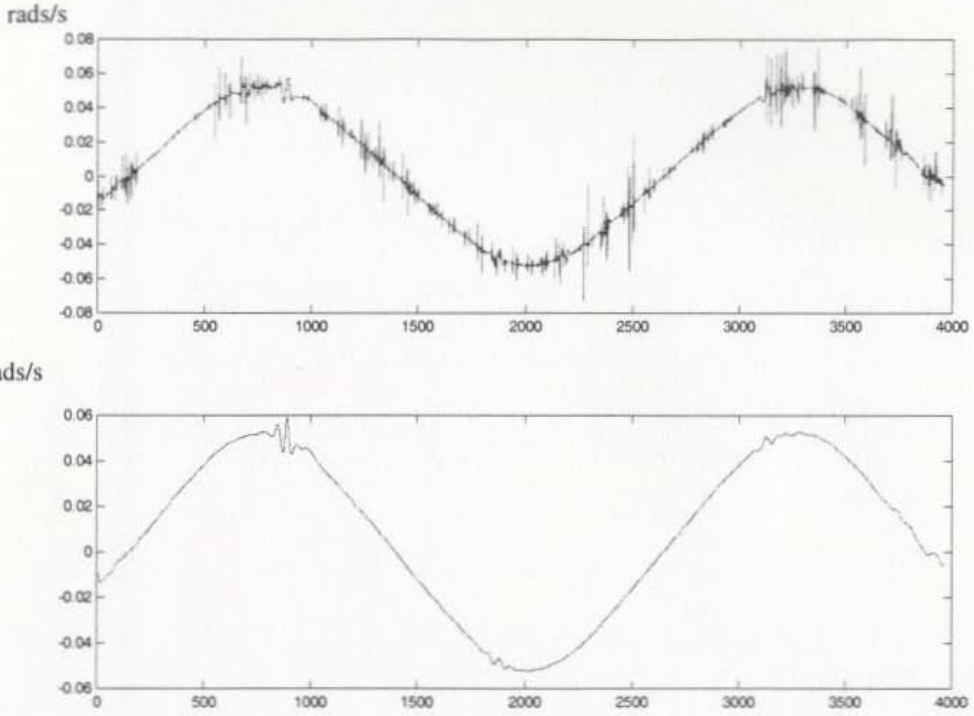

Figure 5-6 displays the results of finite difference numerical method (upper one) and neural network (lower one) applied to the raw data extracted from sinusoidal test rclassmano_40 (level ice, 30mm). It is clear from the graph that the finite difference method produces a noisy result. The results of neural network calculations are much better. This approach can also be used to compute the yaw and sway accelerations.

It is resonable to consider the application of this approach in the derivation of Hydrodynamic coefficients of ship in ice.

We investigated the use of neural network to identify the dependence of sway force and yaw moment on sway velocity and yaw rate. The purpose is to determine the derivatives in equation (3.15 & 3.16). The procedure was as follows:

1. Divide the sinusoidal test data to a number of segments each of a 2-second length (100 points).
2. Train the network using one segment. The network uses 3 inputs (sway velocity, yaw rate and time) and 2 outputs (sway force and yaw moment).
3. Use the weights (training results) and raw data to calculate the required sway velocity dependent derivatives and yaw rate dependent derivatives.
4. Combine the data segments of coefficients to one file and save it.

This technique did not provide satisfactory results. The assumption that the hydrodynamic coefficients in equations (3.15 & 3.16) are linear with small variations is not valid.

Figure 5-8 Hydrodynamic coefficients calculated by neural network method

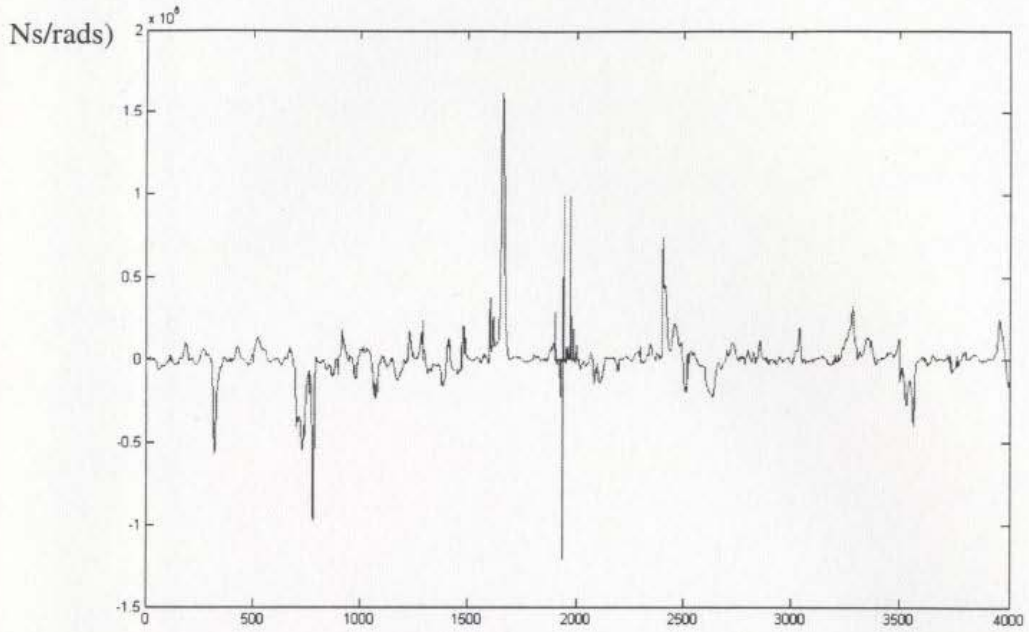

This result shows that a general linear dynamic equation does not reflect the local variations of ice forces acting on ship hull. To explain the problem of this approach, we need a more comprehensive study of the ice breaking dynamics and a careful review of the details of the experimental set-up. The neural network result's probability distributions are also discussed in the next section.

5.4 Statistical Analysis

5.4.1 Spectral Analysis

In the previous sections in this chapter, we applied a series of data analysis techniques to the test data, including data retrieval, conversion, reduction, validation, arithmetic calculation, wavelet filter and neural network differentiation. Now the data are ready for further statistical analysis, which includes sway force, yaw moment, sway velocity and yaw rate (differentiate yaw angle with time by means of neural network computation).

Although the errors in the calculation are reduced, and most of the instrumental and system noises in the signal are removed, there are still significant high frequency components in the processed test data. This is due to the nature of ship-ice interaction. The random variation in the time series of ice force is a realistic phenomenon. It is necessary to check the frequency information of the ice forces. I designed a MATLAB program to execute the spectrum analysis. I plotted the spectral density functions of the measured ice forces in various ice conditions.

A sinusoidal and a constant radius test data were selected from data of each ice condition. Since six ice conditions, 30mm level, 30mm pack, 30mm rubble, 50mm level, 50mm pack, 50mm rubble, were simulated in this experiment, 12 test files in total were chosen to be inspected.

Figure 5-9 Ice force spectra of rclassmano_001, sinusoidal, 30mm, level

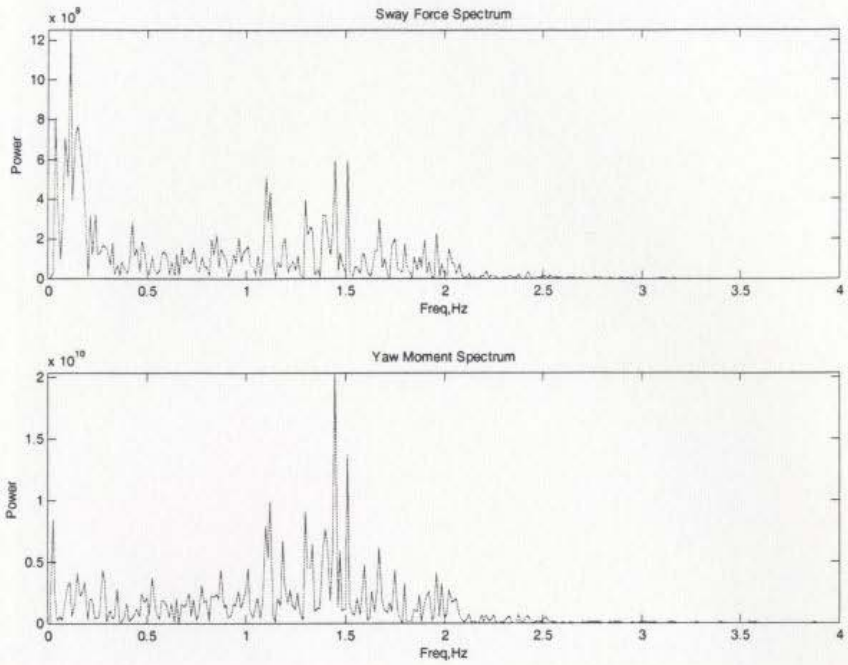

Figure 5-10 Ice force spectra of rclassmano_017, constant radius, 30mm, level

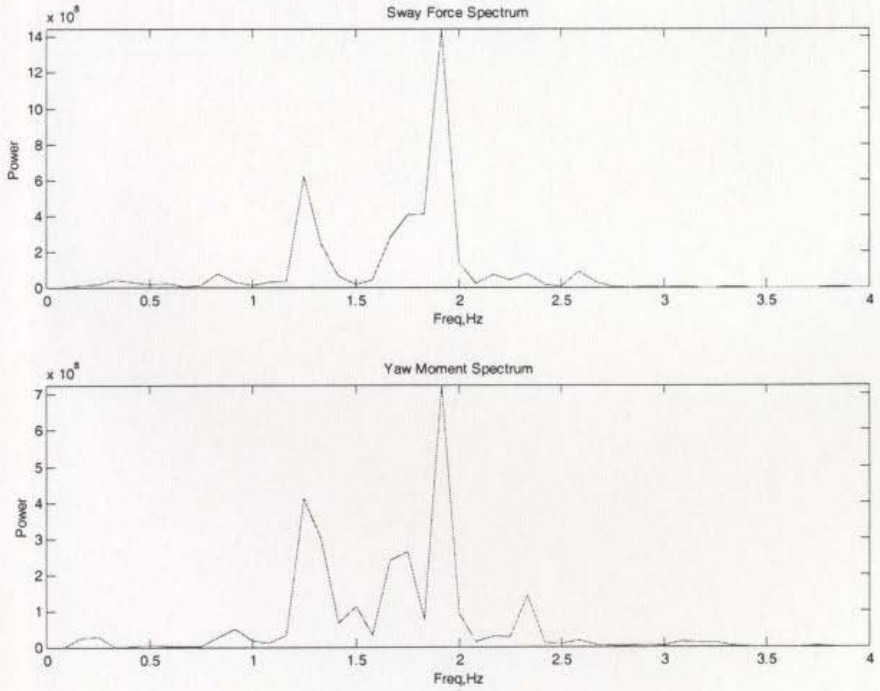

Figure 5-11 Ice force spectra of rclassmano_002, sinusoidal, 30mm, pack

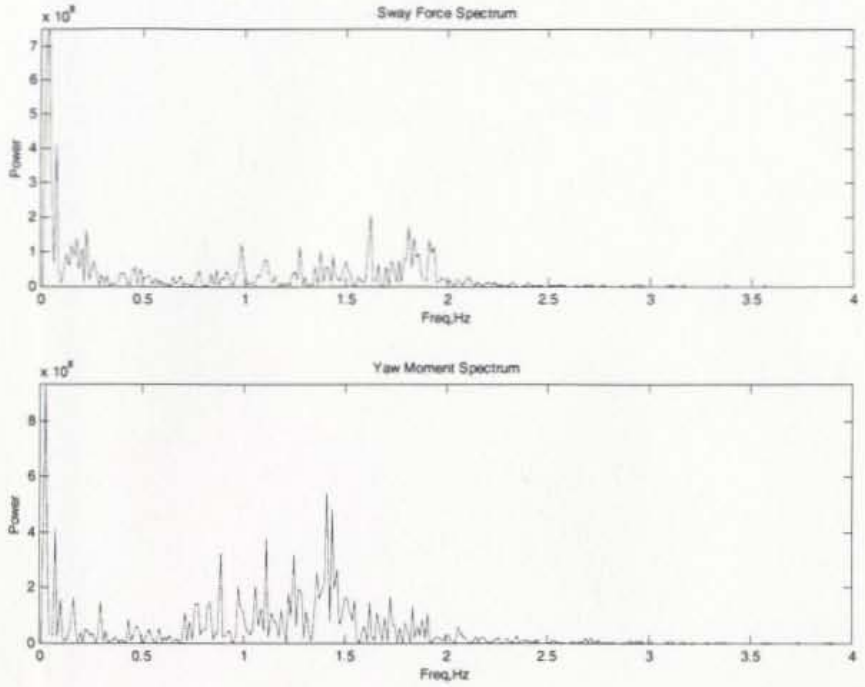

Figure 5-12 Ice force spectra of rclassmano_060, constant radius, 30mm, pack

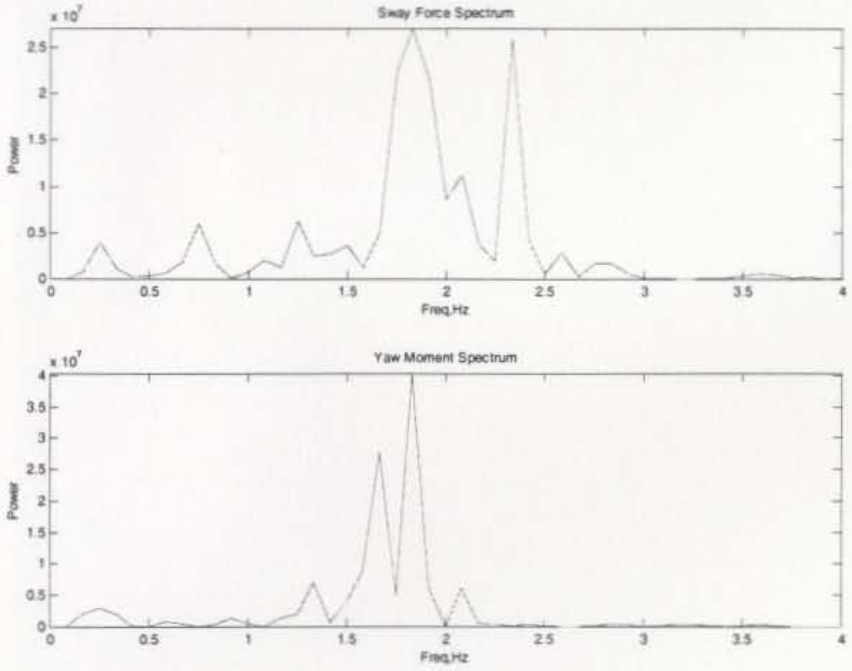

Figure 5-13 Ice force spectra of rclassmano_003, sinusoidal, 30mm, rubble

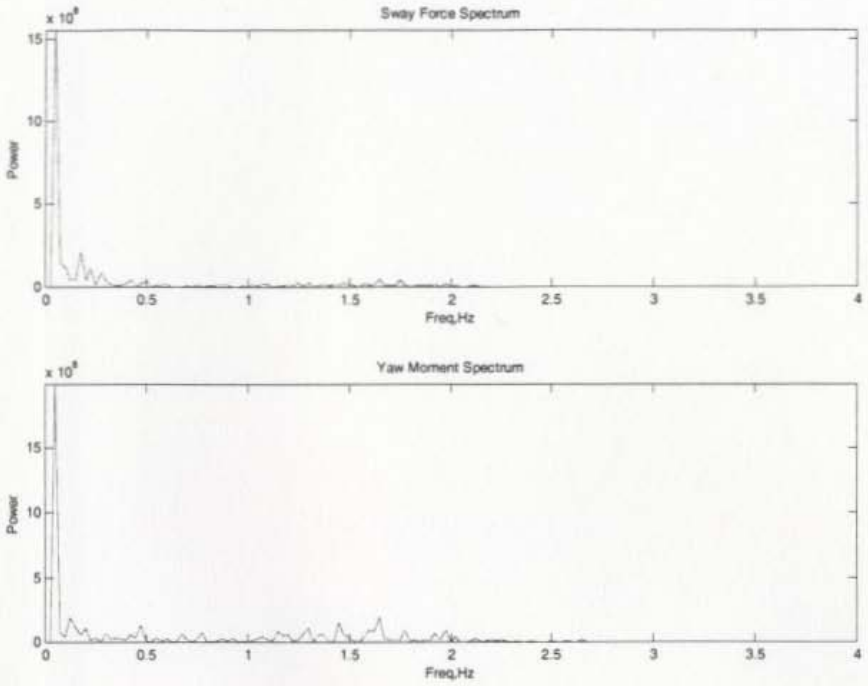

Figure 5-14 Ice force spectra of rclassmano_064, constant radius, 30mm, rubble

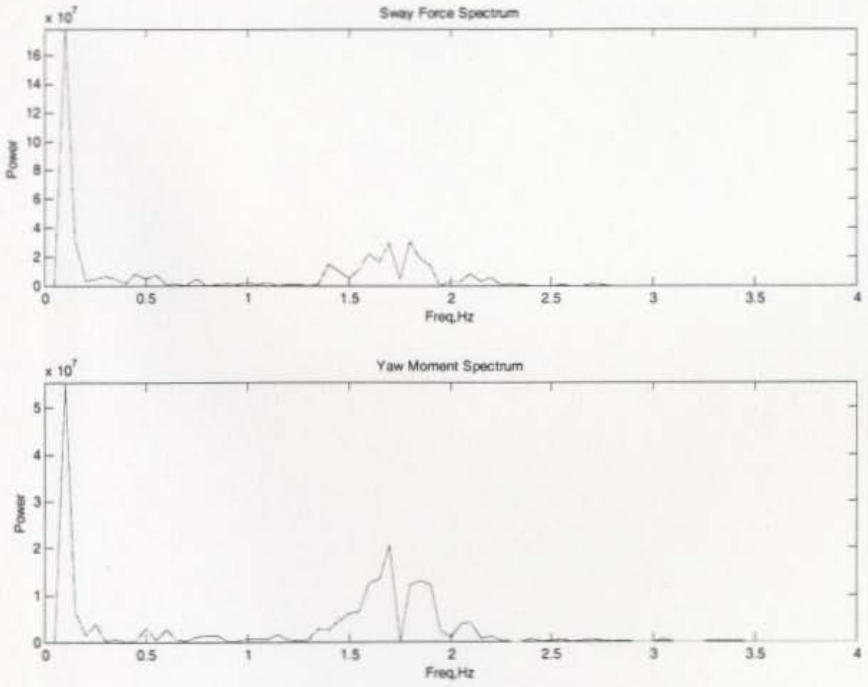

Figure 5-15 Ice force spectra of rclassmano_040, sinusoidal, 50mm, level

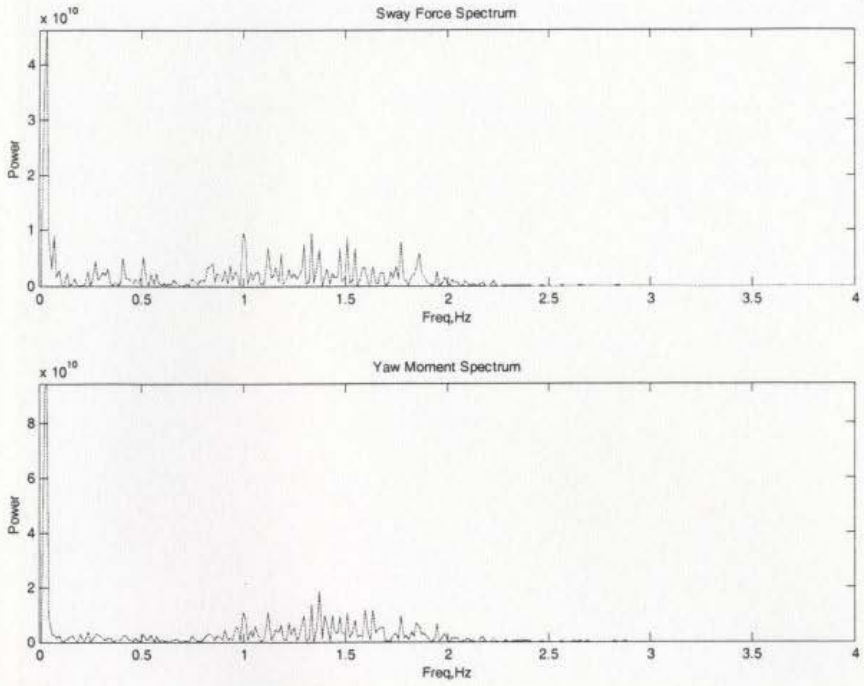

Figure 5-16 Ice force spectra of rclassmano_028, constant radius, 50mm, level

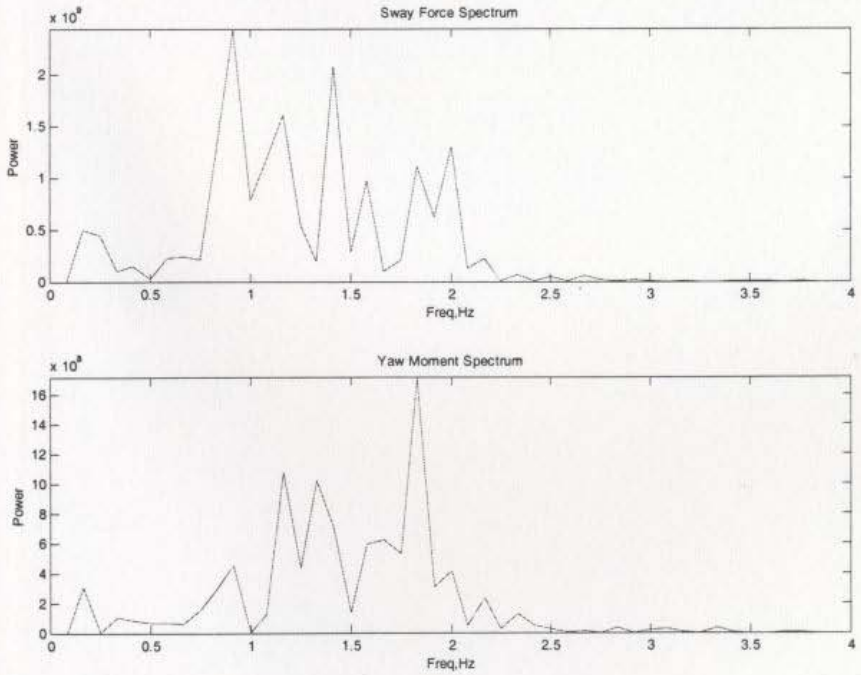

Figure 5-17 Ice force spectra of rclassmano_042, sinusoidal, 50mm, rubble

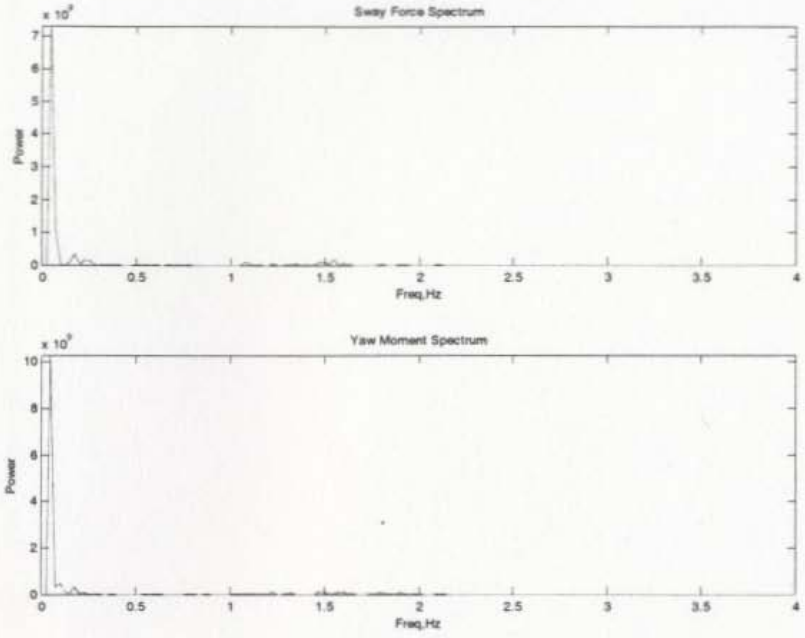

Figure 5-18 Ice force spectra of rclassmano_032, constant radius, 50mm, pack

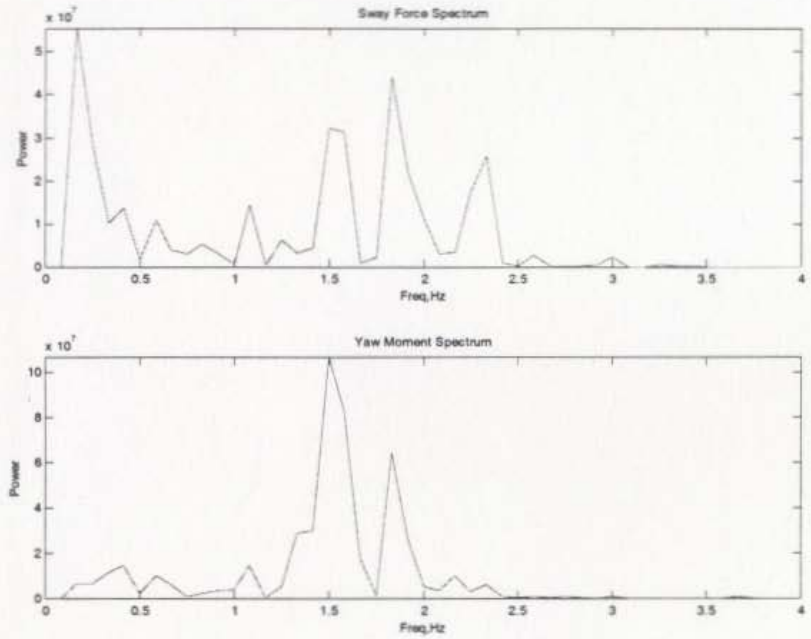

Figure 5-19 Ice force spectra of rclassmano_043, sinusoidal, 50mm, 2rubble

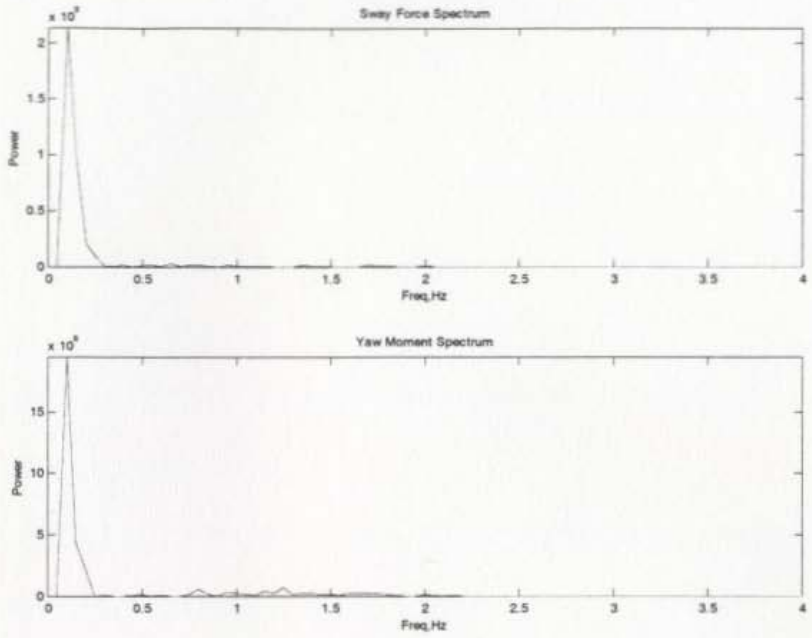

Figure 5-20 Ice force spectra of rclassmano_037, constant radius, 50mm, rubble

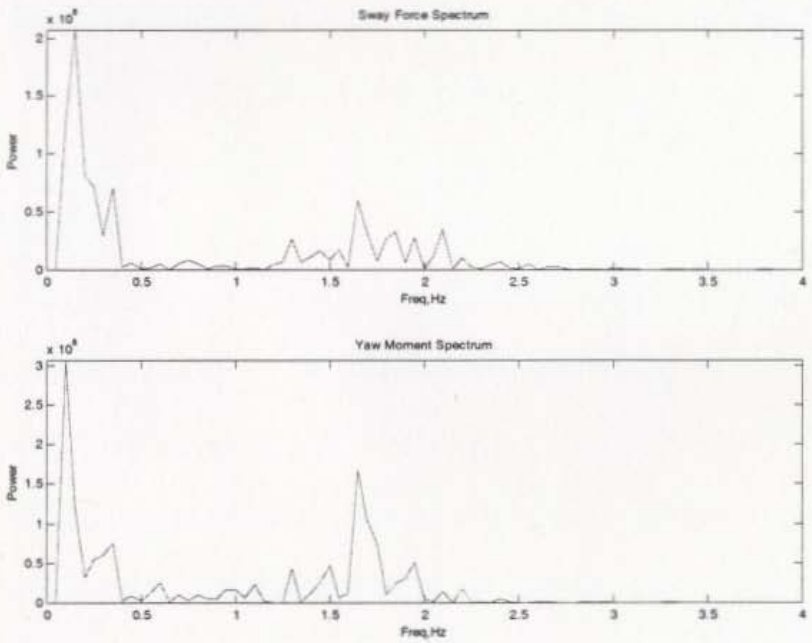

After a careful examination of these spectrum plots, I can arrive at the following conclusions:

- In general, the frequency distributions of ice forces are concentrated on a small range of values in a very low frequency zone.
- The spectrum of the ice force consists of two parts. One is a very low frequency part; the other one is a higher frequency part up to 2.5 Hz. The lower frequency is close to the frequency of the yaw rate; and the higher frequency is similar to the frequency of sway velocity.
- The spectrum in level ice consists of two clearly separated parts as mentioned above. The spectrum of pack ice is similar to that of the level ice. But the two components of the spectrum cannot be distinguished as clearly as that of the level ice.
- The dominant frequency of the ice force in rubble ice (multi-layer broken ice) is very low, no matter what the test pattern and ice thickness.
- The dominant frequency of most tests is below 2.5 Hz, corresponding to a period of 0.4 second.
- The spectra of the sway force and the yaw moment are very similar.
- The spectral distributions of sinusoidal test and constant radius test data for the same ice condition are alike in the ice thickness of 30 mm, but not in 50mm.
- In the same ice condition of 50mm ice thickness, the spectral distributions of sinusoidal test and constant radius test are different. The dominant frequency of sinusoidal test is very low and approximately equal to the frequency of the

sinusoidal maneuver pattern. But in the constant radius test, the dominant frequency of ice force is unevenly distributed between 0 Hz to 2.5 Hz. This is to say that, in thicker ice conditions, the yaw rate is the dominant control motion in ship maneuvering because the yaw rate was assumed constant, or having a very small value, in constant radius test.

- The spectral energy of the ice force is always in the range of 0 –2.5 Hz. This suggests that the test system responds to broad-spectrum excitation by the ice. It is always less energy in rubble ice because the rubble is a plastic material which damps out vibration.

Now, from the study of the spectrum plots, we have a general idea how the model motion parameters determine the dynamic parameters in this physical process. Now we can take a closer look at what the real test data looks like. I plotted a small segment of the data. It just lasts 4 seconds and includes the sway force, yaw moment, sway velocity and yaw rate. The reason to choose only 4-second segment here is that it is too difficult to find some reasonable conclusions from a whole run of the test data. These full run test data are plotted in Appendix 1.2 (P147- P149). In this scale, we cannot find detailed information of the data. So we randomly chose a 4-second segment from test data for the examination. It should be noticed that the data in the time segment will not be consistent in the whole run.

Figure 5-21 Segment of rclassmano_001, sinusoidal, 30mm, level

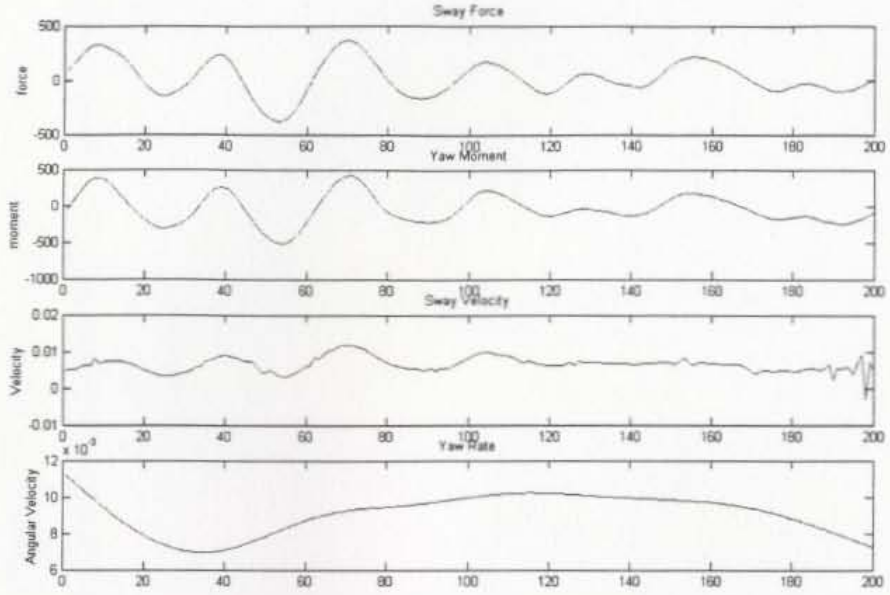

Figure 5-22 Segment of rclassmano_056, constant radius, 30mm, level

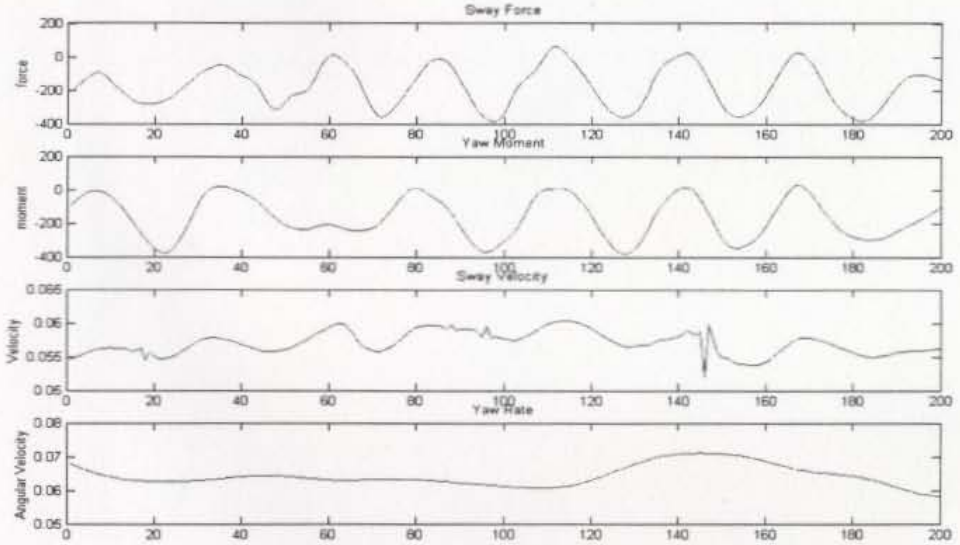

Figure 5-23 Segment of rclassmano_002, sinusoidal, 30mm, pack

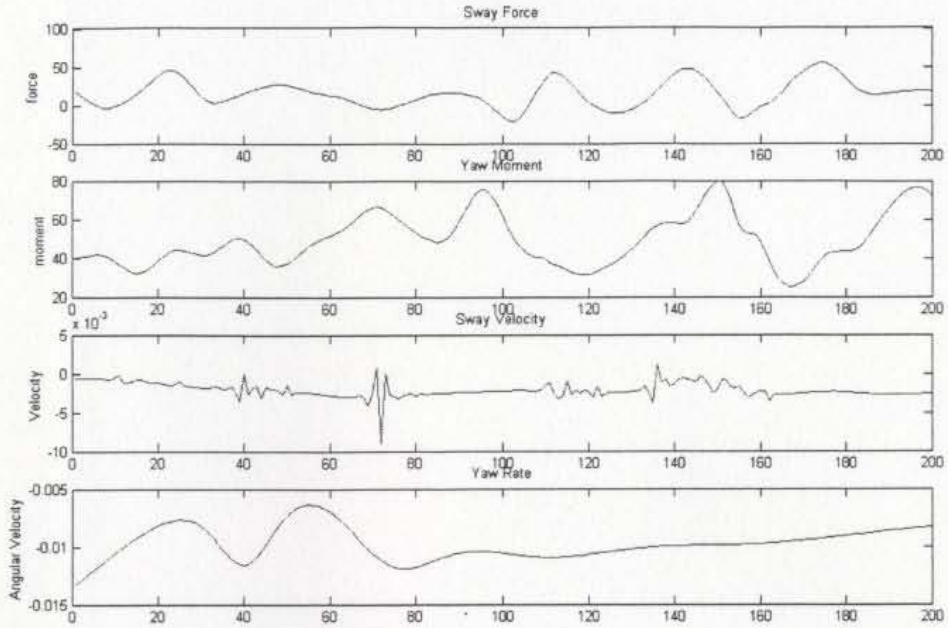

Figure 5-24 Segment of rclassmano_021, constant radius, 30mm, pack

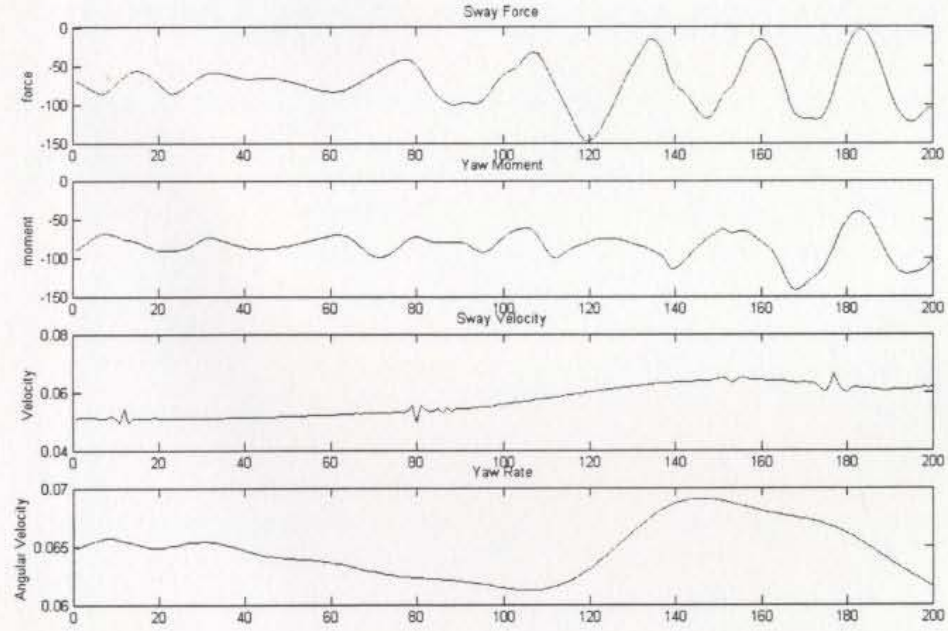

Figure 5-25 Segment of rclassmano_003, sinusoidal, 30mm, rubble

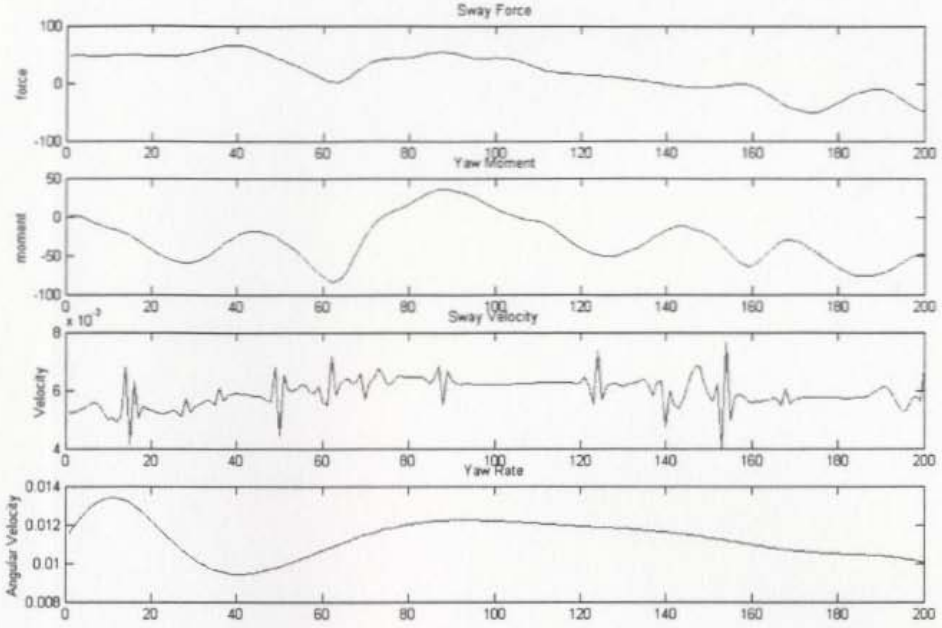

Figure 5-26 Segment of rclassmano_026, constant radius, 30mm, rubble

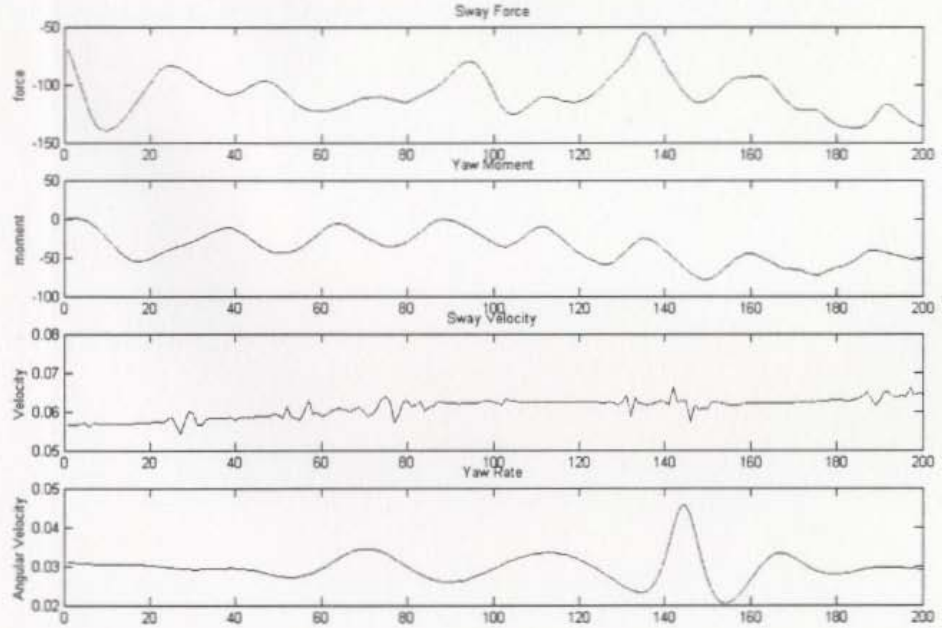

Figure 5-27 Segment of rclassmano_040, sinusoidal, 50mm, level

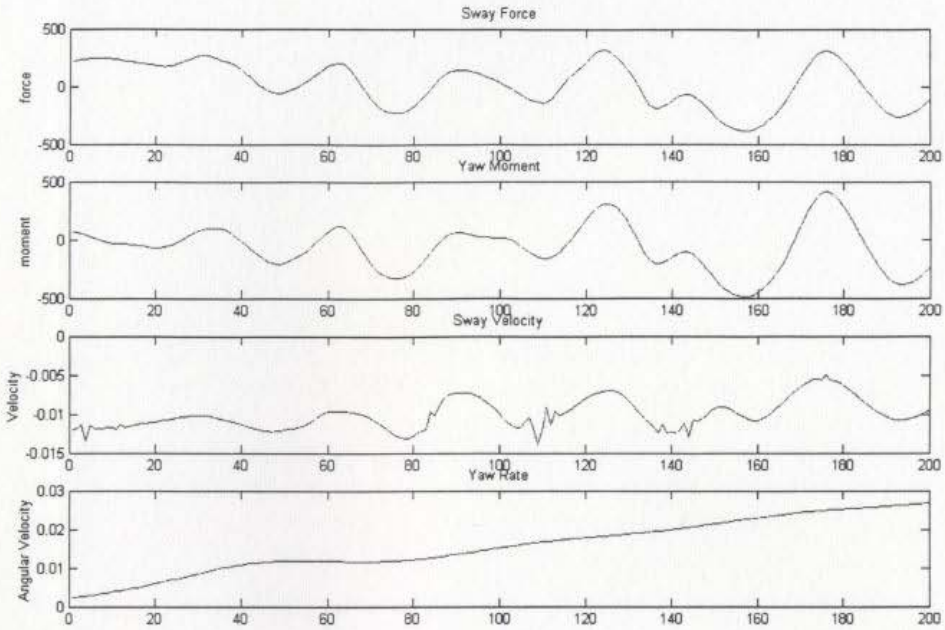

Figure 5-28 Segment of rclassmano_029, constant radius, 50mm, level

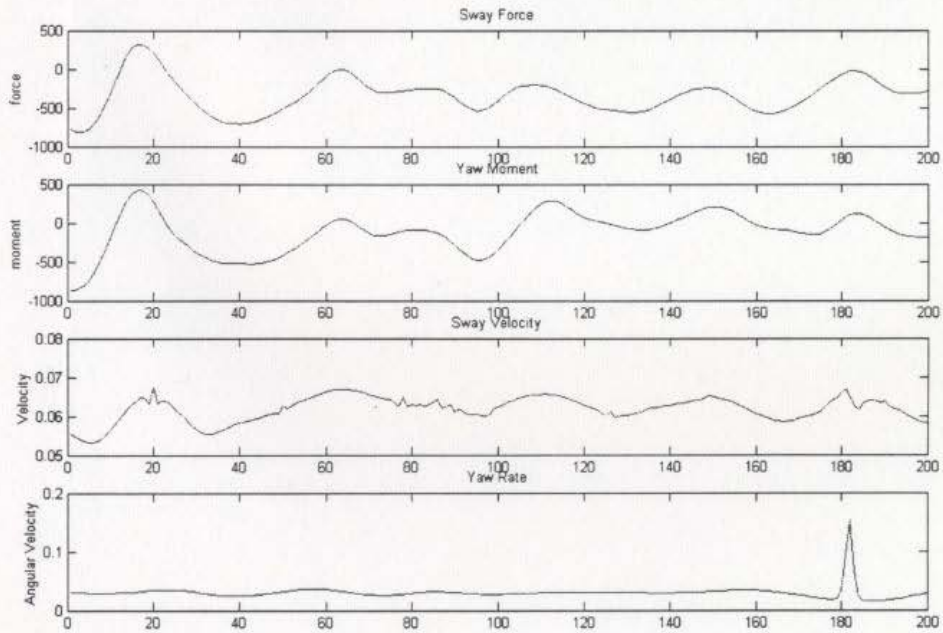

Figure 5-29 Segment of rclassmano_042, sinusoidal, 50mm, pack

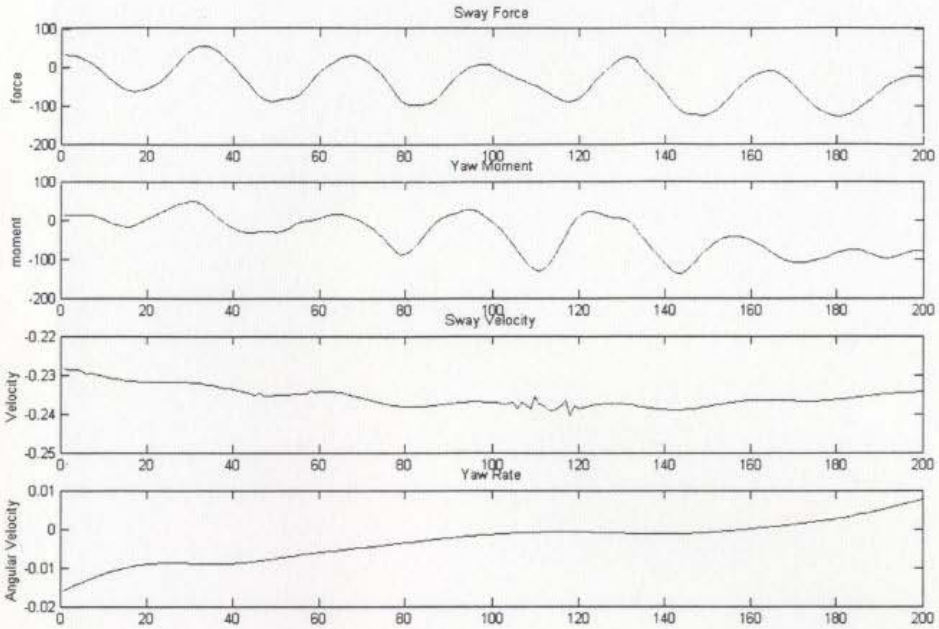

Figure 5-30 Segment of rclassmano_032, constant radius, 50mm, pack

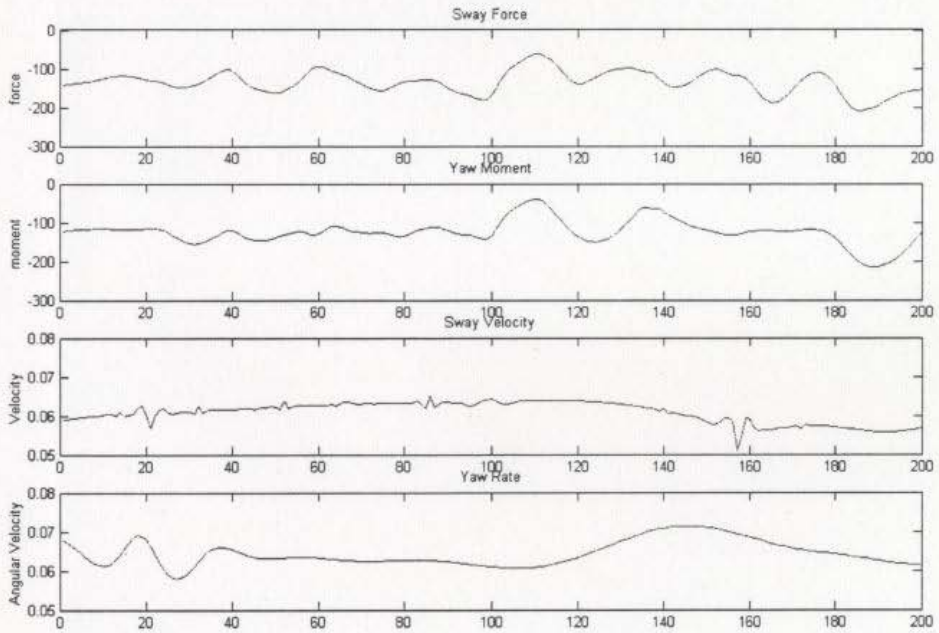

Figure 5-31 Segment of rclassmano_043, sinusoidal, 50mm, rubble

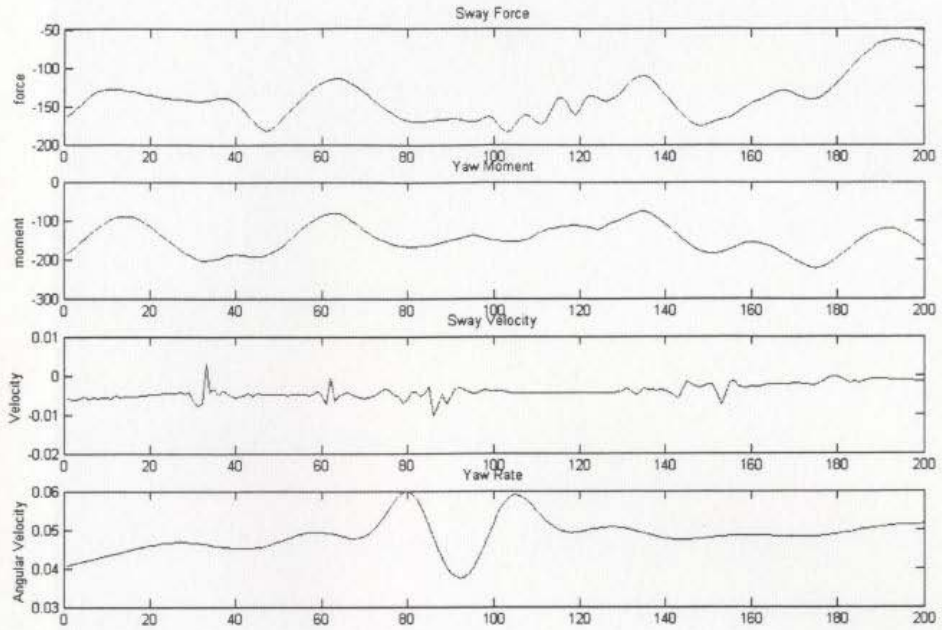

Figure 5-32 Segment of rclassmano_035 constant radius, 50mm, rubble

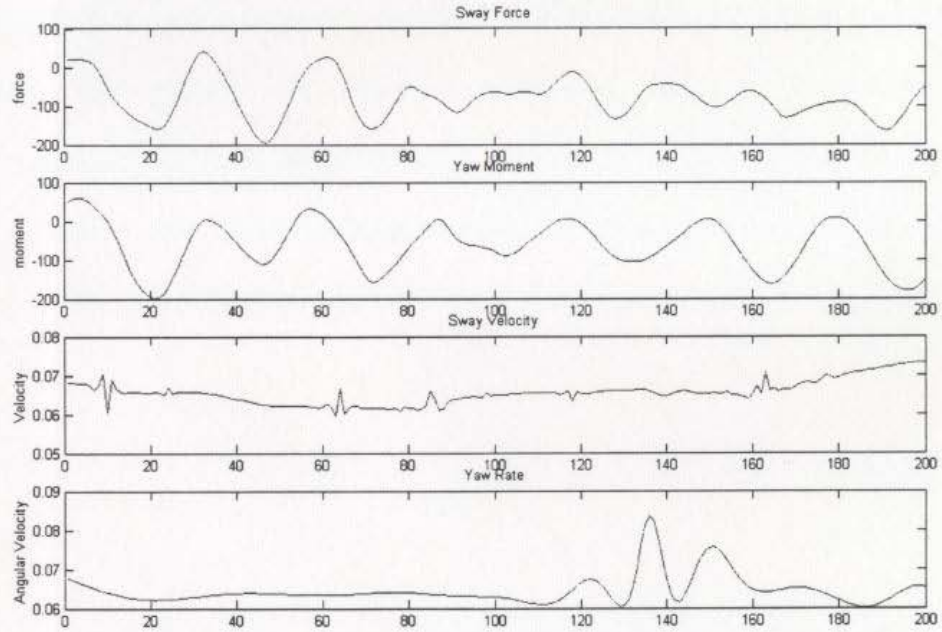

These plots have corroborated some of the conclusions I obtained from the spectral analysis. In level ice condition, there is an apparent matching relationship between the ice forces and the sway velocity. In broken ice conditions, this matching relationship is not clear. Although we assume the sway velocity is very small in sinusoidal test, the small transient sway velocity has a significant influence on the ice force. So we cannot neglect the sway velocity in the ice-ship problem.

5.4.2 Hydrodynamic Coefficients Analysis

In the open water PMM maneuvering tests, we can obtain the hydrodynamic coefficients, which can be used to predict the ship's trajectory and turning radius. In section 5.3 we showed how to use neural network calculation to obtain the Yv, Sway Force derivative with respect to Sway Velocity; Yr, Sway Force derivative with respect to Yaw Rate; Nv, Yaw Moment derivative with respect to Sway Velocity; Nr, Yaw Moment derivative with respect to Yaw Rate. The linear relationship between force and response is clear in open water, that is to say the sway force and yaw moment almost linearly increase with the increase the ship's velocity. But in ice condition, we cannot get the satisfactory results like that in open water test. The following are plots of neural network results for rclassmano_001 test, level 30mm ice.

Figure 5-33 Segments of coefficients obtained from neural network calculation

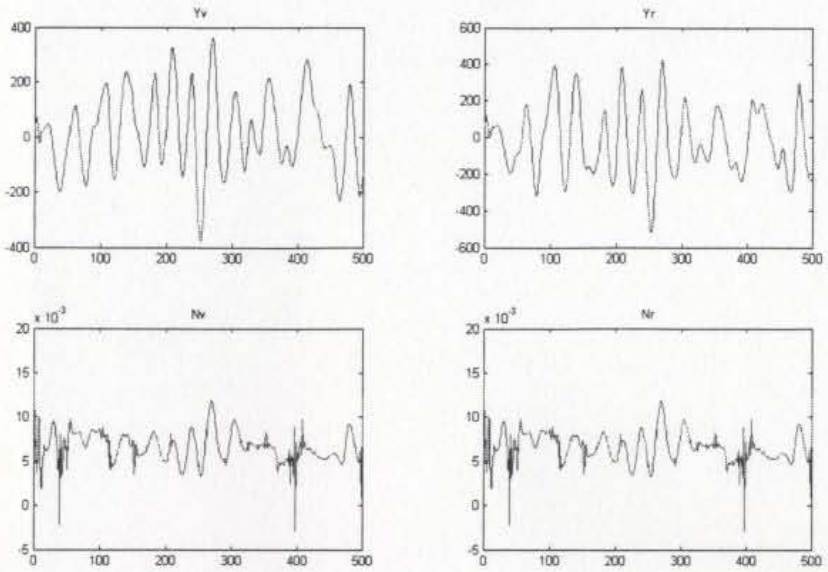

It is clear that the coefficients calculated here demonstrate large variations. This implies that the linear ice force coefficients are random.

In this section we show the distribution of these random variations.

Figure 5-34 Probability distribution of Yv Sinusoidal 30mm r01 (level) and r02 (pack)

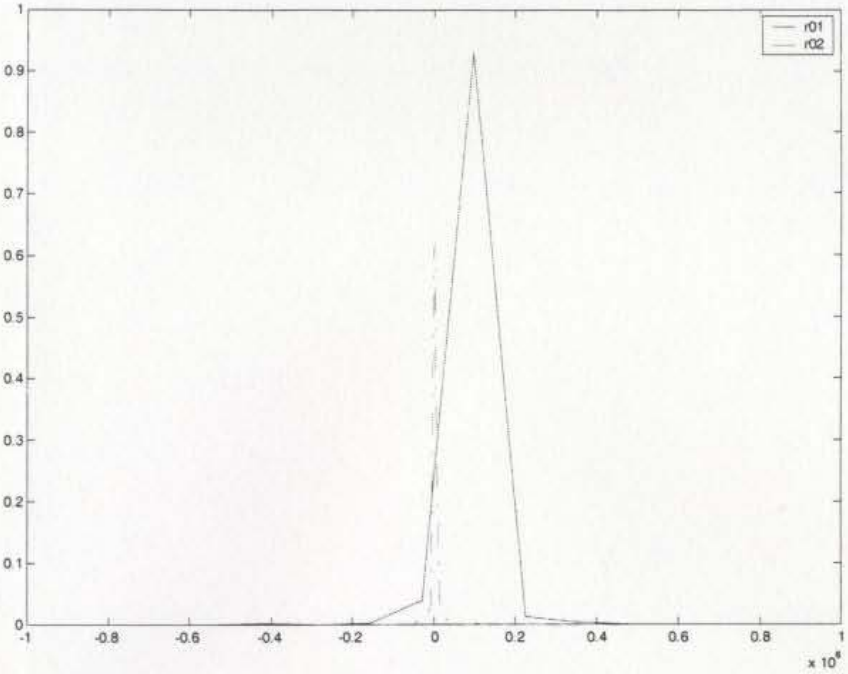

Figure 5-35 Probability distribution of Yv Sinusoidal 30mm r02 (pack), r03 (rubble) and r04 (2rubble)

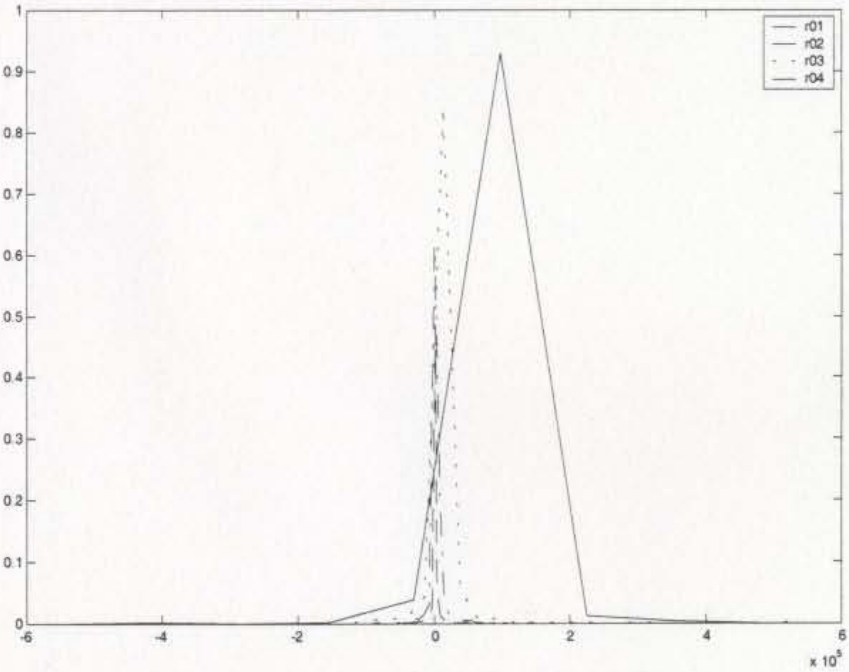

Figure 5-36 Probability distribution of Nv Sinusoidal 30mm r01 (level) and r02 (pack)

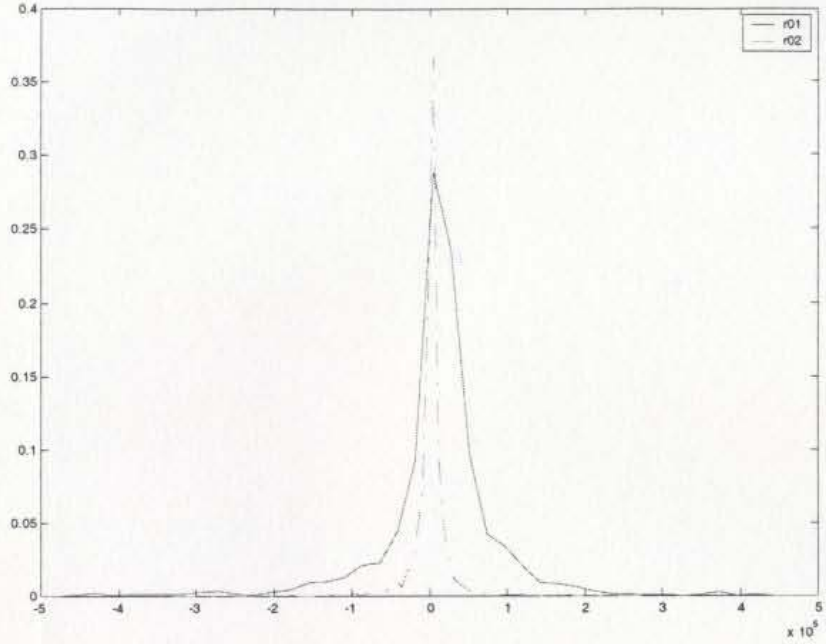

Figure 5-37 Probability distribution of Nv Sinusoidal 30mm r02 (pack), r03 (rubble) and r04 (2rubble)

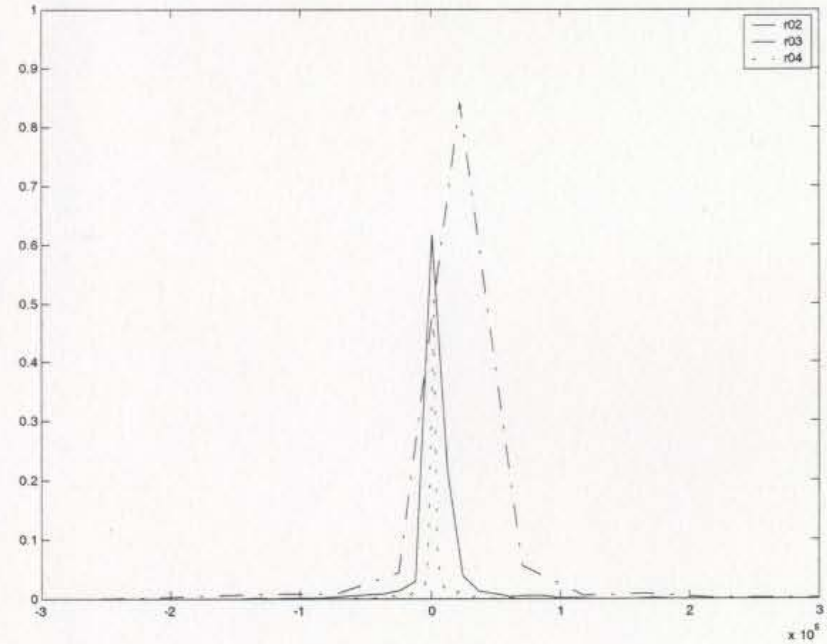

Figure 5-38 Probability distribution of Yv Sinusoidal 50mm r40 (level), and r67 (level)

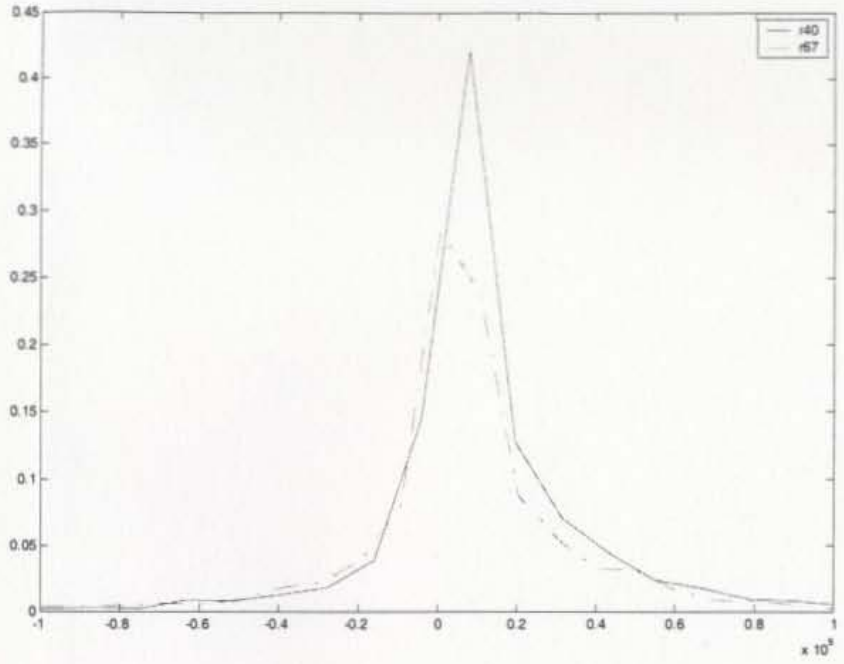

Figure 5-39 Probability distribution of Yv Sinusoidal 50mm r40 (level), r42 (rubble)

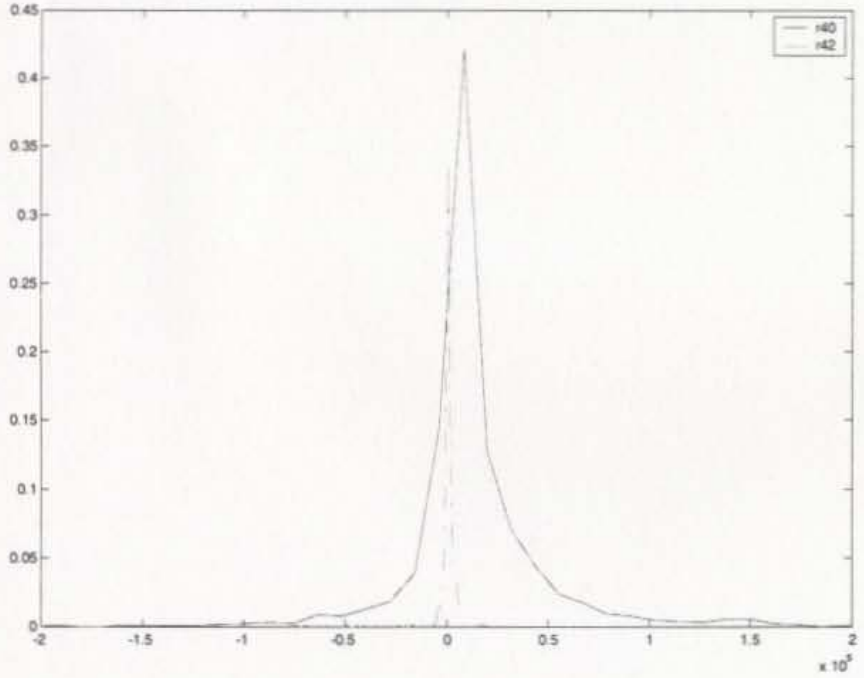

Figure 5-40 Probability distribution of Yv level 50 Constant Radius R28-R30

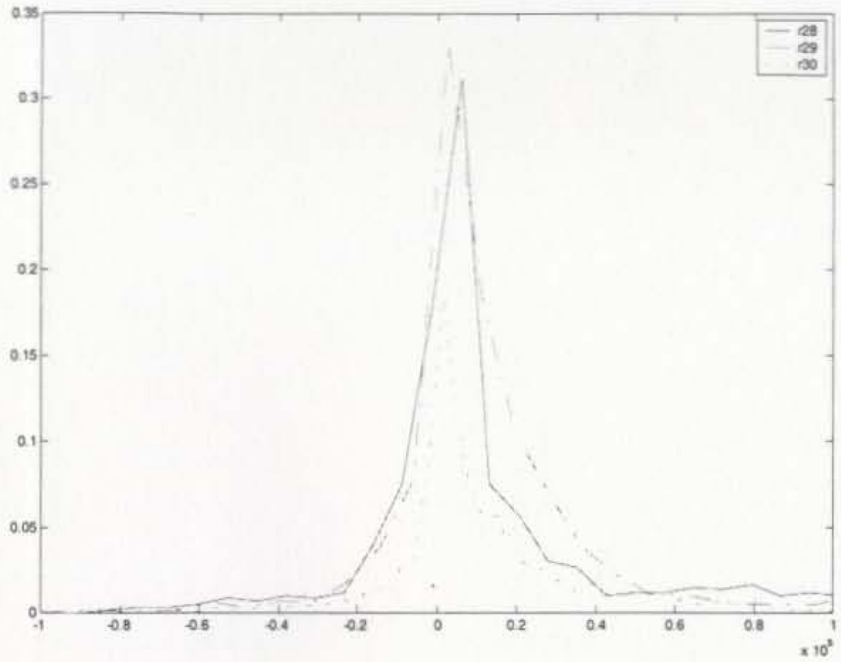

Figure 5-41 Probability distribution of Nv level 50 Constant Radius R28-R30

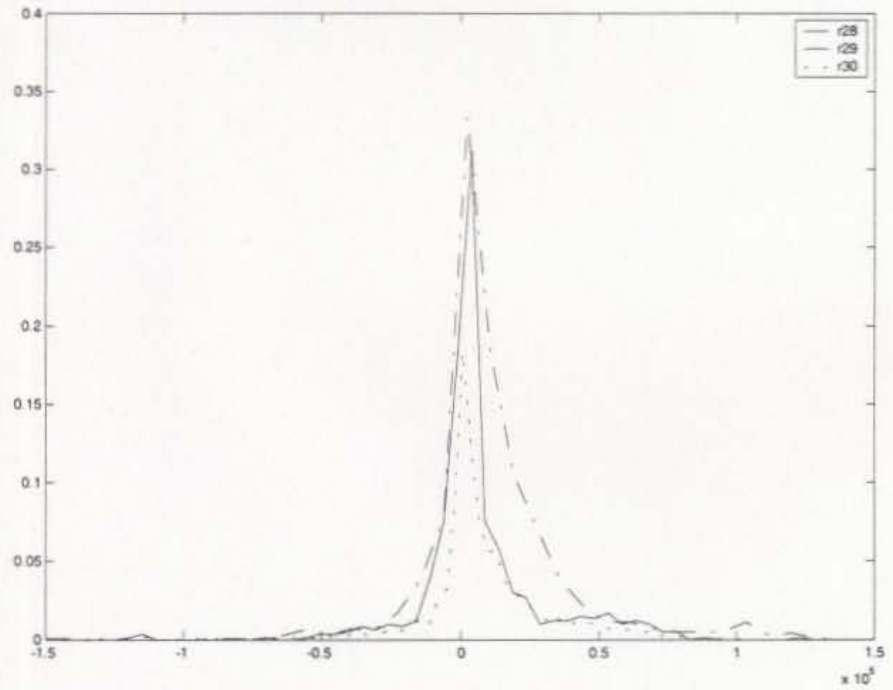

Figure 5-42 Probability distribution of Yv Constant Radius, R28 (level), R32 (pack), R35 (rubble)

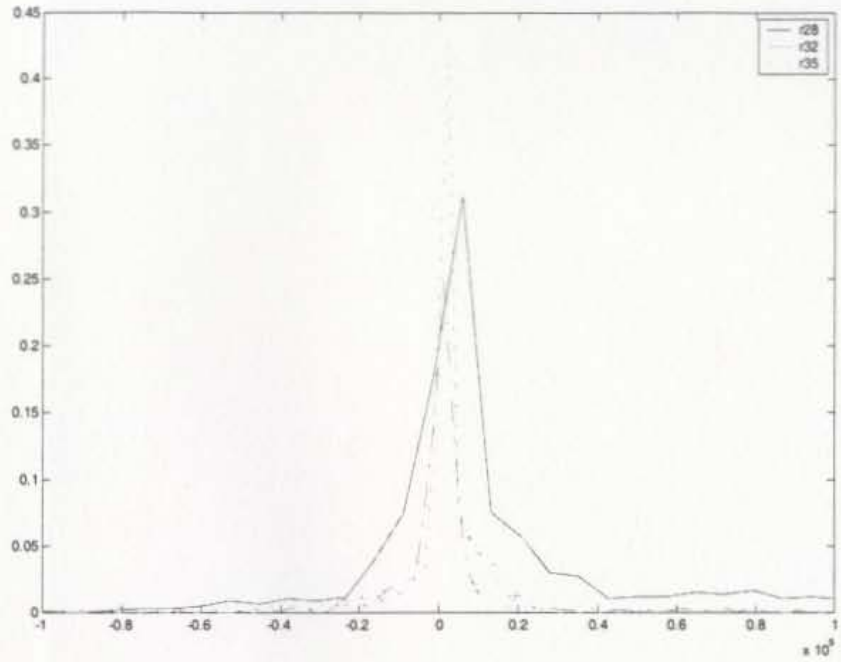

Figure 5-43 Probability distribution of Yv Different thickness: r28(level 50) r56(level 30)

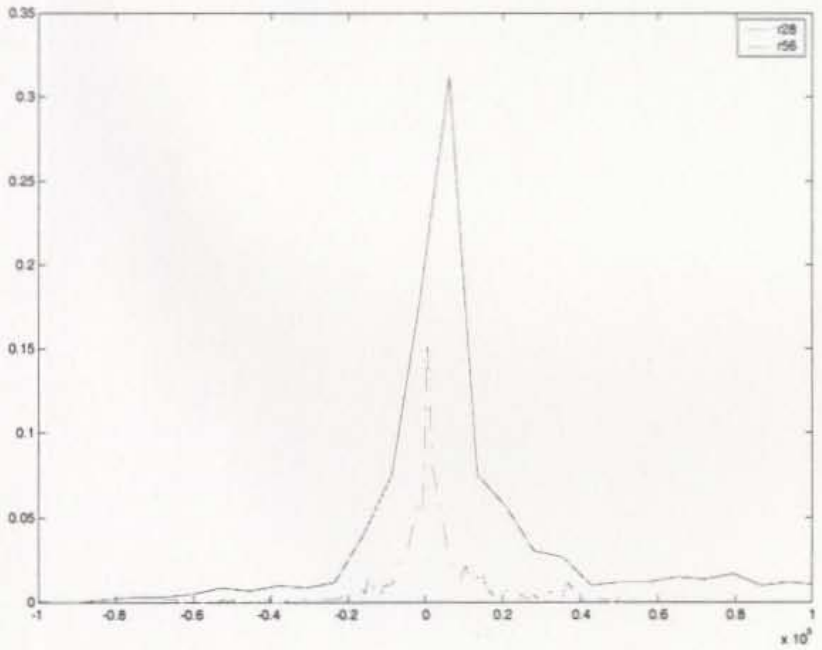

Figure 5-44 Probability distribution of Nv Different thickness: r28(level 50) and r56(level 30)

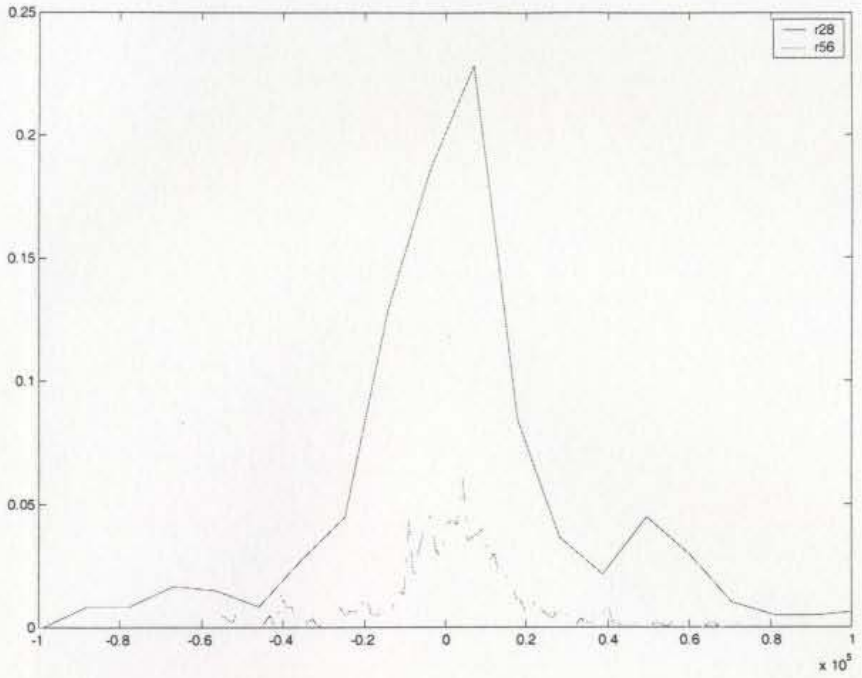

Figure 5-45 Probability distribution of Yv Different thickness: r32(pack 50) and r60(pack 30)

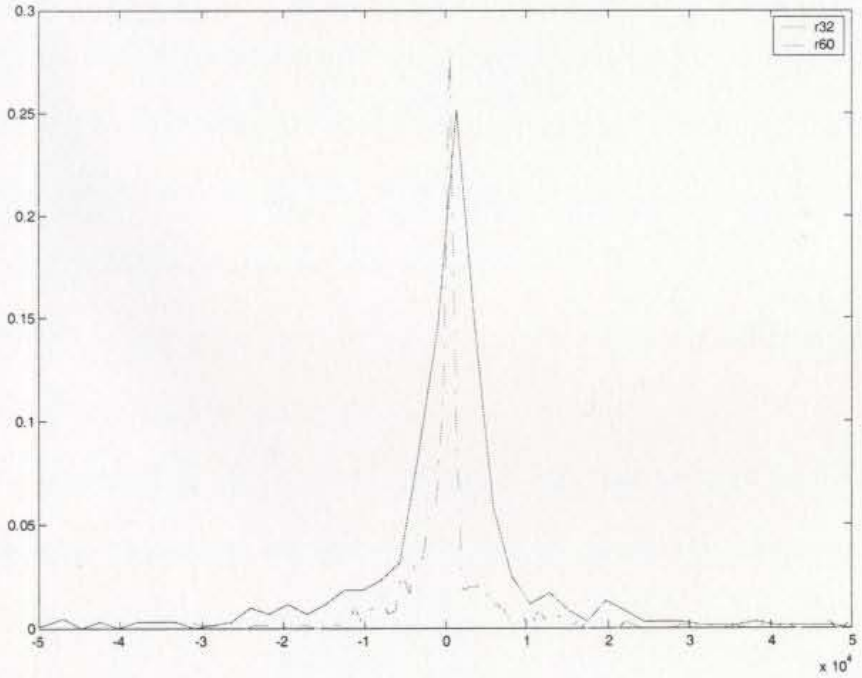

Figure 5-46 Probability distribution of Nv Different thickness: r32(pack50) and r60(pack30)

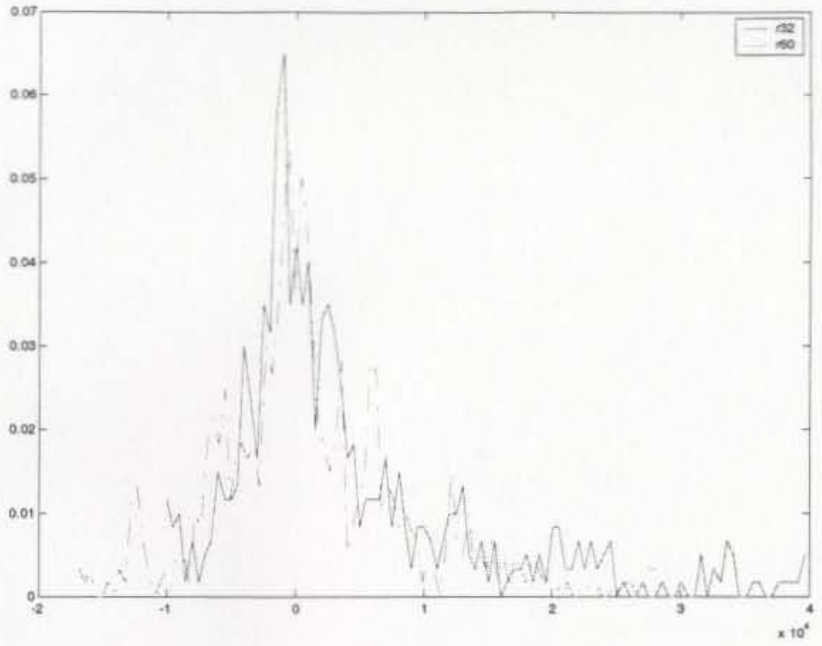

Conclusion:

- In general, the distributions of coefficients are concentrated on a small range of values in comparison with the whole range of possible values of coefficients.
- The coefficients' distributions for tests in same ice condition are similar.
- The coefficients' distributions for broken ice tests have a narrow range of values (smaller standard deviation) compared to that of level ice tests.
- Different broken ice tests (pack, rubble, thick rubble) show the same magnitude of the data range of coefficients.
- The coefficients' distributions for tests in the thinner level ice have a narrow range of values compared to that of thicker level ice tests. (Coefficients in thicker ice are large because force magnitudes are larger.)

- Broken ice tests with different thickness (pack, rubble, thick rubble) show the same magnitude of the data range of coefficients.

5.4.3 Regression Analysis

From the analysis presented in previous sections of this chapter, we have a better understanding of the ice force and moment caused by ship's sway velocity and angular velocity (yaw rate) when it performs maneuvers. The high frequency part in the force is produced by the sway velocity and low frequency part is produced by the yaw rate. But the complexity of the ship-ice interaction means that the methods to extract linear coefficients used in open water condition are inappropriate. The local force and moment cannot be accurately predicted using the linear equations derived in chapter 3 and coefficients calculated using the neural network program. We now focus on the average value of the tests.

We consider a regressed best-fit expression to describe the trend in total measured force as a function of the key ship motion parameters. A regression was run on the average test data to establish a single best-fit expression for the model ice force and moment as a function of model sway velocity and yaw rate.

Table 5-1 presents the average value of the coefficients obtained from the neural network calculation. The average coefficients, yaw moment, sway force and radius / length ratio are shown. The turning radius is prescribed and fixed. The last column of table 5-1 shows the radius ratio calculated using the predicted coefficients.

Table 5-2 presents the mean values of the main parameters in a series of constant radius tests. We can observe that the magnitude of the ice force is similar between two sets of tests with different friction coefficients mentioned in chapter 4, that is to say the influence of friction coefficients on ship maneuverability is not apparent. This conclusion can also be found in [18].

According to the data in table 5-2, we can plot yaw moment v.s. yaw rate for three consecutive constant radius tests (3 yaw rates). Adding a trend line to every plot made some reasonable results. But this is a very rough result. We can use the mean value of a segment of data as a data point. Then we can plot these data points to get a more accurate result. Extensive trials were carried out to select the length of the data segment. Finally 100-point segment (2 second) was taken. Normally a two second segment of data includes at least 5 cycles because the main frequency of variation less than 2.5 Hz. (The main period is 0.4 second) Figure 5-47 shows the scattered plot using one-second-segment (50 points) average value as a point.

Figure 5-47 scatter plot of yaw moment v.s. yaw rate for one-second-segment mean values

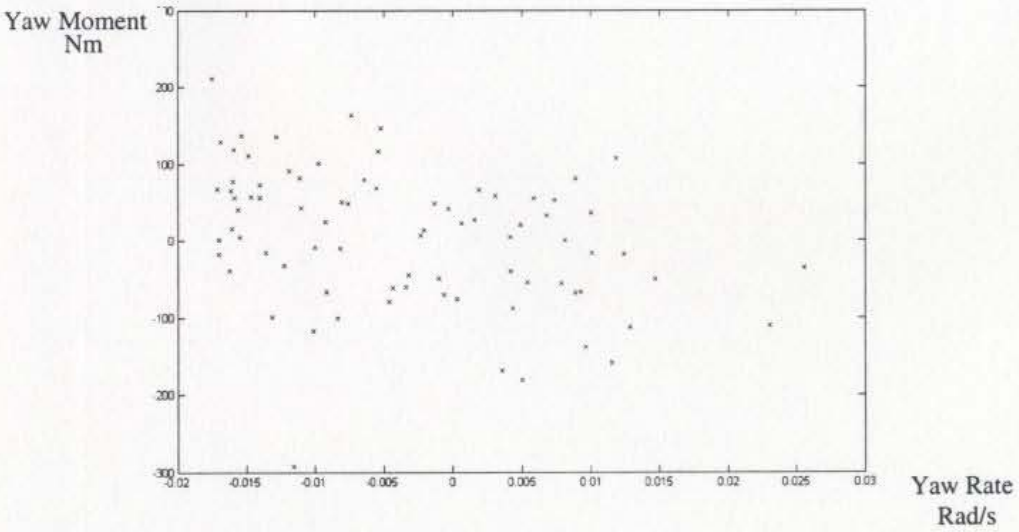

After the regression analysis for constant radius tests, we should take a look at sinusoidal tests. If we plotted all measured yaw moments v.s. yaw rates for the whole sinusoidal run, too much noise would hinder the success of the linear regression analysis. So, again, we took an average value for every 100 data points (2 second) of test data as a data point. For example, for a sinusoidal of 4000 data points (80 second), we got 40 average values. We replace the raw test data with the average value series and plot the average yaw moments vs yaw rates. Then we can add a trend line to every sinusoidal plot. The yaw rate dependent derivatives are displayed on the following plots. We can notice that the trend lines demonstrate the same consistency as that in constant radius tests.

For all the following regression scatter plots (figure 5-48 to figure 5-70), the x-axis is yaw rate or sway velocity, the y-axis is sway force or yaw moment. Every data point is an average value of 100 measured data points. The title of the figure indicates the file name, ice conditions, test pattern. The legend of the plot indicates the linear coefficients we pursued.

Table 5-1 coefficients (from neural network), PMM force and R/L

Filename	Test type	Thickness	Ice form	Yv	Yr	Nv	Nr	Ypmm	Npmm	R/L
rclassmano_001	sinusoidal	30 mm	level	-7416.2653	4358.2586	-9133.2066	5367.24			
rclassmano_017	Const. Radius	30 mm	level	540.86908	-1156.5814	524.56128	-1121.7091	-195.3843	-179.3903	1.9769
rclassmano_018	Const. Radius	30 mm	level	4958.8336	2181.5964	4911.2088	2160.6443	-166.8951	-68.3336	19.7269
rclassmano_019	Const. Radius	30 mm	level	-460.24247	-1596.3093	-517.93114	-1796.3972	-216.3069	-128.6914	4.1425
rclassmano_056	Const. Radius	30 mm	level	1568.3672	370.84261	1291.7664	305.43995	-200.4728	-175.027	1.9922
rclassmano_057	Const. Radius	30 mm	level	3669.6903	-3774.2532	3186.2912	-3277.0803	-179.9666	-113.4516	4.1976
rclassmano_058	Const. Radius	30 mm	level	1574.2132	-1082.4249	1566.3465	-1077.0158	-149.7567	-65.569	19.2238
rclassmano_002	sinusoidal	30 mm	pack	1197.6865	-1292.3449	1928.4461	-2080.8596			
rclassmano_021	Const. Radius	30 mm	pack	-14.224062	-581.63738	-10.431987	-426.57533	-53.2283	-70.5381	1.9246
rclassmano_022	Const. Radius	30 mm	pack	1391.415	2933.9124	834.45488	1759.5164	-53.5632	-54.4373	4.1884
rclassmano_023	Const. Radius	30 mm	pack	3256.1298	776.1871	2720.7845	648.57299	-41.3067	-22.912	19.4948
rclassmano_060	Const. Radius	30 mm	pack	658.9355	1003.3495	572.33078	871.47805	-63.3629	-87.5873	1.9878
rclassmano_061	Const. Radius	30 mm	pack	-131.77283	28.020624	-82.534091	17.550332	-52.1491	-58.8295	4.2277
rclassmano_003	sinusoidal	30 mm	20/10 rubble	12883.725	-543.21372	23264.758	-980.90696			
rclassmano_025	Const. Radius	30 mm	20/10 rubble	9040.7952	1375.6748	7979.0258	1214.1128	-87.8439	-56.3377	4.0962
rclassmano_063	Const. Radius	30 mm	20/10 rubble	2199.7891	-916.21993	2561.7252	-1066.9676	-106.1653	-105.9363	1.9399
rclassmano_064	Const. Radius	30 mm	20/10 rubble	-531.49484	921.94558	-374.41868	649.47695	-101.3431	-57.1397	4.1400
rclassmano_004	sinusoidal	30 mm	30/10 rubble	1101.879	1714.9707	1366.0882	2126.1875			
rclassmano_026	Const. Radius	30 mm	20/10 rubble	913.19727	273.53976	633.84944	189.86371	-128.1441	-57.9167	4.1599
rclassmano_066	Const. Radius	30 mm	30/10 rubble	-669.47625	1285.635	-498.12743	956.58372	-127.0519	-66.7636	4.1358

rclassmano_040	sinusoidal	50 mm	level	8126.8734	106541420	515858090	127753400			
rclassmano_067	Sinusoidal	50 mm	level	2628.7958	30018.698	3135.5929	35805.906			
rclassmano_028	Const. Radius	50 mm	level	6211.8276	18411.957	4191.4011	12423.381	-401.0007	-313.0238	1.9540
rclassmano_029	Const. Radius	50 mm	level	8272.6369	9284.5597	8185.6447	9186.9266	-383.8869	-205.2991	4.1851
rclassmano_030	Const. Radius	50 mm	level	8383.5537	6988.3818	7274.3007	6063.7282	-332.1692	-130.8156	18.8586
rclassmano_045	Const. Radius	50 mm	level	6100.7325	14342.093	5185.6233	12190.781	-370.9582	-293.0964	1.9900
rclassmano_046	Const. Radius	50 mm	level	5903.224	-10179.115	3465.9054	-5976.3695	-365.4292	-226.9234	4.2111
rclassmano_047	Const. Radius	50 mm	level	7379.1405	42.063987	7745.6417	44.153208	-309.9494	-100.1553	20.0035
rclassmano_032	Const. Radius	50 mm	pack	-63.401848	3889.1475	-64.64657	3965.501	-133.4709	-119.9634	1.9805
rclassmano_033	Const. Radius	50 mm	pack	414.63267	3832.4199	489.19303	4521.576	-83.0247	-73.7086	4.1990
rclassmano_034	Const. Radius	50 mm	pack	-608.10419	-900.24941	-599.55875	-887.59856	-112.0249	-24.7008	19.5733
rclassmano_049	Const. Radius	50 mm	pack	-614.1819	-2292.3233	-514.70221	-1921.0333	-87.1727	-93.1496	1.9955
rclassmano_050	Const. Radius	50 mm	pack	1597.3349	5229.0581	1255.2184	4109.1007	-78.9356	-44.766	4.2206
rclassmano_042	sinusoidal	50 mm	pack	-278.73149	1425.5032	-376.6798	1926.4356			
rclassmano_035	Const. Radius	50 mm	20/10 rubble	-2751.5977	-2044.0075	-3426.8862	-2545.6415	-130.3789	-130.1131	1.9579
rclassmano_036	Const. Radius	50 mm	20/10 rubble	178.82112	3690.779	180.57039	3726.883	-172.3603	-98.5204	4.1723
rclassmano_052	Const. Radius	50 mm	20/10 rubble	-2249.9491	679.02444	-2260.9932	682.35747	-95.0393	-116.22	1.9690
rclassmano_053	Const. Radius	50 mm	20/10 rubble	335.82151	153.43219	244.07572	111.51481	-128.361	-79.228	4.1969
rclassmano_043	sinusoidal	50 mm	30/10 rubble	1557.5132	-1139.3847	1720.9477	-1258.9438			
rclassmano_037	Const. Radius	50 mm	30/10 rubble	270.83031	1277.7656	338.49706	1597.0144	-222.2017	-99.6466	4.1687
rclassmano_054	Const. Radius	50 mm	20/10 rubble	1351.1039	43.180826	1159.8778	37.069299	-132.5196	-81.3796	4.1687

Table 5-2 Average values of PMM force, sway velocity and yaw rate

Filename	Condition	Ypmm	Npmm	v	r
rclassmano_017	level 30	-195.3843	-179.3903	0.0596	0.0629
rclassmano_018	level 30	-166.8951	-68.3336	0.0542	0.0063
rclassmano_019	level 30	-216.3069	-128.6914	0.0654	0.0297
rclassmano_056	level 30	-200.4728	-175.027	0.0569	0.0626
rclassmano_057	level 30	-179.9666	-113.4516	0.0634	0.0295
rclassmano_058	level 30	-149.7567	-65.569	0.0518	0.0064
rclassmano_021	Pack 30	-53.2283	-70.5381	0.057	0.0635
rclassmano_022	Pack 30	-53.5632	-54.4373	0.0646	0.0294
rclassmano_023	Pack 30	-41.3067	-22.912	0.0545	0.0063
rclassmano_060	Pack 30	-63.3629	-87.5873	0.063	0.0629
rclassmano_061	Pack 30	-52.1491	-58.8295	0.0644	0.0293
rclassmano_025	Rubble 30	-87.8439	-56.3377	0.0634	0.0297
rclassmano_026	30/10 Rubble 30	-128.1441	-57.9167	0.0669	0.0294
rclassmano_063	Rubble 30	-106.1653	-105.9363	0.0544	0.0626
rclassmano_064	Rubble 30	-101.3431	-57.1397	0.063	0.0295
rclassmano_066	30/10 Rubble 30	-127.0519	-66.7636	0.0643	0.0294
rclassmano_028	level 50	-401.0007	-313.0238	0.0633	0.0628
rclassmano_029	level 50	-383.8869	-205.2991	0.0667	0.0293
rclassmano_030	level 50	-332.1692	-130.8156	0.0548	0.0065
rclassmano_047	level 50	-370.9582	-293.0964	0.056	0.0627
rclassmano_046	level 50	-365.4292	-226.9234	0.0642	0.0294
rclassmano_045	level 50	-309.9494	-100.1553	0.0521	0.0062
rclassmano_032	Pack 50	-133.4709	-119.9634	0.0579	0.063
rclassmano_033	Pack 50	-83.0247	-73.7086	0.0632	0.0295
rclassmano_034	Pack 50	-112.0249	-24.7008	0.0541	0.0063
rclassmano_049	Pack 50	-87.1727	-93.1496	0.0615	0.0627
rclassmano_050	Pack 50	-78.9356	-44.766	0.0622	0.0294
rclassmano_052	Rubble 50	-95.0393	-116.22	0.0627	0.0629
rclassmano_035	Rubble 50	-130.3789	-130.1131	0.0673	0.0632
rclassmano_036	Rubble 50	-172.3603	-98.5204	0.0691	0.0294
rclassmano_037	30/10 Rubble 50	-222.2017	-99.6466	0.0674	0.0294
rclassmano_053	Rubble 50	-128.361	-79.228	0.0657	0.0293
rclassmano_054	30/10 Rubble 50	-132.5196	-81.3796	0.0671	0.0294

The following plots are the linear regression results

Figure 5-48 regression on r of level 30 C. radius r17-r19 and r56 – r58

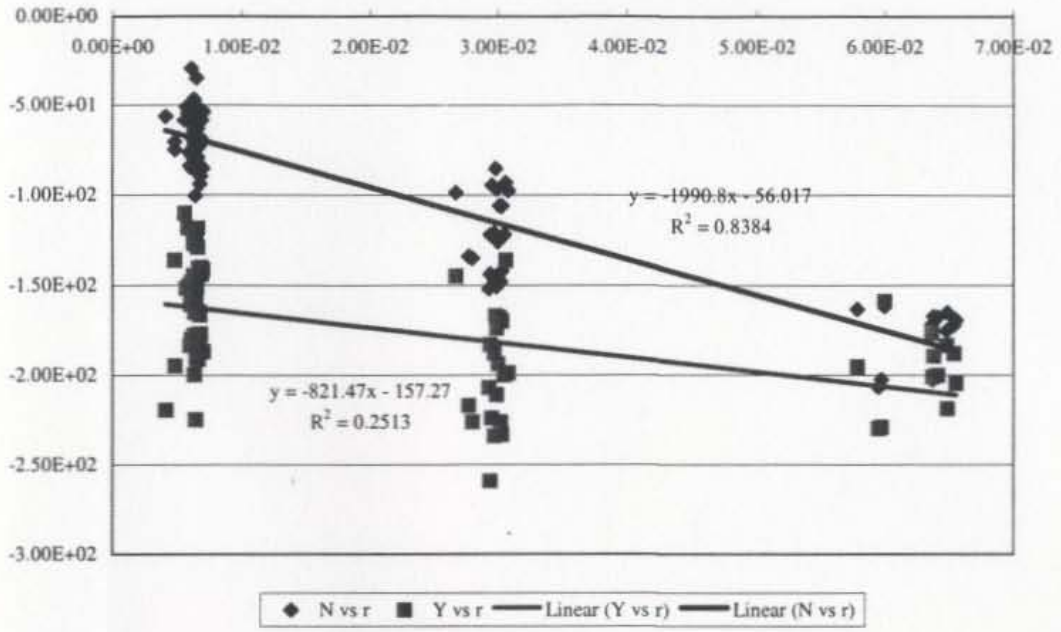

Figure 5-49 regression on v of level 30 C. radius r17-r19 and r56 – r58

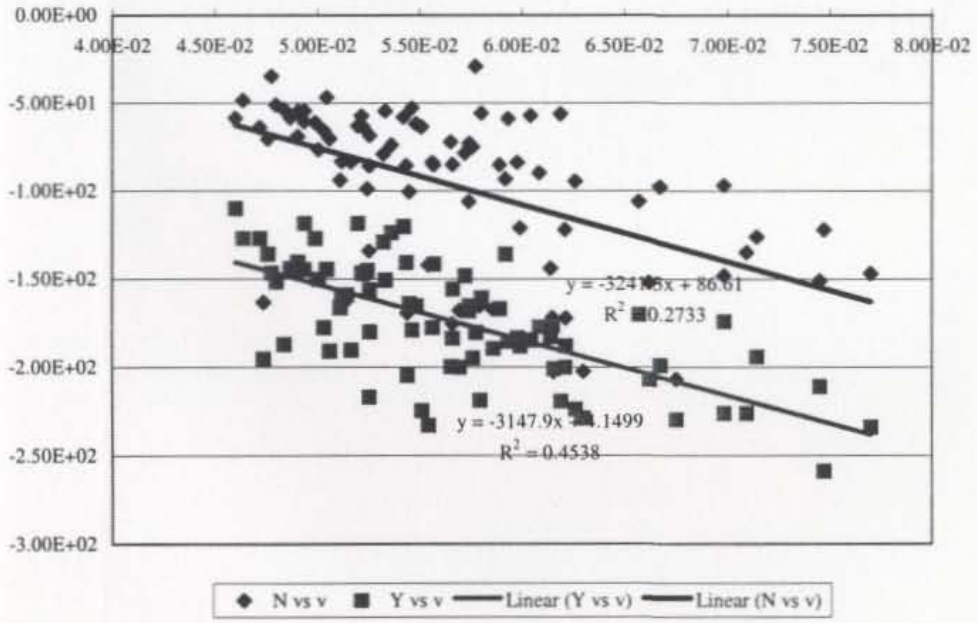

Figure 5-50 regression result of level 30 sinusoidal r01

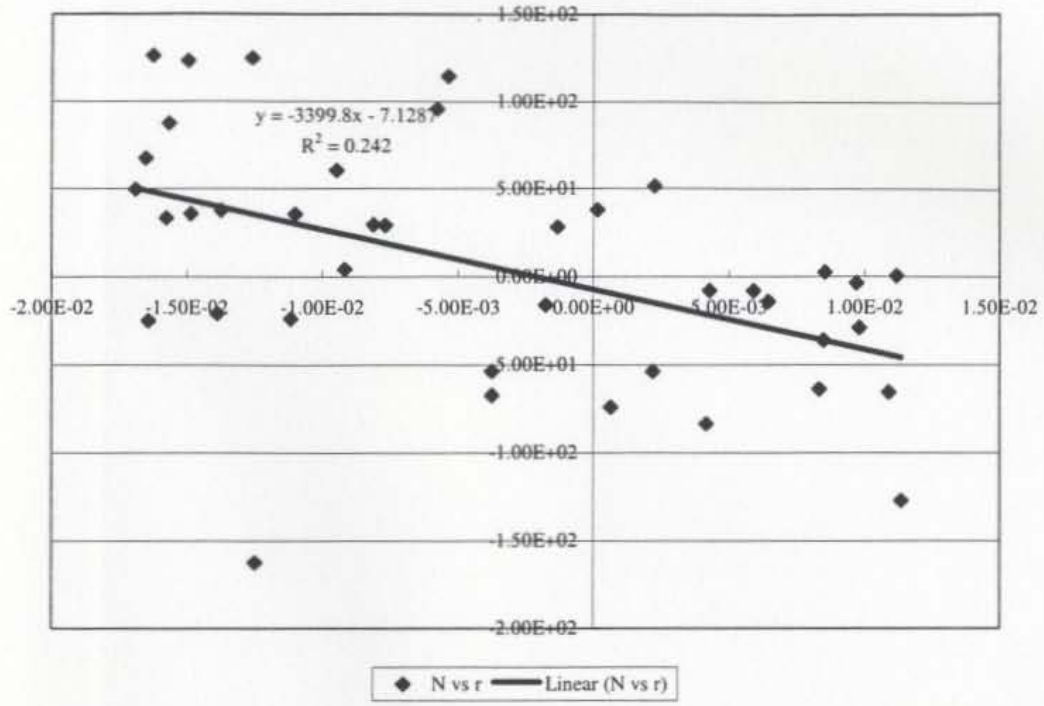

Figure 5-51 Regression result of pack 30 sinusoidal r02

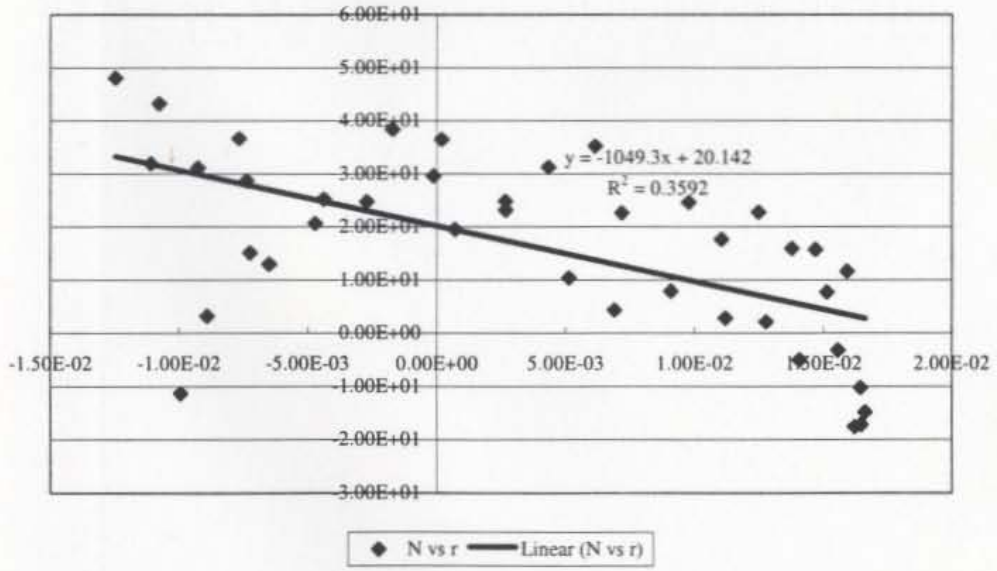

Figure 5-52 Regression result of pack 30 sinusoidal r02

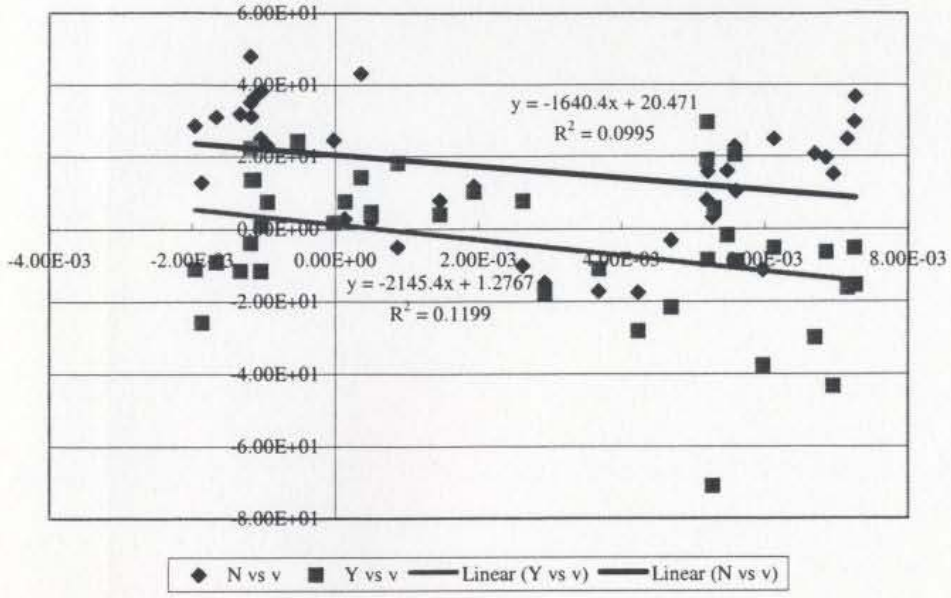

Figure 5-53 Regression result of pack 30 r21-r23 r60-r62

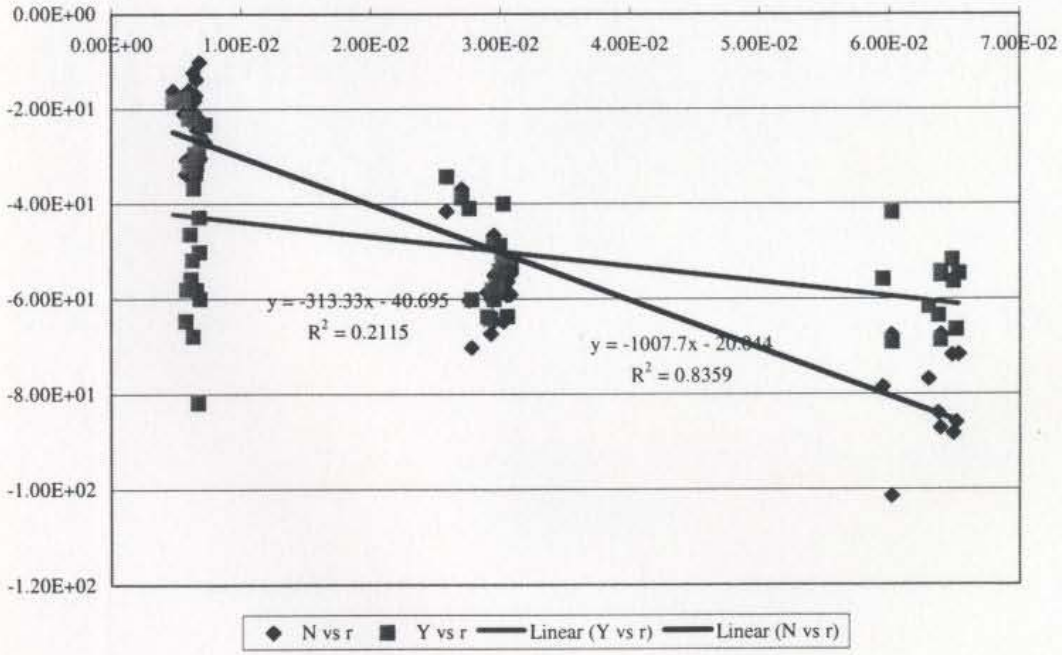

Figure 5-54 Regression result of Pack 30 r21-r23 r60-r62

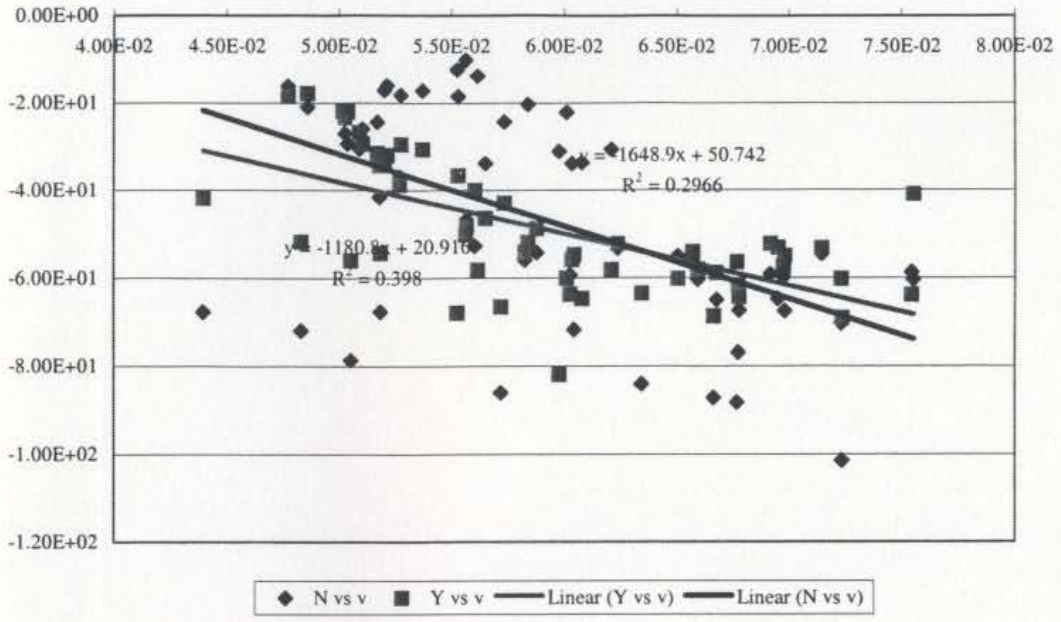

Figure 5-55 Regression result of Rubble 30 sinusoidal r03

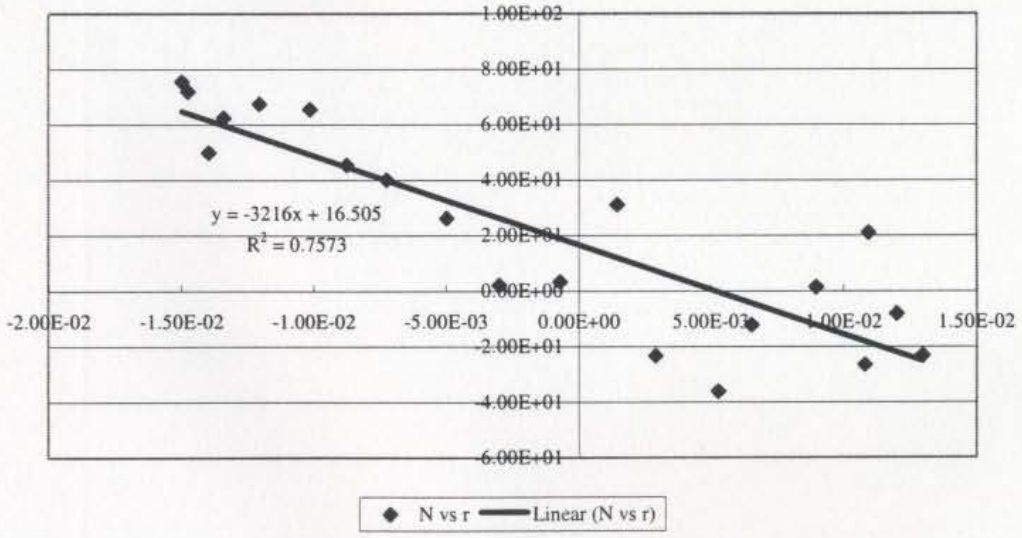

Figure 5-56 Regression result of Rubble 30 sinusoidal r03

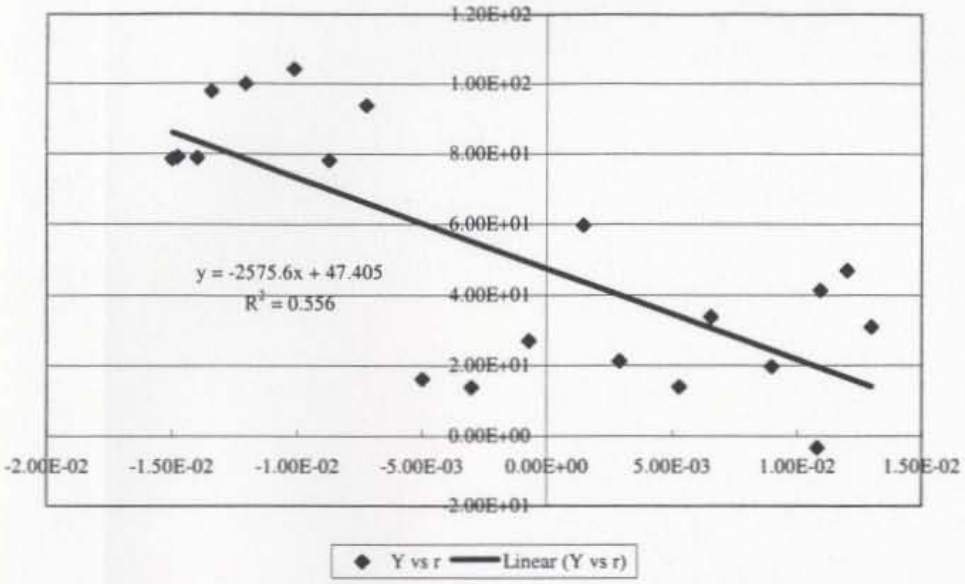

Figure 5-57 Regression result of Rubble 30 sinusoidal r03

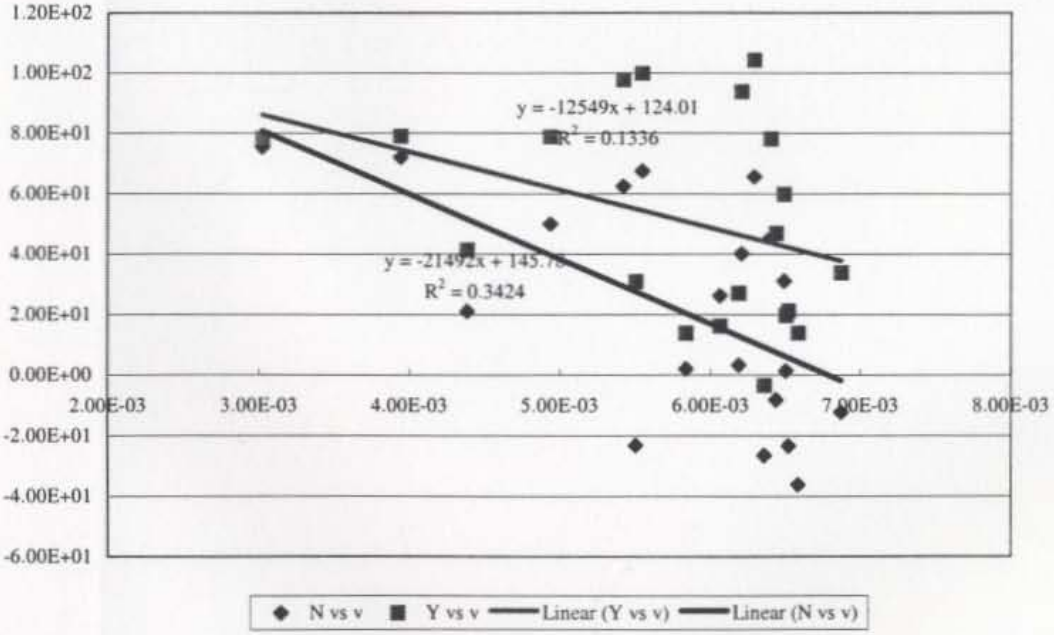

Figure 5-58 Regression result of level 50 C. Radius r24-r25 r63-r64

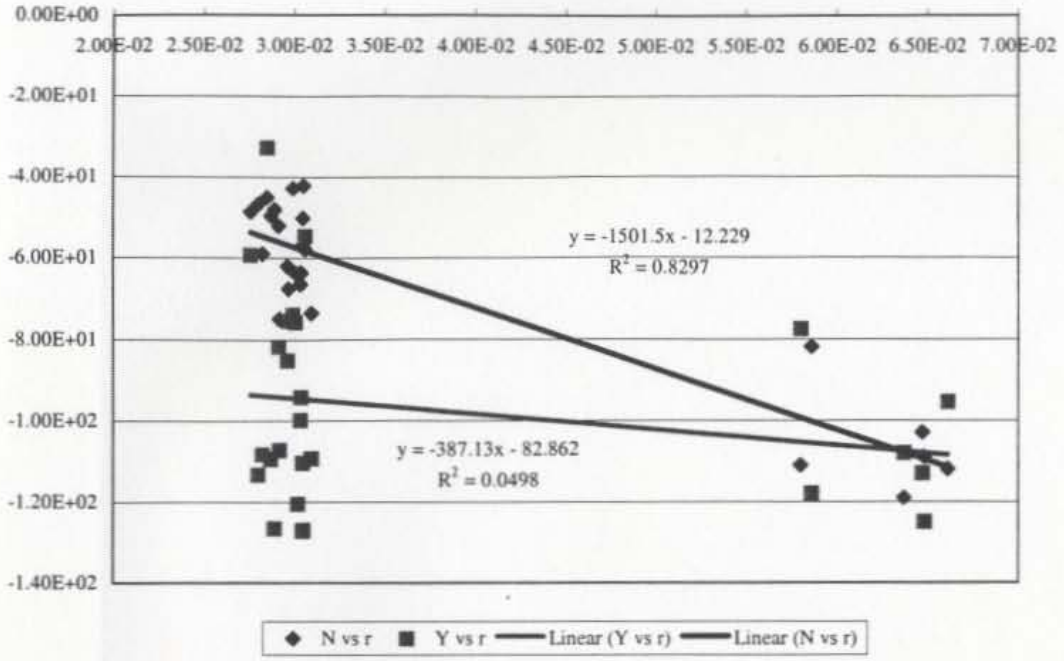

Figure 5-59 Regression result of level 50 C. radius r28-r30 r45-r47

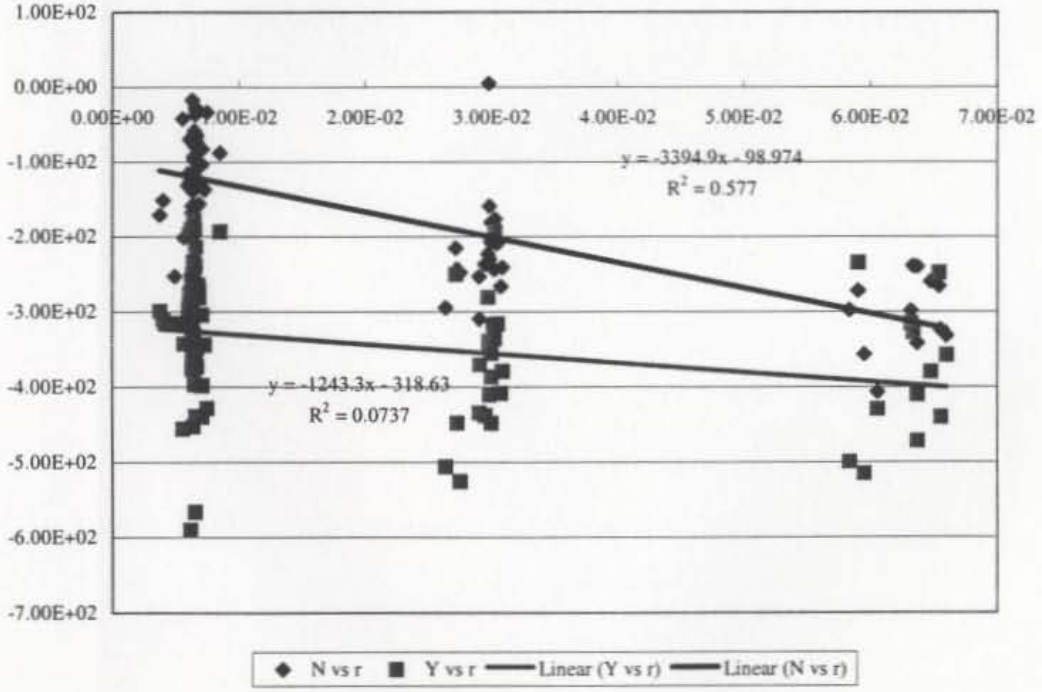

Figure 5-60 Regression result of level 50 sinusoidal r40

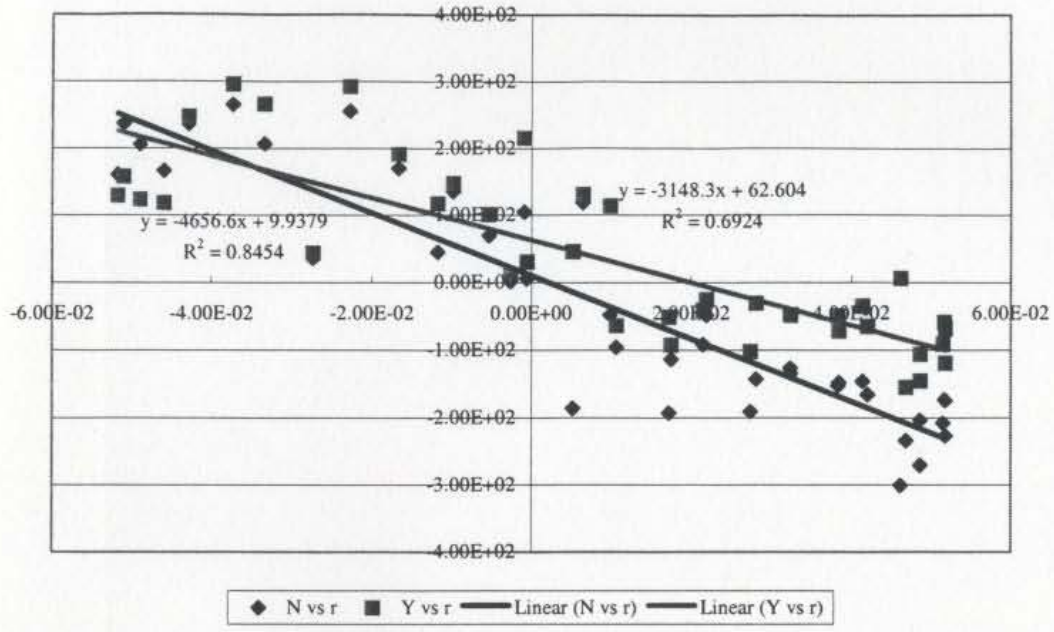

Figure 5-61 Regression result of level 50 sinusoidal r67

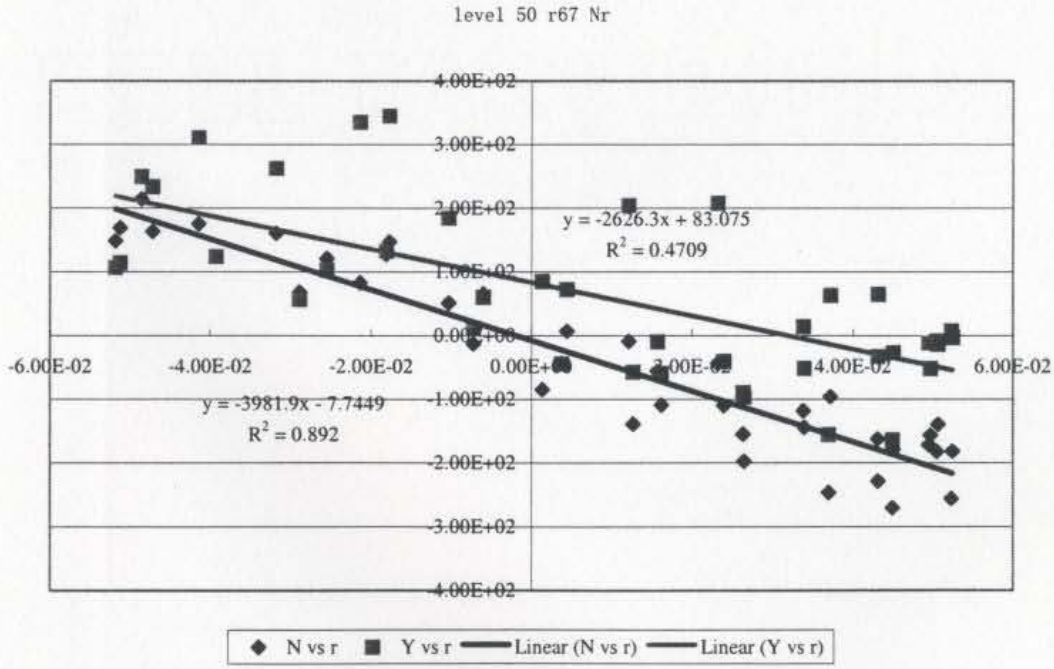

Figure 5-62 Regression result of level 50 sinusoidal r67

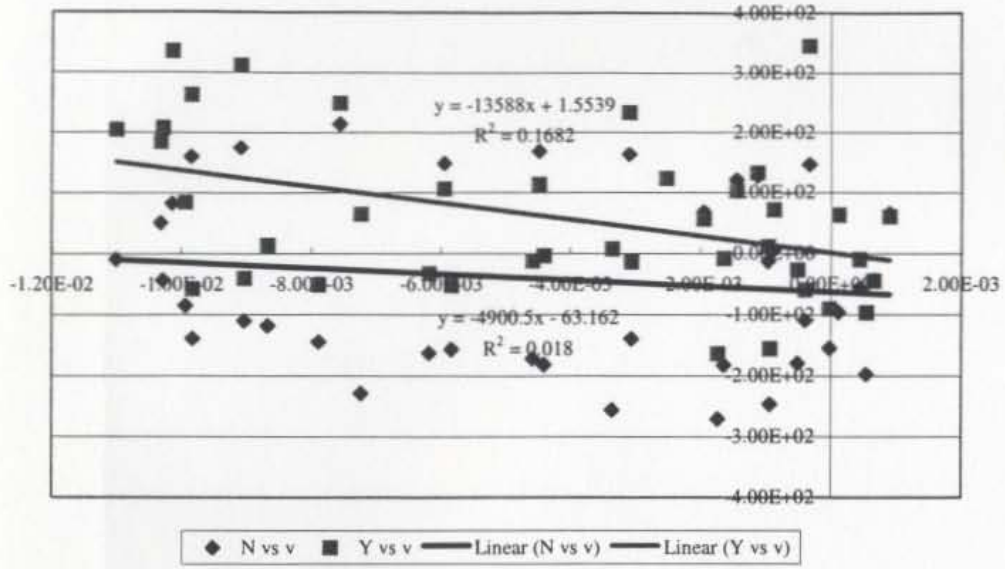

Figure 5-63 Regression result of Pack 50 sinusoidal r41

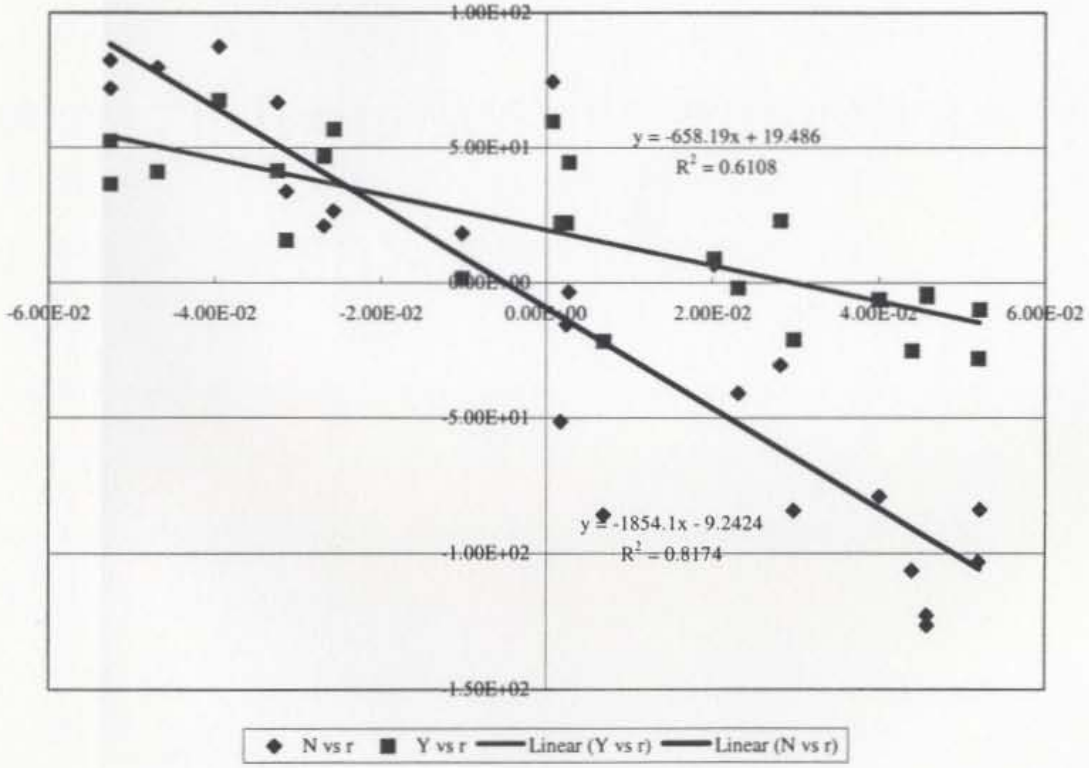

Figure 5-64 Regression result of rubble 50 sinusoidal r42

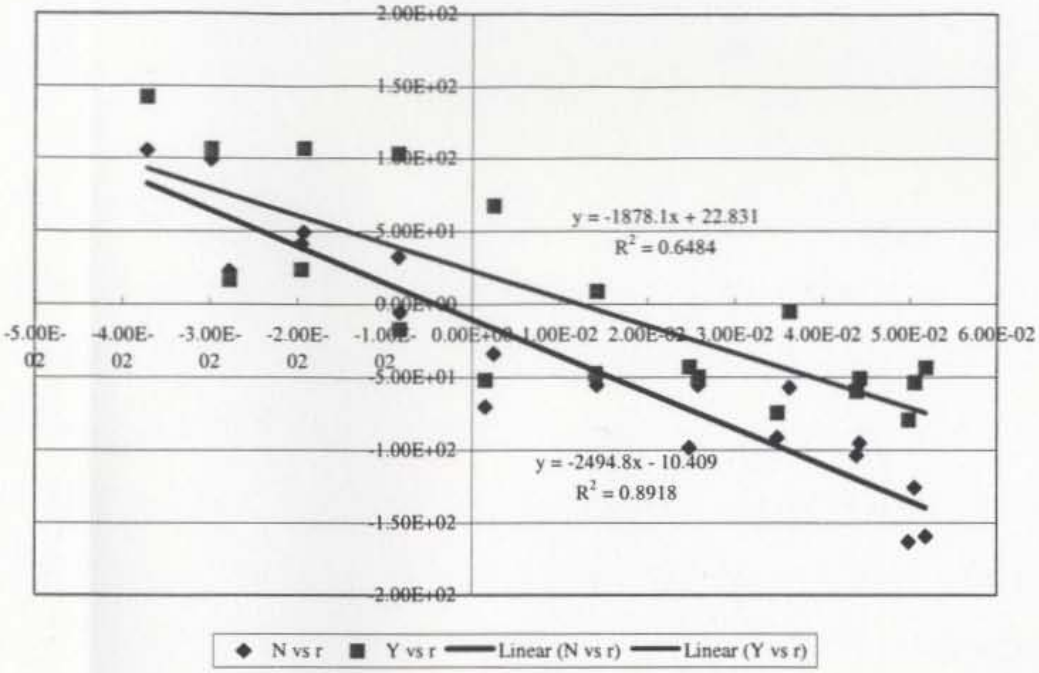

Some results of the linear regression analysis are clearly illustrated by these plots. The goodness of fit of linear regression is different in various ice conditions. Test data in 50mm ice sheet is more convergent to their trend line than the test data in 30mm ice. (refer to Figure 5-50 and Figure 5-60). The linear coefficients we pursued in this work are Nr Yr Nv Yv. Apparently, the results of Nr and Yr are much more reliable than that of Nv Yv. We try to find the correct coefficients with constant radius test data and sinusoidal test data. It is better to make a summary for all the results. (see table 5-3) Please note the linear coefficients we got is the negative value (equations 3-17).

$$-Y_v v-(Y_r-\Delta u_1)r=Y_{pmm}$$

$$-N_v v-N_r r=N_{pmm}+N_{prop}$$

According to the equations, we should change the linear differentiated coefficients to positive and add the term Δu_1 to obtain the Yr. Where Δ is the mass of the model, 965Kg;

and u_1 is the initial forward speed, 0.6 m/s in this test. In the linear regression analysis, we manually removed some strange points in the scatter plots to get the most accurate linear coefficients.

In the sinusoidal test plots, we found the different slopes in different phases of a sinusoidal maneuver. When the ship performs a sinusoidal maneuver, because of the rapid turning direction, especially at the moment of the negative yaw rate changing to positive yaw rate, the midbody of the ship is required to break additional ice to achieve the turn. So in this phase, the yaw rate dependent coefficient Nr is larger than other phases in a sinusoidal maneuver. This phenomenon is not apparent in a thin ice sheet. But we can observe it in thicker ice condition. We divided a sinusoidal test to three phases: lower yaw rate (negative), mid yaw rate (near zero) and higher yaw rate (positive). The results are given as following figures.

Figure 5-65 regression for level 50 r40 low yaw rate

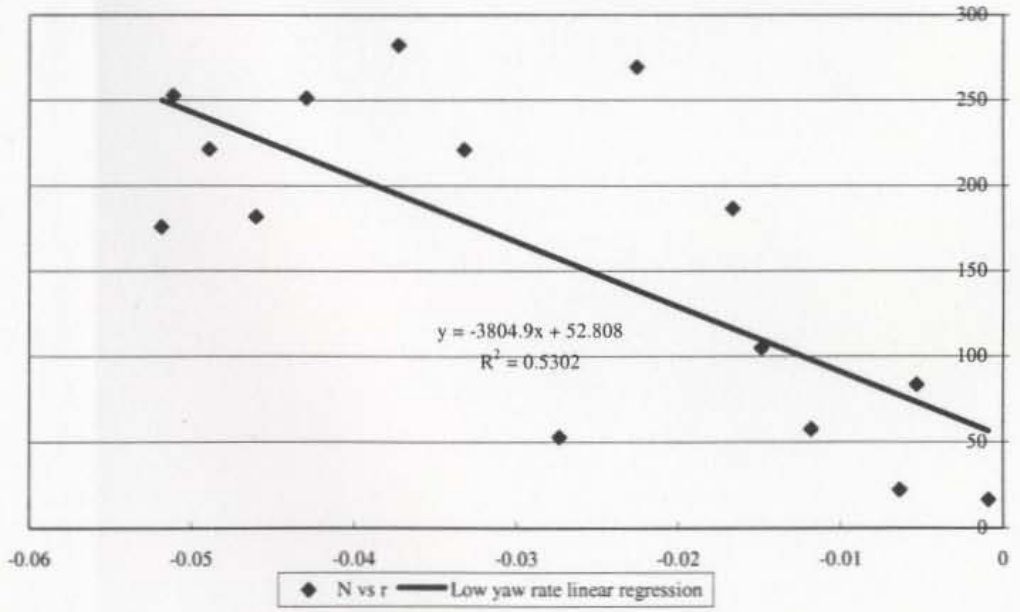

Figure 5-66 regression for level 50 r40 higher yaw rate

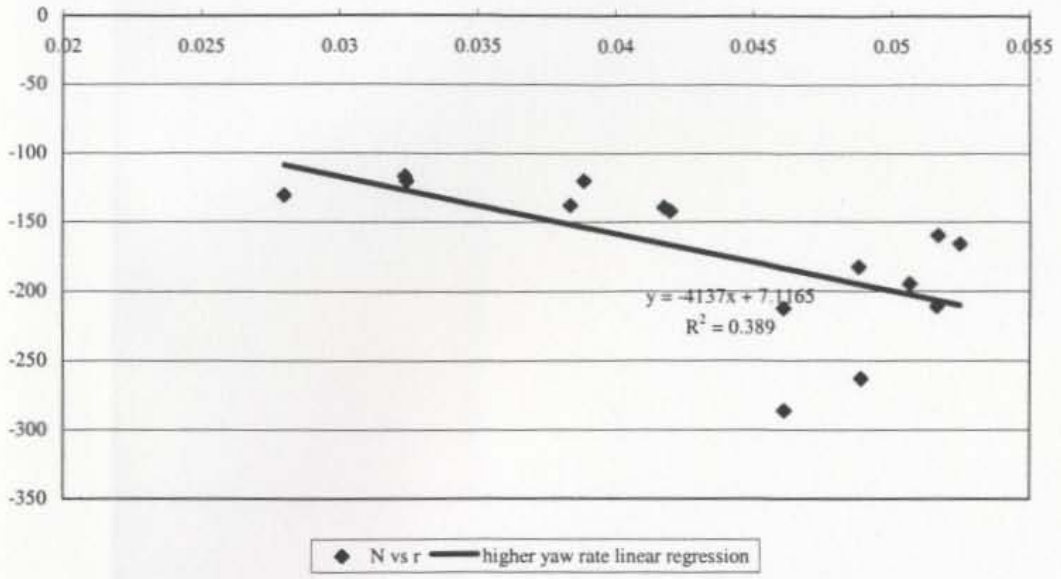

Figure 5-67 regression for level 50 r40 medium yaw rate

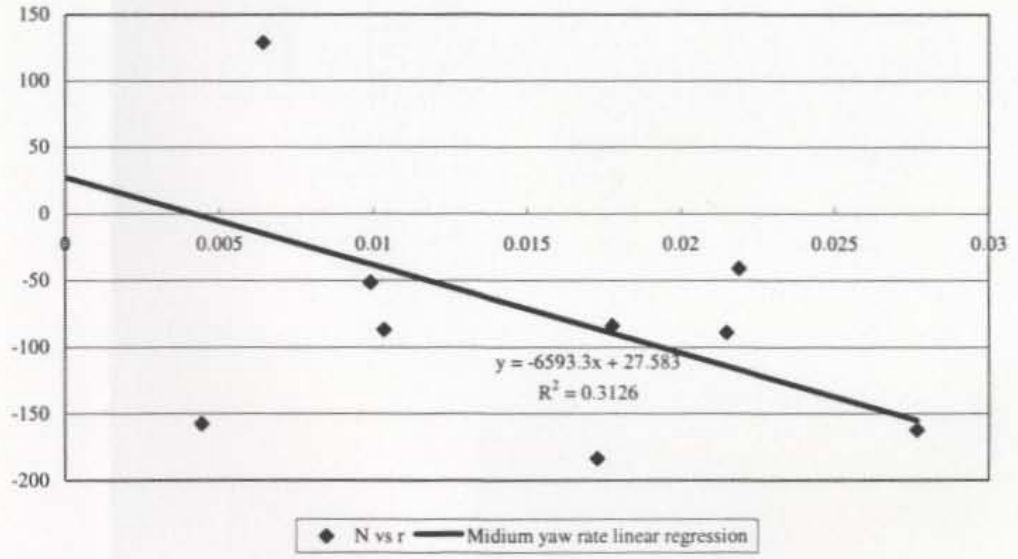

Another Level 50 sinusoidal test

Figure 5-68 regression for level 50 r67 lower yaw rate

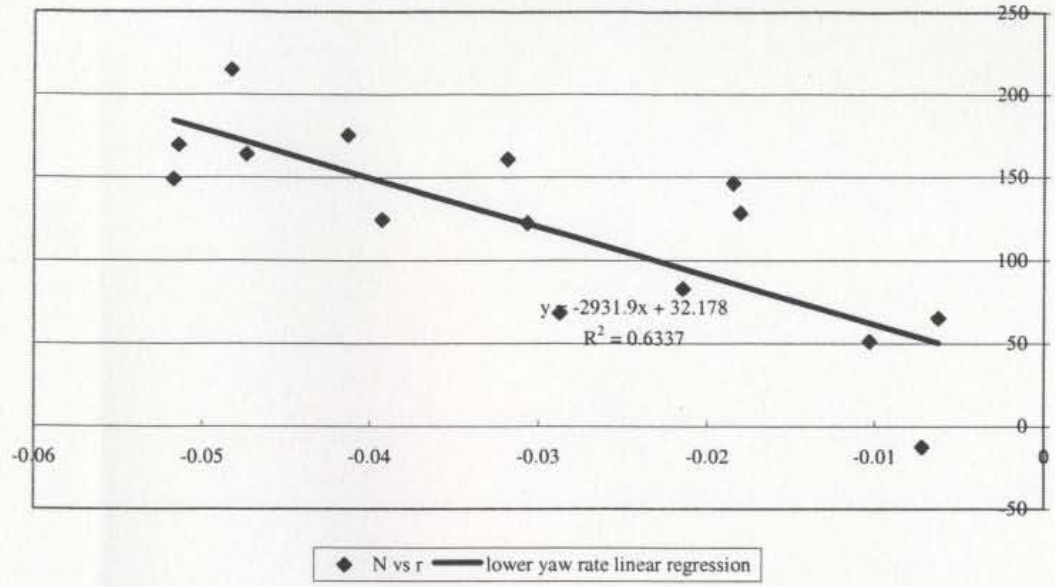

Figure 5-69 regression for level 50 r67 higher yaw rate

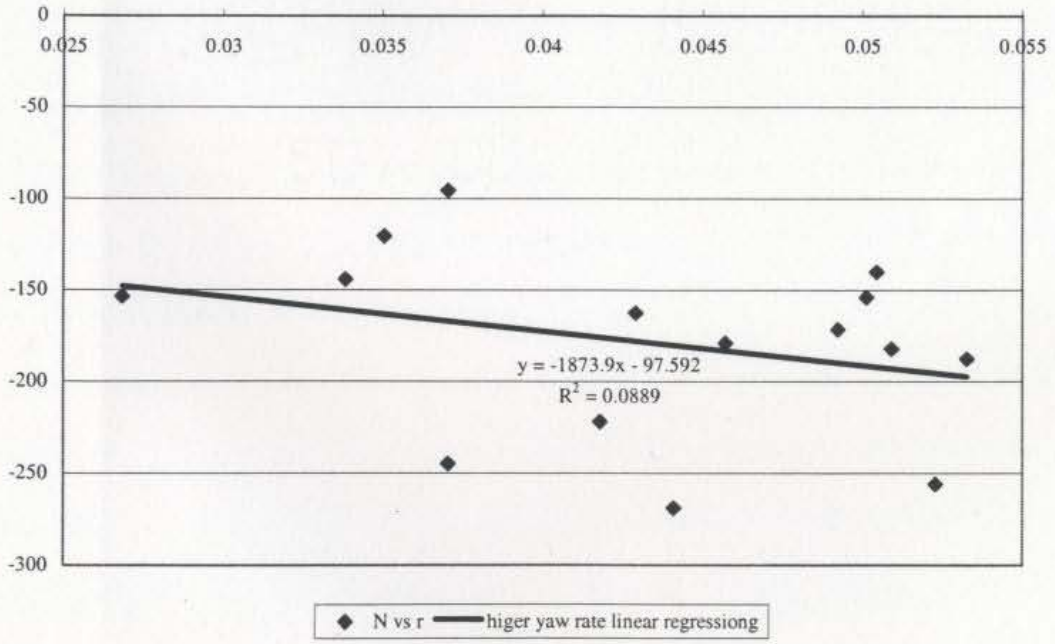

Figure 5-70 regression for level 50 r67 medium yaw rate

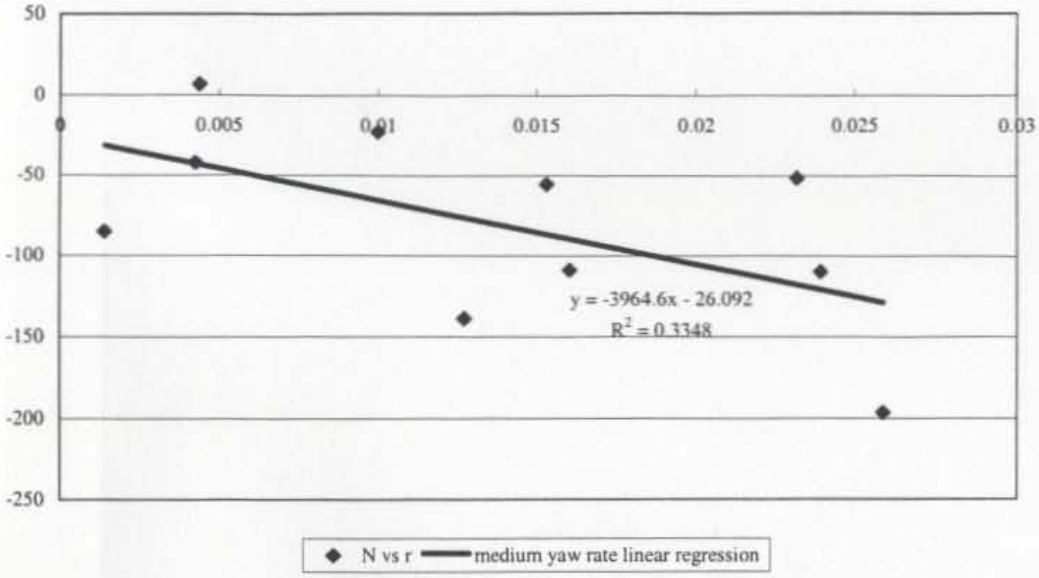

This can explain why the Nr calculated from the sinusoidal test is higher than that of constant radius test. Different physics governs in these two different maneuvers. In the constant radius test, just the bow and one side of the hull take a part in the breaking ice. In sinusoidal test, during the lower and higher yaw rate part, the ship experiences same physics as in the constant radius test. But in the part of that yaw rate changes from negative to positive, both sides of the ship hull have to break the ice sheet. The regression results of Nr obtained from the sinusoidal test are average values in the whole run. So we chose yaw rate dependent coefficients from constant radius tests. But the values of Nv and Yv obtained from constant radius tests are very strange and unstable due to a limited range of sway velocities during the test. So we try to find sway velocity dependent coefficients from sinusoidal test. A larger range of sway velocity is observed during the sinusoidal test. Considering the sway velocity's influence on ice force in the sinusoidal test displayed in Figure 5-21, 5-22, 5-27, sway velocity term $-Y_v v$ and $-N_v v$ should be

added to the left hand side of equations 3-17. The more reliable linear coefficients Nv and Yv can be obtained from the regression analysis of sinusoidal test data.

After carefully reviewing and comparing the regression results from different test data, we determined the four coefficients for eight ice conditions. The final results presented in the row of "summary" in table 5-3. N.A. means we cannot extract the reasonable coefficients from available test data.

Table 5-3 Summary of Coefficients

Ice condition	Data	Yv	Yr	Nv	Nr
30 level	sinusoidal r01	9249.3	1076.5	3255.5	3399.8
30 level	constant radius r17-r19	4401.9	1006.35	5214.9	1933
30 level	constant radius r56-r58	2345.9	1461.86	3517.6	1941.6
30 level	Combination r17-r19 and r56-r58	3147.9	1400.47	3241.3	1990.8
30 level	summary	9249.3	1400.47	3255.5	1990.8
30 pack	sinusoidal r02	3923.9	792.94	1640.4	1049.3
30 pack	constant radius r21-r23	940.49	833.73	1898	898.05
30 pack	constant radius r60-r62	N.A.	1065.01	N.A.	1080.6
30 pack	Combination r17-r19 and r56-r58	1180.8	892.33	1648.9	1007.7
30 pack	summary	3923.9	892.33	1640.4	1007.7
30 rubble	sinusoidal r03	12549	3154	16841	3216
30 rubble	constant radius r24-r25	N.A.	1370.97	N.A.	939.12
30 rubble	constant radius r63-r64	N.A.	724.69	N.A.	1474.2
30 rubble	Combination r24-r25 and r63-r64	1969.6	966.1	N.A.	1501.5
30 rubble	summary	12549	966.1	16841	1501.5
30 rubble 30/10	sinusoidal r04	29645	7601.5	39747	5412.1
30 rubble 30/10	constant radius r26 r66	N.A.	6893.9	N.A.	1199
30 rubble 30/10	summary	29645	6893.9	39747	1199
50 level	sinusoidal r40	7919.5	3727.3	9488.3	4656
50 level	sinusoidal r67	13588	3205.3	4900.5	3981.9
50 level	constant radius r28-r30	5067.5	1748.6	9177.8	3234.8
50 level	constant radius r45-r47	3774.8	1595.3	7619.3	3315.7
50 level	Combination r28-r30 and r45-r47	2852.8	1822.3	5933.8	3394.9
50 level	summary	13588	1822.3	4900.5	3394.9
50 pack	sinusoidal r41	N.A.	1237.19	N.A.	1854.1
50 pack	sinusoidal r69	N.A.	639.39	N.A.	1047.3
50 pack	constant radius r21-r23	5643.7	1037.04	5385.5	1658.9
50 pack	constant radius r60-r62	N.A.	1065.01	N.A.	1080.6
50 pack	Combination r21-r23 and r60-r62	7517.6	N.A.	2193.7	1447
50 pack	summary	7517.6	1037.04	2193.7	1447
50 rubble	sinusoidal r42	21833	5320.1	16756	4505.8
50 rubble	constant radius r35-r36	N.A.	N.A.	N.A.	934.7
50 rubble	constant radius r63-r64	N.A.	724.69	N.A.	1474.2
50 rubble	Combination r35-r36 and r63-r64	4580.5	N.A.	4247.5	1065.3
50 rubble	summary	21833	724.69	16756	1474.2
50 rubble 30/10	sinusoidal r43	N.A.	6026.2	N.A.	5069.3
50 rubble 30/10	constant radius r37, r54	20779	8090.5	11927	N.A.
50 rubble 30/10	summary	20779	8090.5	11927	5069.3

5.5 Turning Radius Prediction

We can use the basic equations 3-17 derived from Chapter 3 and the coefficients obtained from last section to develop a Turning Radius Predictor.

In the PMM model test, the basic equations 3-17 in steady turning motion are:

$$-Y_v v - (Y_r - \Delta u_1) r = Y_{pmm}$$

$$-N_v v - N_r r = N_{pmm} - N_{prop}$$

In steady state constant turning maneuver,

$$r = \frac{d\psi}{dt} = \frac{V}{R} \tag{5.7}$$

So, turning radius R is

$$R = \frac{V}{r} \tag{5.8}$$

After transformation and simplification, we obtain turning radius-ship length ratio:

$$\frac{R}{L} = \frac{V}{L}\left[\frac{Y_v N_r - N_v (Y_r - \Delta \cdot V)}{Y_{pmm} N_v - N_{pmm} Y_v}\right] \tag{5.9}$$

Table 5-4 presented the results calculated by using equation 5-9, corresponding coefficients and measured test data. (The last column is the real turning radius ratio)

In the constant radius turning maneuver for real ship, the ship dynamic equations are given by:

$$\begin{aligned} -Y_v v - (Y_r - \Delta u_1) r &= Y_\delta \delta_R \\ -N_v v - N_r r &= N_\delta \delta_R \end{aligned} \tag{5.10}$$

Where

δ_R . the rudder angle:

Y_δ . the rudder force coefficient on rudder angle:

N_δ . the moment coefficient on rudder angle.

Replacing the PMM forces with rudder forces $Y_\delta \delta_R$ and $N_\delta \delta_R$. we get

$$\frac{R}{L} = \frac{V}{L}\left[\frac{Y_v N_r - N_v (Y_r - \Delta \cdot V)}{Y_\delta \delta_R N_v - N_\delta \delta_R}\right] \qquad (5.11)$$

It is convenient to use an empirical method to obtain rudder coefficients Y_δ and N_δ . Hence equation 5.11 can be used as a helpful tool to predict a ship's turning radius in various ice conditions. The Captain can simply calculate the turning radius if she/he knows the ship speed and the executed rudder angle. The accuracy of the prediction depends on the precision of the coefficients.

The following table 5-4 shows the accuracy of the prediction:

1. Regression analysis was carried out for sinusoidal test together with constant radius test data to obtain 4 coefficients.
2. The sway velocity dependent coefficients are fairly unreliable.
3. The R/L2 is calculated by the formula $R = \frac{V}{r}$
4. The R/L is calculated by the equation 5.9.
5. To compare the R/L and R/L2, some results, such as in 50 mm level ice, 30mm level ice, 30mm pack ice, give satisfactory predictions.

6. With reliable sway velocity dependent coefficients from tests, we could develop a more accurate predictor for ship's turning radius in ice and validate with full-scale ship data.

Table 5-4 Results of Turning Radius Prediction

Filename	Test type	Thickness	form	Yv	Yr	Nv	Nr	Ypmm	Npmm	R/L	R/L2	Error
rclassmano_001	sinusoid	30 mm	level	9249.3	1400.47	3255.5	1990.8					
rclassmano_017	Const. Radius	30 mm	level	9249.3	1400.47	3255.5	1990.8	-195.3843	-179.3903	1.9045	1.9769	3.66%
rclassmano_018	Const. Radius	30 mm	level	9249.3	1400.47	3255.5	1990.8	-166.8951	-68.3336	21.9526	19.7269	11.28%
rclassmano_019	Const. Radius	30 mm	level	9249.3	1400.47	3255.5	1990.8	-216.3069	-128.6914	3.9613	4.1425	4.37%
rclassmano_056	Const. Radius	30 mm	level	9249.3	1400.47	3255.5	1990.8	-200.4728	-175.027	2.0233	1.9922	1.56%
rclassmano_057	Const. Radius	30 mm	level	9249.3	1400.47	3255.5	1990.8	-179.9666	-113.4516	4.1849	4.1976	0.30%
rclassmano_058	Const. Radius	30 mm	level	9249.3	1400.47	3255.5	1990.8	-149.7567	-65.569	16.1908	19.2238	15.78%
rclassmano_002	sinusoid	30 mm	pack	3923.9	792.94	1640.4	1049.3					
rclassmano_021	Const. Radius	30 mm	pack	3923.9	892.33	1640.4	1007.7	-53.2283	-70.5381	2.1867	1.9246	13.61%
rclassmano_022	Const. Radius	30 mm	pack	3923.9	892.33	1640.4	1007.7	-53.5632	-54.4373	3.3265	4.1884	20.58%
rclassmano_023	Const. Radius	30 mm	pack	3923.9	892.33	1640.4	1007.7	-41.3067	-22.912	18.8255	19.4948	3.43%
rclassmano_060	Const. Radius	30 mm	pack	3923.9	892.33	1640.4	1007.7	-63.3629	-87.5873	1.7788	1.9878	10.52%
rclassmano_061	Const. Radius	30 mm	pack	3923.9	892.33	1640.4	1007.7	-52.1491	-58.8295	2.9005	4.2277	31.39%
rclassmano_061	Const. Radius	30 mm	pack	3923.9	892.33	1640.4	1007.7	-35.0517	-25.1326	9.8901	20.0717	50.73%
rclassmano_003	sinusoid	30 mm	2 rubble	12549	3154	16841	3216					
rclassmano_024	Const. Radius	30 mm	2 rubble	12549	966.1	16841	1501.5	-111.8407	-84.793	-1.7156	2.0072	185.5%
rclassmano_025	Const. Radius	30 mm	2 rubble	12549	966.1	16841	1501.5	-87.8439	-56.3377	-1.8532	4.0962	145.2%
rclassmano_063	Const. Radius	30 mm	2 rubble	12549	966.1	16841	1501.5	-106.1653	-105.9363	-3.1118	1.9399	260.4%
rclassmano_064	Const. Radius	30 mm	2 rubble	12549	966.1	16841	1501.5	-101.3431	-57.1397	-1.4563	4.1400	135.2%
rclassmano_004	sinusoid	30 mm	3 rubble	29645	7601.5	39747	5412.1					
rclassmano_026	Const. Radius	30 mm	3 rubble	29645	6893.9	39747	1199	-128.1441	-57.9167	7.8477	4.1599	88.65%
rclassmano_066	Const. Radius	30 mm	3 rubble	29645	6893.9	39747	1199	-127.0519	-66.7636	8.5839	4.1358	107.6%

rclassmano_040	sinusoid	50 mm	level	7060.9	3727.3	7914.4	4656					
rclassmano_067	Sinusoid	50 mm	level	13588	3205.3	4900.5	3981.9					
rclassmano_028	Const. Radius	50 mm	level	13588	1822.3	4900.5	3394.9	-401.0007	-313.0238	2.1396	1.9540	9.50%
rclassmano_029	Const. Radius	50 mm	level	13588	1822.3	4900.5	3394.9	-383.8869	-205.2991	5.3857	4.1851	28.69%
rclassmano_030	Const. Radius	50 mm	level	13588	1822.3	4900.5	3394.9	-332.1692	-130.8156	32.6620	18.8586	73.19%
rclassmano_045	Const. Radius	50 mm	level	13588	1822.3	4900.5	3394.9	-370.9582	-293.0964	2.3023	1.9900	15.69%
rclassmano_046	Const. Radius	50 mm	level	13588	1822.3	4900.5	3394.9	-365.4292	-226.9234	3.8236	4.2111	9.20%
rclassmano_047	Const. Radius	50 mm	level	13588	1822.3	4900.5	3394.9	-309.9494	-100.1553	-31.3411	20.0035	256.7%
rclassmano_041	sinusoid	50 mm	pack	N.A.	1237.19	N.A.	1854.1					
rclassmano_069	sinusoid	50 mm	pack	N.A.	639.39	N.A.	1047.3					
rclassmano_032	Const. Radius	50 mm	pack	7517.6	1037.04	2193.7	1447	-133.4709	-119.9634	2.0141	1.9805	1.70%
rclassmano_033	Const. Radius	50 mm	pack	7517.6	1037.04	2193.7	1447	-83.0247	-73.7086	3.2709	4.1990	22.10%
rclassmano_034	Const. Radius	50 mm	pack	7517.6	1037.04	2193.7	1447	-112.0249	-24.7008	-20.1560	19.5733	203%
rclassmano_049	Const. Radius	50 mm	pack	7517.6	1037.04	2193.7	1447	-87.1727	-93.1496	2.4173	1.9955	21.14%
rclassmano_050	Const. Radius	50 mm	pack	7517.6	1037.04	2193.7	1447	-78.9356	-44.766	7.4620	4.2206	76.80%
rclassmano_051	Const. Radius	50 mm	pack	7517.6	1037.04	2193.7	1447	-109.0399	3.4007	-4.4523	20.0717	122.2%
rclassmano_042	sinusoid	50 mm	2 rubble	21833	5320.1	16756	4505.8					
rclassmano_035	Const. Radius	50 mm	2 rubble	21833	724.69	16756	1474.2	-130.3789	-130.1131	5.5347	1.9579	182.7%
rclassmano_036	Const. Radius	50 mm	2 rubble	21833	724.69	16756	1474.2	-172.3603	-98.5204	-4.8706	4.1723	216.7%
rclassmano_052	Const. Radius	50 mm	2 rubble	21833	724.69	16756	1474.2	-95.0393	-116.22	3.8474	1.9690	95.40%
rclassmano_053	Const. Radius	50 mm	2 rubble	21833	724.69	16756	1474.2	-128.361	-79.228	-8.5542	4.1969	303.8%
rclassmano_043	sinusoid	50 mm	3 rubble	20779	6026.2	11927	5069.3					
rclassmano_037	Const. Radius	50 mm	3 rubble	20779	8090.5	11927	5069.3	-222.2017	-99.6466	-3.2559	4.1687	178.1%
rclassmano_054	Const. Radius	50 mm	3 rubble	20779	8090.5	11927	5069.3	-132.5196	-81.3796	17.0909	4.1687	310%

5.6 Uncertainty Analysis

In this work, our purpose for the test setup is to remove sway velocity and achieve a smooth sinusoidal or constant radius test. But in real test data, we found a small variation of speed does affect the force acting on the ship hull. (See 5.4.1)

We can notice that the turning radius prediction model is not perfect from the results of table 5.4. The important reason is the unreliable sway velocity dependent coefficient. For example, the mean measured sway velocity of the test rclassmano_017 (30mm level ice) is 0.0604 m/s. But its standard deviation is up to 0.0056m/s. We can also find the total uncertainty of speed channel of the IMD tank facility is up to 0.3 m/s in open water. [30] The measurement of such a small sway velocity itself is unreliable. So the level of accuracy in the experimental results is another factor contributing to the incorrect prediction in table 5-4.

Chapter 6 Discussion and Conclusions

6.1 Discussion of the Test Program

The use of the planar motion mechanism to study ship maneuverability in open water is well established. In this work, we presented a detailed analysis of experimental data obtained using the planar motion mechanism to study maneuverability in ice. One of the main problems that we encountered is that sway velocity is not zero during a sinusoidal maneuver as would be expected. Table 6.1 shows samples of the average and standard deviation of measured sway velocity during a sinusoidal maneuver.

Table 6-1 sinusoidal test sway velocity

Test type	Conditions	Mean(v) m/s	Std(v) m/s
rclassmano_001	level 30 mm	0.0038	0.0031
rclassmano_002	level 30 mm	0.0019	0.0036
rclassmano_003	level 30 mm	0.0053	0.0015
rclassmano_040	level 50 mm	-0.0040	0.0048

Although the average value of the measured sway velocity is small and is appropriate for the purpose of these tests, the velocity variations are large. This introduces significant sway acceleration values. The ship-ice interactions result in the small sway velocity. In such a condition, the reliability of the yaw-rate dependent coefficients obtained from sinusoidal test was affected by the sway velocity effect.

A similar problem occurred in the constant radius maneuvers. In these maneuvers, the sway velocity and the yaw rate should stay constant during the maneuvers. Table 6.2 shows samples of the average value and standard deviation of the measured sway velocity and yaw rate during some constant radius tests.

Table 6-2 constant radius test sway velocity

Test type	conditions	Mean(v) m/s	Std(v) m/s	Mean (r) rad/s	Std (r) rad/s	V m/s	R/L
rclassmano_017	level30 mm	0.0604	0.0056	0.0642	0.0157	0.57	2.034
rclassmano_018	level30 mm	0.0536	0.0048	0.0062	0.0034	0.57	21.49
rclassmano_019	level30 mm	0.0659	0.0092	0.0301	0.0077	0.56	4.259
rclassmano_021	pack30 mm	0.0577	0.011	0.0644	0.0169	0.56	1.968
rclassmano_022	pack30 mm	0.0649	0.0087	0.0298	0.0105	0.57	5.688
rclassmano_023	pack30 mm	0.054	0.0047	0.0061	0.0061	0.56	22.53
rclassmano_028	level50 mm	0.0638	0.0107	0.0636	0.0138	0.56	1.992
rclassmano_029	level50 mm	0.0666	0.0094	0.0302	0.0131	0.56	4.590
rclassmano_030	level50 mm	0.0542	0.0060	0.0063	0.0042	0.56	20.20
rclassmano_032	pack50 mm	0.0583	0.0064	0.0644	0.0163	0.57	2.038
rclassmano_033	pack50 mm	0.063	0.0068	0.0297	0.0088	0.57	4.501
rclassmano_034	pack50 mm	0.0536	0.0046	0.0061	0.0052	0.57	22.67

In table 6-2, mean(v), std(v), mean(r), std(r) indicate the average values and standard deviations of sway velocity and yaw rate respectively. V is the average value of the resultant velocity in the tests. We can observe large variations in both the measured yaw rate and the sway velocity. These large variations introduced acceleration effects. R/L is the average value of the calculated radius-length ratio according to the equation R/L=V/rL. The results of R/L are not exactly equal to the preset test radius. This is a result of the vibrations of the mechanism during the test runs. The ship model gains

instantaneous velocity and acceleration from the breaking of the ice sheet and impact of the ice floes. It is more difficult to maintain a steady turning motion in ice than in open water.

One of the problems in the test program is the limited range of the tests as a function of the average sway velocity. Both the sinusoidal tests and constant radius tests give a sufficient range of yaw rates to study the ice force as a function of yaw rate. The linear regression results in the previous chapter show the validity of the test design. We obtained acceptable estimates for the yaw rate dependent coefficients from three consecutive constant radius tests. The range for the average sway velocities for which the tests were designed does not allow a good estimate to be obtained for the sway velocity dependent coefficients.

6.2 Data Analysis Methodology

The wavelet denoise approach is a very useful tool and should be considered as a standard signal filter in ship-ice study. The complexity of ship-ice interaction is represented by the random vibration of ship and the stochastic impact between the ship and ice floes. From the plots of the spectrum, we find that the ice force power spectra are evenly distributed in a small range of frequency. But from the plots of CWT (continuous wavelet transform) we know that the dominant frequency changes with the location in a single run. The traditional cut-off filter will indiscriminately remove the higher frequency information based on the fixed cut-off frequency. We need a tool to remove the noise

without losing the fine details of the signal. Wavelet analysis is a powerful method in signal analysis which can denoise the signal adaptively and keep required local information. The wavelet filter was applied in this work and the results are satisfactory. (Refer to figure 5-5).

Neural network is another technique we used in the data analysis. A neural network can be used to directly extract hydrodynamic coefficients in open water maneuvering tests. We did not achieve this goal in ice maneuvering tests due to data and test facilities limitations. However, we were able to calculate reliable values for the yaw rate by differentiating the yaw angle with respect to time. The finite difference method was initially applied and the results were not satisfactory. The neural network method provided better results than that obtained from the finite difference method. (Refer to Figure 5-7)

6.3 Conclusions

The following conclusions can be drawn from the data analysis.

1. The spectrum of the ice force consists of two parts. One is a very low frequency part; the other one is a higher frequency part up to 2.5 Hz. The lower frequency is close to the frequency of the yaw rate; and the higher frequency is similar to the frequency of sway velocity.

2. The power spectrum plots and the distributions of coefficients obtained from the neural network show that ship's dynamic responses are mainly determined by the sway velocity and yaw rate dependent coefficients.

3. Maneuvering performance is not sensitive to the coefficient of friction. (Ch. 5.4.3)

4. Regression analysis revealed that yaw rate dependent coefficients obtained from a sinusoidal maneuver are not unique. Their average value seem to be higher than that obtained from a constant radius test.

5. Reliable estimates for the yaw rate dependent coefficients were easy to obtain. In conclusion, it was not easy to obtain reliable estimates for the sway velocity dependent coefficients.

6. The coefficients obtained from the raw test data can be used to predict turning radius of ship navigating in similar ice conditions. The accuracy of the prediction is dependent on the accuracy of the sway velocity dependent coefficients. This prediction model can be applied to full-scale ship conveniently.

6.4 Recommendations for future work

It is still a tremendous task to exactly predict ice forces acting on the ship when it performs maneuvers in various ice conditions. Several possible reasons are discussed in the previous section. The following are some suggestions for the future research.

- The principal task is to design an experiment to study the ice force response to various sway velocities. A Straight-line Oblique Tow model test in traditional towing tank or with the PMM in IMD's ice tank can be carried out. The measured data of the new experiment combined with present PMM test data can be used to develop and validate a more accurate mathematical model of ship maneuverability in ice.
- The data acquisition system and test facility should be improved or adjusted to match the requirements of ice study. For example, in the constant radius test, the turning radius was maintained constant, but the measured instant velocity and yaw rate were delayed or asynchronous in the test. So the instantaneous turning radius computed by instantaneous velocity and yaw rate did not remain constant.
- An efficient way to calculate the second derivatives of yaw angle (yaw acceleration) and sway acceleration should be developed in order to investigate their contributions on ice forces. A significant sway acceleration and yaw acceleration may occur in the course of the test. They cannot be neglected.
- Nonlinear regression techniques and other nonlinear approaches, such as neural network are worthy of a trial when the required data are supplemented.

References

1. Kendrick. A.M. Dadachanji. N. Quart. B. 1984. *M.V. ARCTIC – Maneuvering Performance in Ice Final Report.* Transport Canada. TP 5684E.
2. Weeks. W.F. and Ackley. S.F. 1982. *The growth. structure. and properties of sea ice.* CRREL Monograph. Vol. 82-1. 1982. 136.
3. Mellor. M. 1983. *Mechanical Behaviour of Sea Ice.* CRREL monograph. Vol. 83-1. 1983. 102.
4. Forland. K.A. and Tatinclaux. J. C. 1985. *Kinetic friction coefficient of ice.* 1985. CRREL: 85-6.
5. Menon. B.C. Glen. I.F. Steele. M. Hardiman. K. 1991. *Investigation of Ship Maneuverability in Ice – Phase I.* Transport Canada. TP 10922E
6. Edwards. R.Y. Major. R.A. Kim. J.K. German. J.G. Lewis. J.W. Miller. D.R. 1976. *Influence of Major Characteristics of Icebreaker Hulls on Their Powering Requirements and maneuverability in Ice.* SNAME Transactions. Vol. 84: 364-407.
7. Peirce. T.H. Peirce. J.C. 1987. *A Survey of the Potential for Improving the Maneuverability of Ice-transiting Vessels.* Transport Canada. TP 8434.
8. Abkowitz. M.A. Liu. G. 1988. *Measurement of ship resistance. powering. and maneuvering coefficients from simple trials during a regular voyage.* Transactions of SNAME. 1988. 96: p. 97-128

9. Menon. B.C. Edgecombe. M. Tue-fee. K. Glen. I.F. 1986. *Maneuvering tests in Ice aboard USCGC Polar Star in Antarctica 1985*. Arctec Canada Limited. Report No. FR1723C-2

10. Zahn. Peter B. Humphreys. David Phillips. Loyd 1987. *Full-scale Towed Resistance Trials of the USCGC Mobile Bay in Uniform Level Ice*. SNAME Transactions. Vol. 95: 45-77.

11. Tatinclaux. Jean-Claude Alekseyev. Junj Enkvist. Ernst Kitagawa. Hiromitsu Narita. Shumei Schwarz. Joachim Takekuma. Katsuyoshi Williams. F. Mary 1989. *Comparative Model Tests in Ice of a Canadian Coast Guard R-Class Icebreaker*. SNAME Transactions. Vol. 97: 31-52.

12. Kitazawa. Takamune Ettema. Robert 1985. *Resistance to Ship-Hull Motion Through Brash Ice*. Cold Regions Science and Technology. 10(1985) 219-234

13. Lewis. Jack W. DeBord. Frank W. Bulat. Vanya A. 1982. *Resistance and propulsion of Ice-Worthy Ships*. SNAME Transactions. Vol. 90: 249-276.

14. Keinonen. Arno Browne. Robin P. Revill. Colin R. Bayly. Ian M. AKAC. 1991. *Icebreaker Performance Prediction*. SNAME Transactions. Vol. 99: 221-248.

15. Brown. Robert C. Haddara. Mahmoud R. 1997. *An Experimental Study of Ship Maneuverability in Simulated Broken Ice Floes*. Proceedings of the 4th Canadian Marine Hydrodynamics and Structures Conference.

16. Molyneux. W. D. *Self-propulsion Experiments for Icebreakers in Ice and Open Water*. Institute for Marine Dynamics. Report No. IR1989-16

17. Williams, F. M., Waclawek, P., 1998 *Physical Model Test for Ship Maneuvering in Ice*. 25th ATTC, Iowa City.

18. Molyneux, W. D. et. al. 1998. *Evaluation of Performance Limitations for Ships Navigation to and from Voisey's Bay part 5: Maneuvering experiments in Level, Pack and Rubble ice*. Institute for marine Dynamics: TR-1998-05, St. John's.

19. Mellor, Malcolm *Ship Resistance in Thick Brash Ice*. 1980. Cold Regions Science and Technology, 3(1980) 305-321.

20. Ettema, Robert Matsuishi, Masakatsu Kitazawa, Takamune *Model Tests on Ice-Rubble Size and Ship Resistance in ice Rubble*. 1986. Cold Regions Science and Technology, 12(1986) 229-243.

21. Levine, George H. Voelker, Richard P. Mentz, Paul B. *Advances in the Development of Commercial Ice-Transiting Ships*. 1974. SNAME Transactions, Vol. 82

22. Spencer, D. S. Williams, F. M. *Development of a New Large Amplitude Planar Motion mechanism at IMD*. 1998. ATTC, Iowa City: Iowa Institute for Hydraulic Research.

23. Dick, R. A. Prior, A. D. Melville Shipping Ltd., Peirce, T.H. Transportation Development Centre. *Resistance and propulsion in Ice Using System Identification Techniques*. 1995. SNAME Transactions, Vol. 103: 237-254.

24. Abkowitz, Martin A. Liu, Gengshen *Measurement of Ship Resistance, Powering and Maneuvering Coefficients from Simple Trials During a Regular Voyage*. 1988. SNAME Transactions, Vol. 96: 97-128.

25. Waclawek. P. *A Neural Network to Identify Ship Hydrodynamic Coefficients.* 1996. IMD IR-1996-14. MARSIM 96. pp 509-513

26. Lamar. Williams. *Artificial Neural network Applications to Naval and Commercial Ships.* 1993. Newport News Shipbuilding.

27. Zahn. Peter B. *Ice model Testing, A Review of Current Procedures, Materials and Results.* 1984. Sr. Naval Architect Marine Technology Corporation. IMD NM451 Z19

28. Alan Reynolds. *Ship Maneuvering Workshop at NRC, Physical Modeling Summary.* 1992. IMD VM156 S556 1992.

29. Molyneux. D. Williams. F. M. *Ship Power Performance in Multiple Layers of Broken Ice.* Proceedings of OMAE. 18. 1999 St. John's. Newfoundland. Canada.

30. Hermanski. Greg Derredji-Aouat. Ahmaed Hackett. Peter *Uncertainty Analysis – Preliminary Data Error Estimation for Ship Model Experiments.* 2001. 6th Canadian Marine Hydro-mechanics and Structures Conference. Vancouver. BC. Canada.

31. Kristin Hoffmann. *Ship maneuvering in Ice with the Planar Motion Mechanism R-class Testing.* 1998. IMD LM-1998-19.

32. Forsman. Bjorn Sandkvist. Jim SSPA Maritime Consulting AB. *Brash Ice Effects on Ship Operations- A Presentation of the SSPA Maneuvering Simulation Model and other Brash ice related projects.* POLARTECH'86 VTT Symposium 71.

33. Lindstrom. Carl-Anders *Numerical Simulation of Ship Maneuvering Motion in Level Ice.* POLARTECH'90 Proceedings.

34. The Math Works Inc. *Wavelet Toolbox User's Guide.*

35. Abkowitz, M.A. *Lectures on Ship Hydrodynamics – steering and maneuverability.* 1964. Report No. Hy-5, Hydro and Aerodynamics Laboratory, Lyngby, Denmark.

36. Cox, G. F. N., and Weeks, W. F. (1982). *"Equations for determining the gas and brine volumes in sea ice samples." CRREL Report 82-30.* CRREL.

37. Williams, F. M. Waclawek, Piotr and Kim, Hyunsoo (1996). *"Simulation of Maneuvering in Ice IMD-Samsung Collaborative Project Status report"* 1996. Institute for marine Dynamics: TR-1996-28, St. John's.

38. Nordco Limited, 1989. *A study of Ship Resistance in Pack Ice.* 1989 Institute for marine Dynamics: VM1 C765 CR-1989-29, St. John's.

39. Kashteljan, V.I. et al. 1969 *Ice Resistance to Motion of a Ship.* 1969 Institute for Marine Dynamics: VM451 K19e, St. John's.

40. Tronin, V. A. 1969. *Calculating Ice Resistance of a Ship During Rectilinear Motion in Broken Ice.* Institute for marine Dynamics: VM451 T853e, St. John's.

41. Sorensen, C., *Interaction between floating ice sheets and sloping structures.* Lyngby, Denmark 1978. Technical University of Denmark, Institute of Hydrodynamics and Hydraulic Engineering, Series Paper 19, 175p.

42. Timco, G.W. 1986 *EG/AD/S: a new type of model ice for refrigerated towing tanks.* Hydraulics Laboratory, National Research Council of Canada, Ottawa

43. Scragg, Carl A. *The determination of stability derivatives by impulse response techniques.* SNAME, Northern California Section, 1976.

APPENDIX 1 Test Data Manipulation

1.1. Data retrieval and conversion

The PMM test data was initially analyzed using GEDAP command procedures, which are developed by IMD in order to analyze the data acquired during the test runs. The test data were initially stored on the IMD server with a GEDAP (General Experimental Data Acquisition, Control and Analysis Package) format. An ftp program is prepared to transfer the test data files from VMS OS to Windows OS automatically. It is convenient to conduct test data analysis with other available tools in Windows environment a binary format.

GEDAP can handle the test data to some degree, but it is not as powerful as Matlab Program which provides us all mathematical tools that can analyze the test data as well as programmable language. Matlab includes all tools involved in my research, Wavelet toolbox, Neural Network toolbox, Statistical toolbox, Signal processing tool box. So it is necessary to convert all .DAC files to .MAT files. A shorter program was developed to carry out this conversion called "*convert*". It can manually convert .DAC files to .MAC files without losing any useful information. The short program "*convert*" is given in appendix 1.

1.2. Data Structure

After the conversion of all .DAC files to .MAT files by "convert.com" program (GEDAP programming language), the data structure of Matlab file should be introduced.

The raw test data are saved in 18 different data channels. The last channel is a time series. The interval between two measured data points is 0.02 second. The data structure is displayed in the following table and diagram.

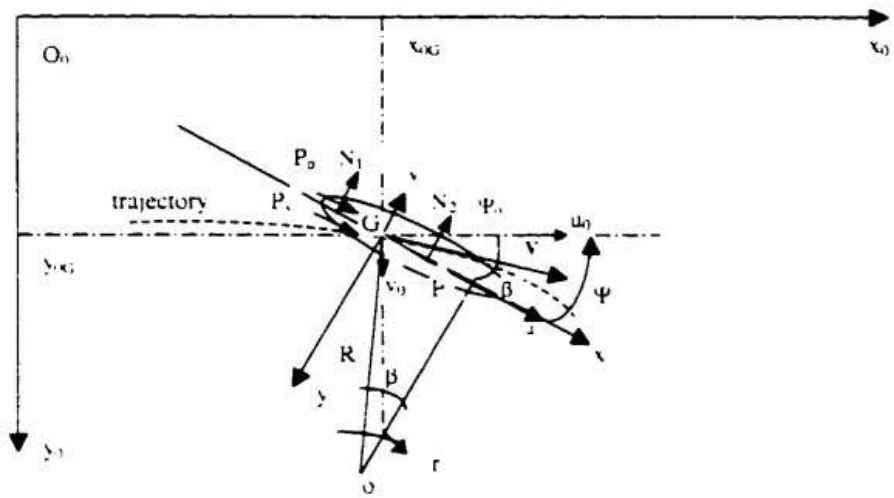

Referring to the free body diagram, two right-hand coordinate systems were used to identify the main parameters measured in test. One is $o_0x_0y_0z_0$, which is fixed in the tank; another is oxyz, which is fixed on the center of gravity of model, moving with the motion of the ship model.

Channel	Data	Remark	Unit
1	Surge-Center	Surge Force (along the x direction)	N
2	Fwd Sway	Forward sway force (N_2)	N
3	In line load		N
4	Aft Sway	After sway force (N_1)	N
5	Stbd Torque	Starboard torque	Nm
6	Stbd Thrust	Starboard thrust (P_s)	N
7	Port Torque	Port torque	Nm
8	Port Thrust	Port thrust (P_p)	N
9	Sway Velocity	Transverse Velocity ($v_0 = \dot{y}_{0G}$)	m/s
10	Sway Displacement	Transverse Displacement (x_{0G})	m
11	Fwd-yo-yo-pot		m
12	RVDT	Yaw Angle (ψ)	deg
13	Aft-LVDT		m
14	Port shaft speed	Port shaft speed	rps
15	Stbd shaft speed	Starboard shaft speed	rps
16	Model Position		m
17	Model Speed	Carriage Speed ($u_0 = \dot{x}_{0G}$)	m/s
18	time		s

The measured data of two typical test runs are plotted. These plots represent measured raw test data against time. A total of eight channels of test data were chosen to be plotted. The first group of plots comes from the data measured during a constant radius test in 30mm level ice. (file no.: rclassmano_014). The second group of plots corresponds to the data measured during a sinusoidal test in 30mm level ice. (file no.: rclassmano_001).

On inspection of the plots, one can see that the sway velocity increases while the carriage velocity slows down in the constant radius test. This combination resulted in making the model to travel along a part of a circular path. The plots of sway force, surge force and thrust revealed the random property of the ice–related dynamic data series.

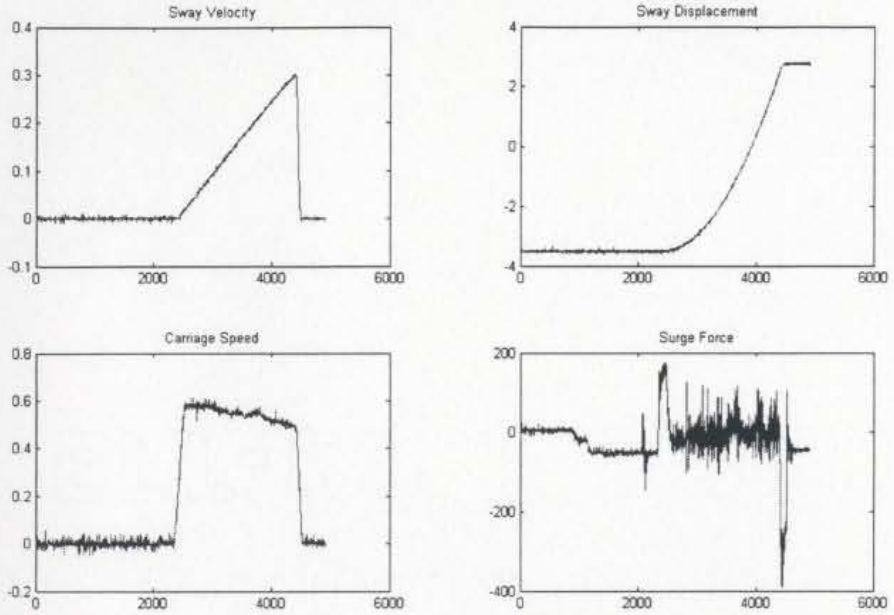

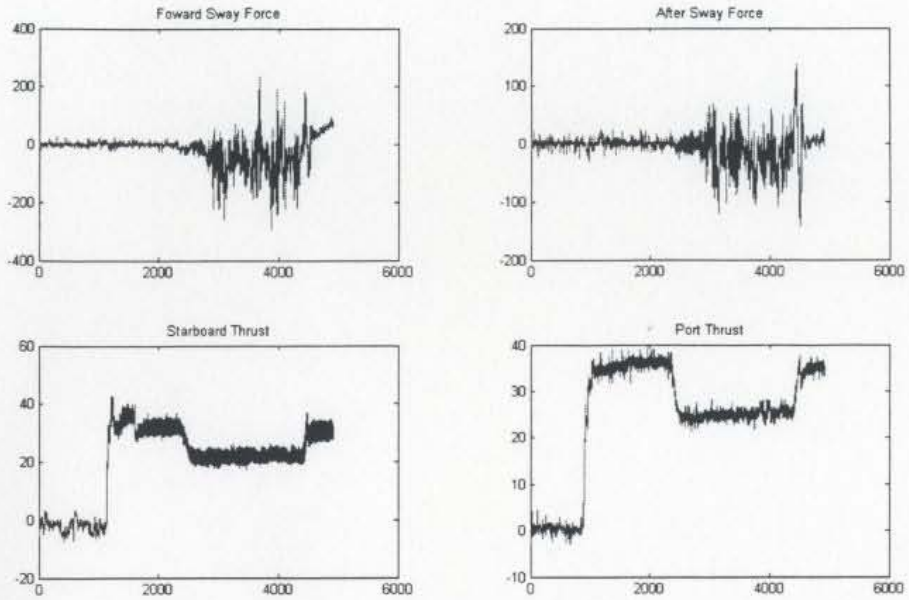

In sinusoidalal test run, the sway velocity is controlled to perform a sinusoidalal maneuver pattern, while the carriage velocity stays constant. So this forced the model to perform a sinusoidalal maneuver. The plots of sway force, surge force and thrust also reflected the parameter's stochastic nature.

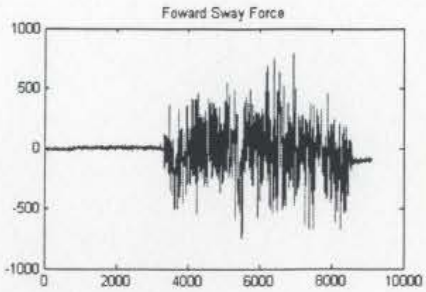
Foward Sway Force
1000
500
0
-500
-1000
0
2000
4000
6000
8000
10000

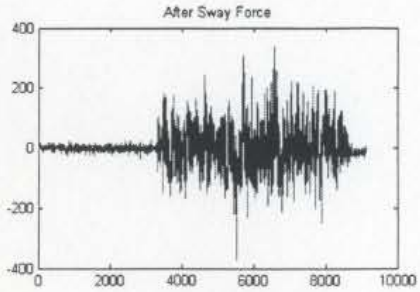
After Sway Force
400
200
0
-200
-400
0
2000
4000
6000
8000
10000

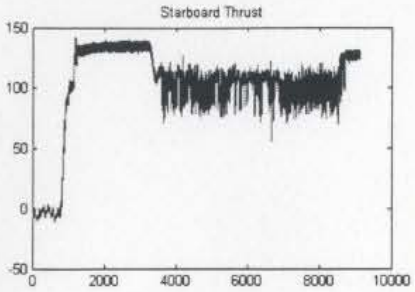
Starboard Thrust
150
100
50
0
-50
0
2000
4000
6000
8000
10000

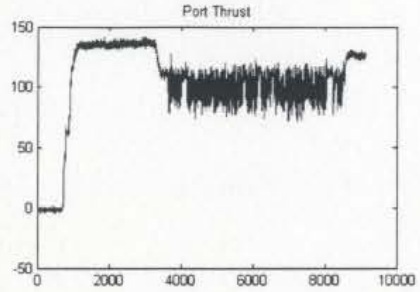
Port Thrust
150
100
50
0
-50
0
2000
4000
6000
8000
10000

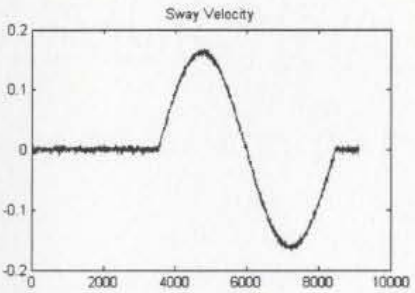
Sway Velocity
0.2
0.1
0
-0.1
-0.2
0
2000
4000
6000
8000
10000

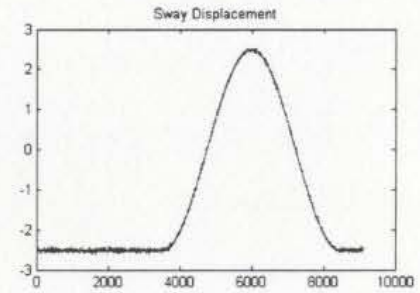
Sway Displacement
3
2
1
0
-1
-2
-3
0
2000
4000
6000
8000
10000

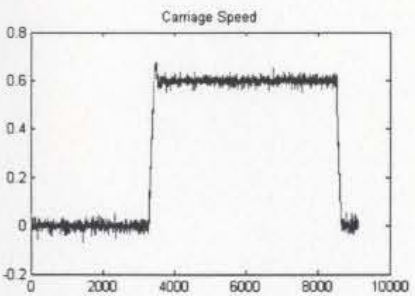
Carriage Speed
0.8
0.6
0.4
0.2
0
-0.2
0
2000
4000
6000
8000
10000

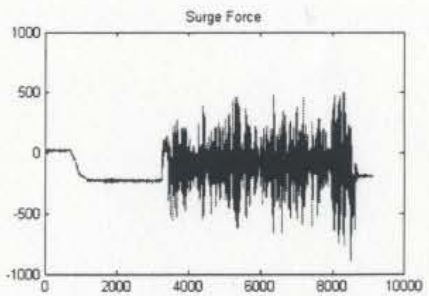
Surge Force
1000
500
0
-500
-1000
0
2000
4000
6000
8000
10000

1.3. Data Reduction and Validation

It is obvious that the measured test data, especially the ice-caused forces, are noisy and stochastic in nature with a reference to previous plots and not all information stored in the raw test data is useful for our analysis. So we have to extract the valuable information from the raw data. What we want is the information in the time duration of the tests when the model executes exact maneuvers in the desired ice condition. In this section, we present analysis techniques to extract useful information at the appropriate level of complexity in the data.

Selection of the appropriate interval over which to examine the data is a key step. In the constant radius turns, the model quickly reaches steady state in the turn. The average ship velocity, yaw rate, and turning moment, taken over the steady state portion, adequately describe the maneuver. In this case, the appropriate interval is the length, or time period, of the steady state portion. From sinusoidal maneuvers we wish to determine N_I as a function of r and $\dot{r}$. A pure yaw test with a sinusoidal motion eliminates sway velocity and acceleration, and provides information over a range of r and $\dot{r}$. The measured yaw moment N is the sum of N_I and hydrodynamic forces. The main component of N is due to the test pattern, usually one cycle or less. Other components appear in different portions of the turn, depending on the nature and location of the ice contact zones. The measured N signal also contains a component which is the test system (carriage together with PMM and attached model) response to the transient ice forces. For

the 1:20 R-class. the frequency of this component is approximately 2.1 Hz. The valuable segment of test data is selected using visual inspection and judgment.

The Matlab program we prepared is able to plot all measured information simultaneously on a time base scale. After a visual inspection we can decide to get rid of useless information manually. In this program. we just set the initial time point and end time point and extract data record in this interval. We set initial point for some time after the carriage start moving and the end point before the carriage stops. In these two time zones. velocity. force and moment changed greatly and suddenly. So these two parts of information have to be removed in order to obtain an objective evaluation of the ice force. After above-mentioned process. we can get the valid test data.

Detailed procedures are presented here with reference to the Matlab program.

- Choose the useful columns of data from raw data

  Surge force. forward and after sway load. starboard and port thrust. sway velocity. model speed. yaw angle. sway displacement. a total of 9 columns.

- Cut the raw test data

  Input the numbers of beginning data point and end data point after a visual inspection. (To eliminate the disturbed effects of engine start and stop)

- Finally. to cut data segments between start point and end point and subtract the average value before intermediate data point to get absolute value of measured test data.

1.4. Filter Program

Detail procedure and the design of the wavelet filter was documented as following

- Multi-level 1-D wavelet decomposition command WAVEDEC performs a multi-level 1-D wavelet analysis:
- DDENCMP command calculates the default parameter for de-noising:
- De-noising wavelet command WDENCMP performs the actual de-noising process.

Note that we pass in to WDENCMP with the results of the decomposition (C and L) that we calculated in the first step. After a number of trials, we specify the most desirable wavelet filter parameters, "sym8" wavelet to perform the original analysis, maximum wavelet decomposition level 10, and global thresholding option 'gbl' which is applied to the whole data series. Wavelet filter were applied to 9 channels of raw data, surge force, forward and afterward sway force, Starboard and Port thrust, model carriage velocity and transverse velocity, yaw angle and sway displacement.

1.5. Arithmetic Operation

This step is necessary because only a free body, the model, will be considered when we study the ship responses to ice forces. So we should do everything about ice forces acting on ship in the moving coordinate system. But the data measured in the test

are corresponding to the fixed coordinate system. A Matlab program is used to make a coordinate transformation from earth coordinates to ship coordinates and include the extra forces and moments provided by propellers. This arithmetic calculation resulted in a matrix of test data which is ready to analyze.

The following equations outline the operations involved in the Matlab program. As to the algorithm, please refer to *Code for GEDAP Command Procedures* prepared by IMD, which has been used in the initial analysis of the tests.

Surge force = surge center load + starboard thrust + port thrust

Sway force = forward sway load + after sway load

Yaw Moment = forward sway load × 0.9969 - after sway load × 0.9144 + (starboard thrust - port thrust) × 0.204

Sway Velocity = $v = \sqrt{u_0^2 + v_0^2}\sin\left[\tan^{-1}\left(\frac{v_0}{u_0}\right) - \psi\right]$

Surge Velocity = $\sqrt{u_0^2 + v_0^2}\cos\left[\tan^{-1}\left(\frac{v_0}{u_0}\right) - \psi\right]$

Yaw Rate = $\frac{\sqrt{u_0^2 + v_0^2}}{R}$ (for Constant Radius Test only, in the case of Sinusoidal test, neural network technique was used to obtain yaw rate)

Where u_0 is the carriage speed. v_0 is sway velocity corresponding to fixed axes. ψ is yaw angle and R is Instant Turning Radius of the ship.

APPENDIX 2 Application Program

2.1 Program "convert.com"

Run under VMS OS convert .DAC file to .MAT file.

```
S SPLIT_DACICE:[TEST_PJ96802.VB22]'P1' ! name of DAC input file [.DAC]
! GEDAP file name option [1]
! output data scale option [0]S!S!S EXPORT_MAT2'P1'
! output MATLAB mat file name [.MAT]17
! number of GEDAP input files (1-20) [1]G1.001
! name of GEDAP input file no. 1 [.001]G1.002
! name of GEDAP input file no. 2 [.001]G1.004
! name of GEDAP input file no. 3 [.001]G1.005
! name of GEDAP input file no. 4 [.001]G1.017
! name of GEDAP input file no. 5 [.001]G1.018
! name of GEDAP input file no. 6 [.001]G1.019
! name of GEDAP input file no. 7 [.001]G1.020
! name of GEDAP input file no. 8 [.001]G1.021
! name of GEDAP input file no. 9 [.001]G1.022
! name of GEDAP input file no. 10 [.001]G1.023
! name of GEDAP input file no. 11 [.001]G1.024
! name of GEDAP input file no. 12 [.001]G1.025
! name of GEDAP input file no. 13 [.001]G1.031
! name of GEDAP input file no. 14 [.001]G1.032
! name of GEDAP input file no. 15 [.001]G1.046
! name of GEDAP input file no. 16 [.001]G1.047
! name of GEDAP input file no. 17 [.001]Y
```

! Export GEDAP data? [Yes]: GEDAP_DATA

! name of data matrix (19 char max)Y

! Export GEDAP header parameter? [Yes]:

! string for missing char headers [ ]

! integer number for all missing numeric headers [0]4

! number of header parameters to export (1-100) [1]DATA_CHAN_1

! name of header parameter no. 1DATA_CHAN_2

! name of header parameter no. 2UNITS_CHAN_1

! name of header parameter no. 3UNITS_CHAN_2

! name of header parameter no. 4N

! Convert all matrix names to lower case? [No]:

2.2 MATLAB program "extract.m"

Extract and filter data

```
% load raw test data
fn1=input('enter file name ','s');
file_load= [fn1,'.mat'];
eval(['load ',file_load]);

% Extract useful information
% Suge Force
ch1=GEDAP_DATA(:,1);
% Forwar and After Sway Load
ch2=GEDAP_DATA(:,2);
ch4=GEDAP_DATA(:,4);
% Starcoard and Port Thrust
ch6=GEDAP_DATA(:,6);
ch8=GEDAP_DATA(:,8);
% Sway Velocity
ch9=GEDAP_DATA(:,9);
% Model Speed
ch17=GEDAP_DATA(:,17);
% Yaw Angel
ch12=GEDAP_DATA(:,12);
% Sway Displacement
```

```
ch10=GEDAP_DATA(:,10);

plot(ch10)

% Input the keypoints
pi=input('please enter initial point');
pe=input('please enter end point');

% Cut the data
% Suge Force
x1=ch1(pi:pe);
% Forwar and After Sway Load
x2=ch2(pi:pe);
x3=ch4(pi:pe);
% Starcoard and Port Thrust
x4=ch6(pi:pe);
x5=ch8(pi:pe);
% Sway Velocity
x6=ch9(pi:pe);
% Model Speed
x7=ch17(pi:pe);
% Yaw Angel
x8=ch12(pi:pe);
% Sway Displacement
x9=ch10(pi:pe);

% Filter
x=x1;
[c,l]=wavedec(x,10,'sym8');
[thr,sorh,keepapp]=ddencmp('den','wv',x);
x1f=wdencmp('gbl',c,l,'sym8',10,thr,sorh,keepapp);

x=x2;
[c,l]=wavedec(x,10,'sym8');
[thr,sorh,keepapp]=ddencmp('den','wv',x);
x2f=wdencmp('gbl',c,l,'sym8',10,thr,sorh,keepapp);

x=x3;
[c,l]=wavedec(x,10,'sym8');
[thr,sorh,keepapp]=ddencmp('den','wv',x);
x3f=wdencmp('gbl',c,l,'sym8',10,thr,sorh,keepapp);

x=x4;
[c,l]=wavedec(x,10,'sym8');
```

```
[thr,sorh,keepapp]=ddencmp('den','wv',x);
x4f=wdencmp('gbl',c,l,'sym8',10,thr,sorh,keepapp);

x=x5;
[c,l]=wavedec(x,10,'sym8');
[thr,sorh,keepapp]=ddencmp('den','wv',x);
x5f=wdencmp('gbl',c,l,'sym8',10,thr,sorh,keepapp);

x=x6;
[c,l]=wavedec(x,10,'sym8');
[thr,sorh,keepapp]=ddencmp('den','wv',x);
x6f=wdencmp('gbl',c,l,'sym8',10,thr,sorh,keepapp);

x=x7;
[c,l]=wavedec(x,10,'sym8');
[thr,sorh,keepapp]=ddencmp('den','wv',x);
x7f=wdencmp('gbl',c,l,'sym8',10,thr,sorh,keepapp);

x=x8;
[c,l]=wavedec(x,10,'sym8');
[thr,sorh,keepapp]=ddencmp('den','wv',x);
x8f=wdencmp('gbl',c,l,'sym8',10,thr,sorh,keepapp);

x=x9;
[c,l]=wavedec(x,10,'sym8');
[thr,sorh,keepapp]=ddencmp('den','wv',x);
x9f=wdencmp('gbl',c,l,'sym8',10,thr,sorh,keepapp);

raw=[x1f,x2f,x3f,x4f,x5f,x6f,x7f,x8f,x9f];

%Save the extracted data
f='save';
fn2=input('please enter the file name','s');
file_save1=[fn2,'data.txt'];
feval(f,file_save1,'raw','-ascii');

clear
```

2.3 MATLAB program "calcu.m"

Calculate the required test data for further analysis

```
% Load raw test file
fn1=input('enter test data file name','s');
file_load= [fn1,'data.txt'];
data=load(file_load);

x1=data(:,1);
x2=data(:,2);
x3=data(:,3);
x4=data(:,4);
x5=data(:,5);
x6=data(:,6);
x7=data(:,7);
x8=data(:,8);
x9=data(:,9);

% Calculation
% Suge Force
c1=x1-x4+x5;
% Sway force
c2=x2-x3;
% Yaw Moment
c3=x2*0.9969-x3*0.9144+(x5-x4)*0.204;
% Sway Velocity
ve=sqrt(x6.^2-x6-x7.^2);
c4=ve.*sin(atan(x6./x7)-x8*pi/180);
% Surge Velocity
c5=ve.*cos(atan(x6./x7)-x8*pi/180);
% Yaw Rate
c6=ve;
% Yaw Angel
c7=x8;
% % Sway Displacement
c8=x9;

result=[c1,c2,c3,c4,c5,c6,c7,c8];

f='save';
file_save= [fn1,'c.txt'];
feval(f,file_save,'result','-ascii');
```

2.4 MATLAB program "mynn.m"

Execute the neural network calculation for the purpose of getting yaw rate and differential coefficients

```
% Load raw test file
fn1=input('enter test data file name ','s');
file_load= [fn1,'e.txt'];
data=load(file_load);

% extract useful data
f=data(:,2);
m=data(:,3);
v=data(:,4);
q=data(:,7)*pi/180;

% data preparation for neural network calculation
n=length(f);
t=0:0.02:(n-1)*0.02;
p=q';

lp=squash(p);
lt=squash(f);

% neural network calculation for yaw rate
si=round(1+sqrt(n));
net=newff(lp,[min(lt) max(lt)],[si 1],{'tansig' 'purelin'});
net.trainParam.epochs=150;
net=train(net,lt,lp);

wei1=net.iw{1,1};
wei2=net.lw{2,1};
b1=net.b{1,1};
b2=net.b{2,1};

for i=1:n
  in=lp(:,i);
  for j=1:si
    A(j,i)=in'*wei1(j,:)+b1(j);
```

```
    H(j)=tansig(A(j));
    DH(j)=(1+H(j))*(1-H(j));
    We(j)=wei1(j)*wei2(j);
  end
  r(i)=sum(DH.*We);
end

at=2/(max(t)-min(t));
ap=2/(max(p)-min(p));

r=(at/ap)*r;

clear net t i n A H DH We

% data reparation for neural network calculation to get differentiate coefficients
da=[f';m';v';r];
t=0:0.02:1.98;
lt=squash(t);

len=length(da);

seg=len/100;

for se=1:seg

  das=da(:,100*se-99:se*100);

lf=squash(das(1,:));
lm=squash(das(2,:));
lv=squash(das(3,:));
lr=squash(das(4,:));

af=2/(max(f)-min(f));
am=2/(max(m)-min(m));
av=2/(max(v)-min(v));
ar=2/(max(r)-min(r));

% neutal network calculation
P=[lv;lr;lt];
Y=lf;
N=lm;
PR=[-1 1;-1 1;-1 1];
si=12;
[R,n]=size(P);
```

```
net=newff(PR,[si 1],{'tansig' 'purelin'});
net.trainParam.epochs=300;
net=train(net,P,Y);

w1=net.iw{1,1};
w2=net.lw{2,1};
b1=net.b{1,1};
b2=net.b{2,1};

for i=1:n
  in=P(:,i);
  for j=1:si
    A(j)=sum(w1(j,:)*in)+b1(j);
    H(j)=tansig(A(j));
    DH(j)=(1+H(j))*(1-H(j));
    We(j)=w1(j,1)*w2(j);
  end
  Y(i)=sum(DH.*We);
end

Y=(av/af)*Y;

for i=1:n
  in=P(:,i);
  for j=1:si
    A(j)=sum(w1(j,:)*in)+b1(j);
    H(j)=tansig(A(j));
    DH(j)=(1+H(j))*(1-H(j));
    We(j)=w1(j,2)*w2(j);
  end
  Y(i)=sum(DH.*We);
end

Y=(av/af)*Y;

clear net

net=newff(PR,[si 1],{'tansig' 'purelin'});
net.trainParam.epochs=300;
net=train(net,P,N);

for i=1:n
  in=P(:,i);
  for j=1:si
```

```
    Aj=sum(w1j.*in)+b1j;
    Hj=tansig(Aj);
    DHj=(1+Hj).*(1-Hj);
    Wej=w1j.*w2j;
  end
  Nv(i)=sum(DH.*We);
end

Nv=(av/am).*Nv;

for i=1:n
  in=Pr(:,i);
  for j=1:st
    Aj=sum(w1j.*in)+b1j;
    Hj=tansig(Aj);
    DHj=(1+Hj).*(1-Hj);
    Wej=w1j.*w2j;
  end
  Nr(i)=sum(DH.*We);


end

Nr=(ar/am).*Nr;

co=[Yv' Yr' Nv' Nr'];
coe(100*se-99:se*100,:)=co;
%geocose(:,:)=[mean(Yv) mean(Yr) mean(Nv) mean(Nr)];

end

df=da';

% saving the files
fi='save';
file_save=[fn1,'coe.txt'];
feval(fi,file_save,'coe','-ascii');
file_save1=[fn1,'re.txt'];
feval(fi,file_save1,'df','-ascii');


clear
```

```
% Linear Squash function from -1 to 1

function y=squash(x)

maxx=max(x);
minx=min(x);

a=2/(maxx-minx);
b=1-a*maxx;
y=a*x+b;
```